Oncogenic Phosphoinositide 3-Kinase signalling in Venous Malformations

Jasmina Zanoncello

Oncogenic Phosphoinositide 3-kinase signalling in Venous Malformations

Jasmina Zanoncello

PHD THESIS, BARCELONA, JUNE 2020

UNIVERSITAT DE BARCELONA

FACULTAT DE MEDICINA

Programa de Doctorat en Biomedicina 2016-2020

Oncogenic Phosphoinositide 3-Kinase signalling in Venous Malformations

Memòria presentada per

Jasmina Zanoncello

per optar al títol de doctora per la Universitat de Barcelona.

Aquesta tesi ha estat realitzada sota la co-direcció de

Mariona Graupera i Garcia-Milà

Sandra Castillo

en el Laboratori de Senyalització Vascular ubicat en l'Institut d'Investigació Biomedica de Bellvitge (IDIBELL).

Directora de tesi

Dra. Mariona Graupera i Garcia-Milà

Directora de tesi

Dra. Sandra Castillo

Tutor

Dr. Francesc Viñals Canals

This thesis work titled "Oncogenic Phosphoinositide 3-Kinase signalling in Venous Malformations" has been developed in the Vascular Biology and Signalling Laboratory (Graupera Lab) at Institut d'Investigació Biomèdica de Bellvitge (IDIBELL), L'Hospitalelt de Llobregat, Barcelona.

To myself.

To remember that everything is possible even when it appears otherwise.

Perseverance and self belief give you the instruments.

The rest is magic.

To Sergio.

Acknowledgements

I would like to thank Dra. Mariona Graupera for giving me the opportunity to join her lab and the group of beautiful people in it: Judith, Helena, Piotr, Anabel, Pilar, Pau, Leonor, Laia Sandra and the old Anas. Special thanks to Sandra for being my direct support during these years.

In particular, I want to thank Mariona and Sandra for giving me the opportunity to learn autonomously and independently, especially during the writing part of my PhD thesis. This experience has been revelatory for my professional and personal growth.

I would also like to thank the Marie Curie Action Program for giving me the opportunity to have such a beautiful experience and meet many wonderful people and scientists.

I would especially like to thank to my family. Without them, this experience would never have been possible. To my mother and my father from Italy, to my sister from the difficult situation in South Sudan and her boyfriend Michele from London, and to all my best friends around Europe: Caterina, Michela, Linda, Lin, April, Martina, for sharing precious moments and for supporting me in tricky times.

And last but not least, a special thank goes to my lovely Paolo, my first supporter and a unique presence in this journey, who gave me all the love I needed.

I feel extremely grateful to have lived this enormous experience with all of you.

Thank you very much.

Abstract

Venous malformations (VM), the most frequent type of vascular malformations, are localized developmental defects occurring during vascular morphogenesis that generate dilated, tortuous venous channels surrounded by erratically distributed mural cells and a disorganized extracellular matrix. VM often manifest sporadically at birth and grow over the time. They can be of different sizes and be present in any tissue resulting in chronic pathologies that are painful and lead to recurrent bleeding, infection and organ dysfunction. Current standard treatments are not fully efficient and are associated with high risk of recurrence and progression, claiming for an urgent need for targeted therapies.

From a biological perspective VM are considered as congenital errors affecting endothelial cells (ECs) or early endothelial progenitors, characterized by a constitutive activation of PI3K signalling pathway. Key discovering studies identified mutually exclusive somatic gain-of-function mutations in the endothelial *PIK3CA* gene or in the upstream endothelial tyrosine-kinase receptor *TEK*, as the genetic causes generating VM lesions. However, the molecular and cellular mechanisms driven by PI3K signalling activation in ECs underlying the pathogenesis of VM remain unknown.

Here, by using an innovative approach that combines untargeted transcriptomics with unique *in vitro* and *in vivo* models, we investigated the pathogenic mechanisms induced by the expression of the oncogenic PIK3CA-H1047R activating mutation in ECs.

We confirm that ECs hyperproliferation is the triggering mechanism leading to abnormal dilated hyperplastic vascular channels *in vivo*. In addition, we discover that expression of the mutation induces a unique shift in the adhesive molecular signature of ECs, with a specific impact on the integrins profile, which can be rescued by the use of PI3K pathway inhibitors. Also, $Pik3ca^{H1047R}$ expression leads to an increased capacity of ECs to migrate.

We postulate that altogether, the combination of an altered proliferative and migratory ECs behaviour causes defects in angiogenesis, showing a novel scenario for the pathogenesis of PI3K-driven VM. We identified the integrin-α9 as the most up-regulated integrin upon $Pik3ca^{H1047R}$ expression in ECs and we propose that its role is key in mediating the aberrant ECs behaviour underlying the pathogenesis of VM.

Finally, we developed *in vivo* and *in vitro* pre-clinical models, which can be used in combination, to study the biology of VM, enabling the investigation and development of new personalized therapies on a patient-to-patient basis.

TABLE OF CONTENTS

List of Figures

List of Tables

List of Abbreviations

4E-BP Eukaryotic translation-initiation factor 4E binding p

4-OHT 4-hydroxytamoxifen, the active form of Tamoxifen

αSMA Smooth muscle alpha actin

AKT Serine/Threonine Protein kinase B

ANGs Angiopoietins

ANG1 Angiopoietin 1

ANG2 Angiopoietin 2

Angpt2 Angiopoietin 2 gene encoding for ANG2

ARAP3 ArfGAP With RhoGAP Domain, Ankyrin Repeat And PH Domain 3

BYL719 PIK3CA-specific inhibitor; alpelisib

BM Basement membrane

CLOVES Congenital Lipomatous Overgrowth, Vascular malformations, Epidermal nevi and Skeletal/Scoliosis/ Spinal abnormalities

CLVM Capillary-lymphatico-venous malformation

CVM Capillary venous malformations

CXCR4 Chemokine (C-X-C Motif) Receptor 4

DAPI 4',6-diamidino-2-phenylindole

DEGs Differentially expressed genes

DMSO Dimethyl sulfoxide

DNA Deoxyribonucleic acid

DTT Dithiothreitol

ECs Endothelial cells

ECM Extracellular matrix

EdU 5-ethynyl-2-deoxyuridine

EEL External elastic laminae

eNOS Endothelial nitric oxide synthase

ERG ETS-related gene

FAK Focal adhesion kinase

FBS Fetal bovine serum

FGF Fibroblast growth factor

FN Fibronectin

Flk-1 Fetal liver kinase 1 gene encoding for **VEGFR2**

Flt1 Fms-like tyrosine kinase 1 gene encoding for **VEGFR1**

Flt4 Fms related tyrosin kinase 4 gene encoding for **VEGFR3**

FOXO Forkhead box O transcription factors

GAP GTPase-activating protein

GEF Guanine nucleotide exchange factor

GFP Green fluorescent protein

GPCR G-protein-coupled receptor

GVM Glomuvenous malformation

HDECs Human dermal endothelial cells

hECs human ECs

HIF-1 Hypoxia Inducible Factor 1

HIF-1α Hypoxia inducible factor α

HUVECs Human umbilical vein endothelial cells

IEL Internal elastic laminae

IF Immunofluorescence

ILK Iintegrin-linked kinase

ISSVA International Society for the Study of Vascular Anomalies

Itgα9 Integrin α9 subunit

KTS Klippel–Trénaunay syndrome

LM Lymphatic malformations

MAPK Mitogen-activated protein kinase

mECs mouse ECs

MEFs Mouse embryonic Fibroblasts

MIC Matrix-integrin-cytoskeletal

MLCP Myosin light chain phosphatase

MMP Matrix metalloproteinase

mTORC1 Mammalian target of rapamycin complex 1

mTORC2 Mammalian target of rapamycin complex 2

MVM Multifocal venous malformations

NO Nitric oxide

ON Overnight

p110α Protein encoded by the PIK3CA gene; **PI3Kα**

PBS Phosphate-buffered saline

PBST Phosphate-buffered saline-Tween 20

PCs Pericytes

PCR Polymerase chain reaction

PDGF Platelet derived growth factor

Pdgfb Platelet-derived growth factor-B gene encoding for **PDGF-B**

PDGF-B Platelet-derived growth factor-B

PDK-1 Phosphoinositide-dependent kinase 1

PFA Paraformaldehyde

PH Pleckstrin homology

PI3K Phosphoinositide 3-kinase

PIK3CA Phosphatidylinositol-4,5-Bisphosphate 3-Kinase Catalytic Subunit Alpha gene encoding for **p110α/ PI3Kα**

PIP Phosphatidylinositol 3-phosphate; see also PtdIns(3)P

PIP$_2$ Phosphatidylinositol-4,5-bisphosphate; see also PtdIns(4,5)P2

PIP3 Phosphatidylinositol 3,4,5-trisphosphate; see also to PtdIns (3,4,5)P3

PTEN Phosphatase and tensin homologue deleted on chromosome 10

PtdIns Phosphatidylinositide; see also PI

PtdIns(3)P Phosphatidylinositol 3-phosphate; see also PIP

PtdIns(3,4)P2 PtdIns 3,4-bisphosphate

PtdIns(3,4,5)P3 PtdIns 3,4,5-trisphosphate; see also PIP3

PtdIns(4,5)P2 Phosphatidylinositol 4,5-bisphosphate; see also PIP2

PROS *PIK3CA*-related overgrowth syndromes

PX Phox homology

RBD Ras‑binding domain

RT Room temperature

RTK Receptor tyrosine kinase

RT-qPCR Real Time Quantitative polymerase chain reaction

SEM Standard error of the mean

SH2 Src-homology 2

SHIP 1 and 2 SH2-domain containing inositol 5' phosphatase 1 and 2

SMCs Smooth muscle cells

SPF Specific pathogen-free

S6K1 70-kDa S6 kinase

TBS Tris-buffered saline

TBST Tris-buffered saline with tween

TEK Endothelial specific Tyrosine Kinase Receptor gene encoding **TIE2** receptor

TEM Transmission electron microscopy

VCAM-1 Vascular cell adhesion molecule 1

VE-cadherin Vascular endothelial cadherin

VEGF Vascular endothelial growth factor

VEGFs Vascular endothelial growth factors

VEGFRs Vascular endothelial growth factors receptors

VM Venous Malformations

VMCM Cutaneomucosal venous malformation

VSP34 Vacuolar protein sorting 34, Class III isoform

WB Western Blot

1   Introduction

1.1   Angiogenesis

The growth of a functional blood vessels network is essential for normal development, tissue homeostasis, repair and fertility (Graupera and Potente 2013). Since a blood vessels network nourishes all tissues, it is not surprising that structural or functional vessels abnormalities contribute to many diseases. Inadequate vessels maintenance or growth causes ischemia in diseases such as myocardial infarction, stroke, and neurodegenerative or obesity-associated disorders, whereas excessive vascular growth or abnormal vascular remodelling promote many ailments including vascular malformations, cancer, inflammatory disorders and eye diseases (Carmeliet, 2003; Folkman 2007). Vessels are also used as routes for tumor cells to metastasise (Potente et al., 2011).

Although vessels can form via different mechanisms, angiogenesis (the sprouting of new vessel branches from existing ones) accounts for the majority of vascular growth (Potente et al., 2011). Angiogenesis is required for the progression of normal physiological events, such as embryonic development, wound healing, reproductive cycling and ocular maturation, but it can be activated in pathogenic processes, e.g. chronic inflammation, tumour growth and tumour metastasis, where vessels are abnormally formed in growth, shape and function (Carmeliet and Jain 2011).

The vessels' wall is composed of endothelial cells (ECs), which line up the inner part of the vascular tubes, covered by mural cells (referred to as pericytes (PCs) in capillaries and to vascular smooth muscle cells (SMCs) in bigger vessels); which are embedded in a basement membrane (BM) comprised of extracellular matrix (ECM) proteins, that forms a sleeve around endothelial tubules (Eble et al., 2009) (**Figure 1.1**). This BM and the coat of mural cells prevent resident ECs from leaving their positions. Following exposure to pro-angiogenic stimuli, ECs undergo dynamic and complex morphological changes that allow them to invade and expand in avascularised tissues.
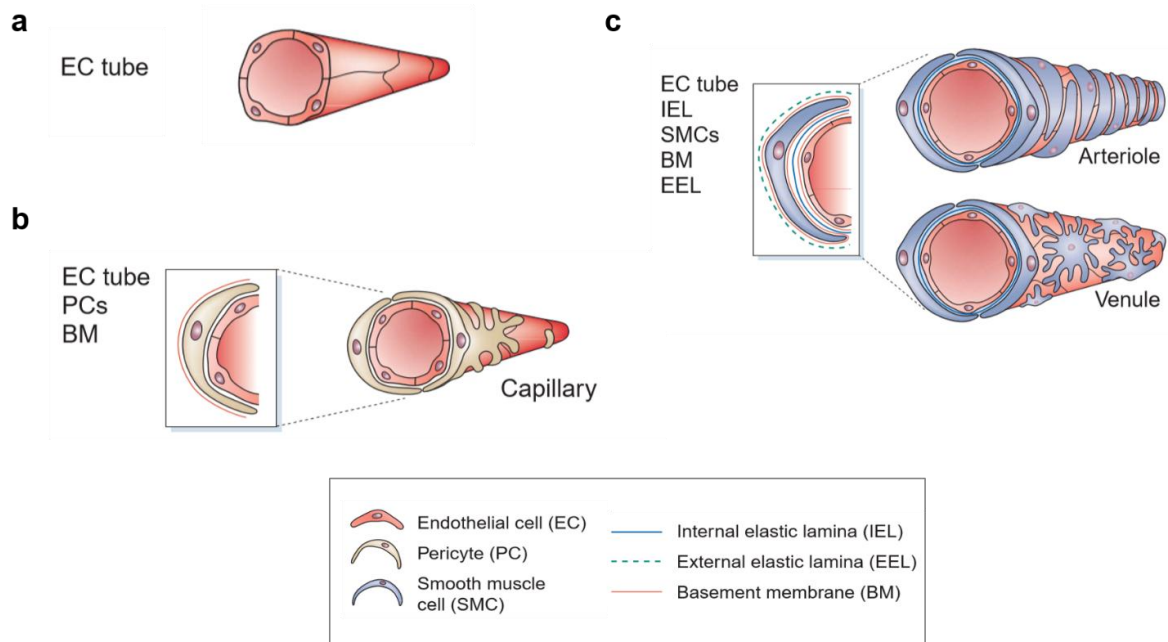
Figure 1.1. Vessel wall composition of nascent versus mature vessels.

a) Nascent vessels consist of a tube of ECs. These mature into specialised structures of capillaries, arteries and veins. b) Capillaries, the most abundant vessels in our body, consist of ECs surrounded by basement membrane and a sparse layer of pericytes embedded within the ECs BM. c) Arterioles and venules have an increased coverage of mural cells compared with capillaries, called smooth muscle cells (SMCs) and present additional inner and outer limiting matrix elastic laminae called internal elastic laminae (IEL) and external elastic laminae (EEL). (Adapted from (Jain 2003)).

Briefly, sprouting angiogenesis is initiated by tissue hypoxia and/or nutrient deprivation, which upregulate the expression of a number of growth factors and chemokines genes involved in vessel formation, patterning and maturation, including endothelial nitric oxide synthase (eNOS), vascular endothelial growth factor (VEGF) and angiopoietin-2 (ANG2). Therefore, several signalling pathways are implicated in promoting correct vascular development (Adair and Montani, 2010; De Spiegelaere et al., 2012). Upon the release of pro-angiogenic factors, existing vessels dilate in response to nitric oxide (NO) produced by eNOS and become leaky and hyperpermeable to blood plasma proteins in response to VEGF. The basement membrane and ECM dissolve in response to activation of proteases (such as matrix metalloproteinase (MMP)2, MMP3 and MMP9 and urokinase plasminogen activator) and suppression of protease inhibitors (such as tissue inhibitors of metalloproteinases). Plasma proteins leaked from these nascent vessels serve as a provisional matrix. Thus, some ECs start to protrude numerous filopodia and

become motile and invasive (**Figure 1.2**). ECs that acquire migratory properties, referred to as "tip cells", lead and guide emerging vessel sprouts and are followed by trailing proliferative "stalk cells", which make up the structure of the nascent vessel and form a lumen. This tip and stalk ECs selection and specification process is controlled by the Notch pathway (Eilken and Adams, 2010; Phng and Gerhardt, 2009) and is not a static process. Tip cell is in continuous exchange during vascular sprouting due to the mechanism of competition that ensures the optimal migration towards the VEGF gradient, assuring proper guidance and elongation of the sprout (Jakobsson et al., 2010). Thus, ECs migrate through interactions between integrins and the matrix, and proliferate in response to VEGF and other endothelial cell mitogens. Tip cells eventually anastomose with other tip cells from neighbouring sprouts, forming new vascular loops and networks. Then, to become functional, the nascent vessels must mature and become stable, which requires the formation of firm endothelial cell–cell junctions, the recruitment of mural cells and the dynamic deposition of ECM from endothelial and mural cells (Potente et al., 2011). The timing of most of these processes overlaps, allowing the vasculature to evolve seamlessly to maturation and the angiogenic process continues until pro-angiogenic signals are silenced and ECs' quiescence can be established again. In this way, blood vessels exhibit a unique plasticity and are capable of continuous adaptive structural changes in response to varying conditions and functional demands.

a *Sprout initiation and elongation*

b *Sprout anastomosis*

c *Vessel remodelling and maturation*

d *Reestablishment of quiescence*
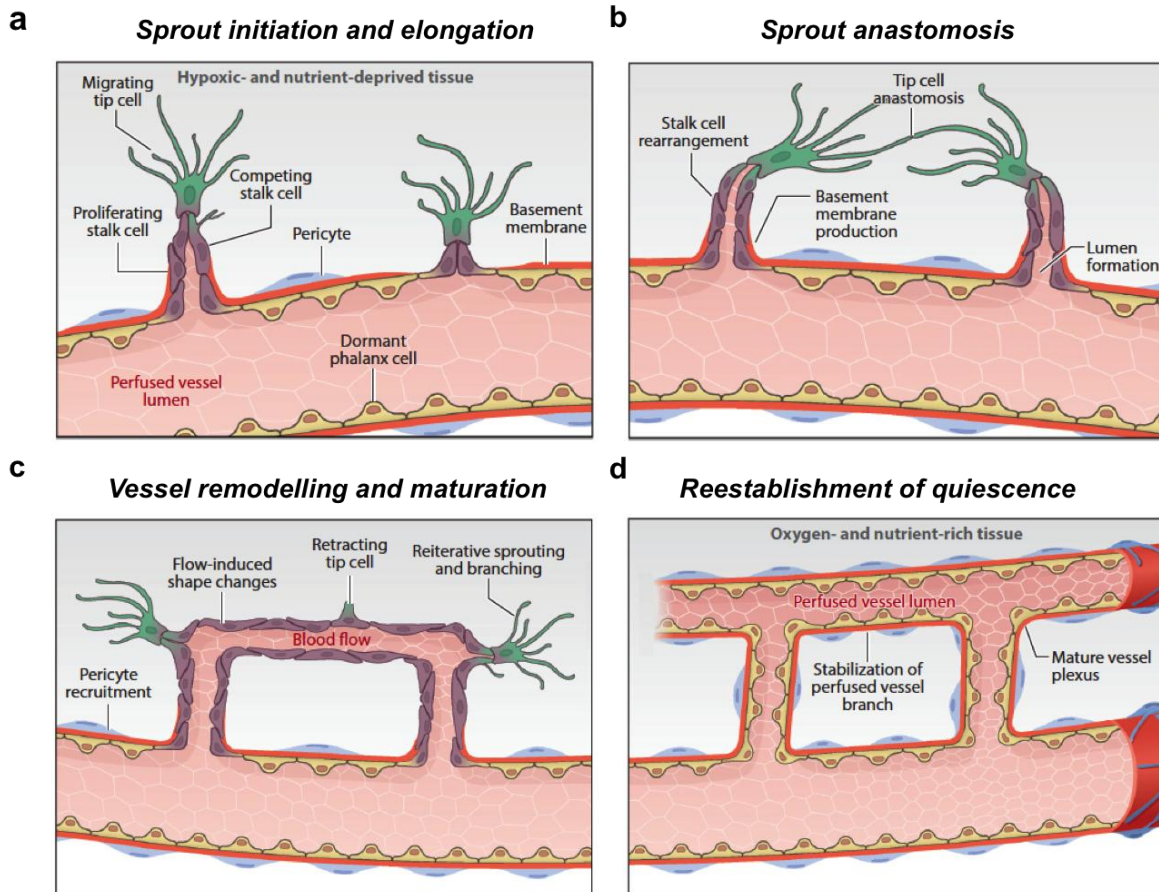
Figure 1.2. The different steps of angiogenesis.

The sprout initiation and elongation, sprout anastomosis, vessel remodelling and the reestablishment of vessel quiescence. a) Activation of quiescent vessel. Tissues in need of O2 and nutrients secrete proangiogenic molecules, thus BM and ECM dissolve, PCs start to detach from the vessel and quiescent vessels are activated, triggering ECs to become invasive and protrude filopodia. Specification in migratory tip and proliferating stalk cells is dynamic, and ECs continuously compete for the lead position. b) Sprout anastomosis and lumen formation. Tip cells connect with tip cells from adjacent sprouts to establish new vessel circuits, which eventually stabilise in one location. To generate a functional vessel a proper lumen has to be formed and expanded c) and d) the sprouting process continues until nutrients and O2 supply meet tissue demand, proangiogenic factors are silenced and ECs become quiescent again. The recruitment of pericytes, the establishment of a basement matrix and the onset of blood flow consolidate the quiescent endothelial phenotype, which has a cobblestone shape and tight monolayer organisation. Because of its resemblance to a Spartan military formation, this phenotype has been named a phalanx cell (Adapted from (Potente and Carmeliet, 2016)).

Of note, angiogenesis has been traditionally viewed from the perspective of how ECs coordinate migration and proliferation in response to growth factors activation, forming new vessel branches. However, during the sprouting phase, ECM binding to

integrins provides critical signalling support for ECs proliferation, survival, and migration (Senger and Davis 2011). ECM also signals the ECs cytoskeleton, through a matrix-integrin-cytoskeletal (MIC) signalling axis,to initiate blood vessel morphogenesis (Davis et al., 2002) (**Figure 1.3**). Furthermore, ECM provides a binding scaffold for a variety of cytokines that exert essential signalling functions during angiogenesis; thus, ECM serves as a storage for various growth factors and proenzymes involved in vessel development. During sprouting angiogenesis, the dynamic remodelling of ECM, particularly by proteases, releases various pro-angiogenic growth factors (such as VEGF and basic fibroblast growth factor (FGF)), that are sequestered in the matrix and generate anti-angiogenic molecules by cleaving plasma proteins (such as angiostatin from plasminogen) and matrix molecules (such as tumstatin from collagen type IV) or the proteases themselves (such as PEX from MMP2) (Davis et al. 2002; Senger and Davis, 2011). Thus, the spatial and temporal concentration profiles of these growth factors and protein fragments coordinate the formation of vascular tubes with lumens, presumably by regulating ECs proliferation and migration, and thus providing guidance tunnels for pericytes that assist ECs in the assembly of vascular basement membrane (Senger and Davis 2011).
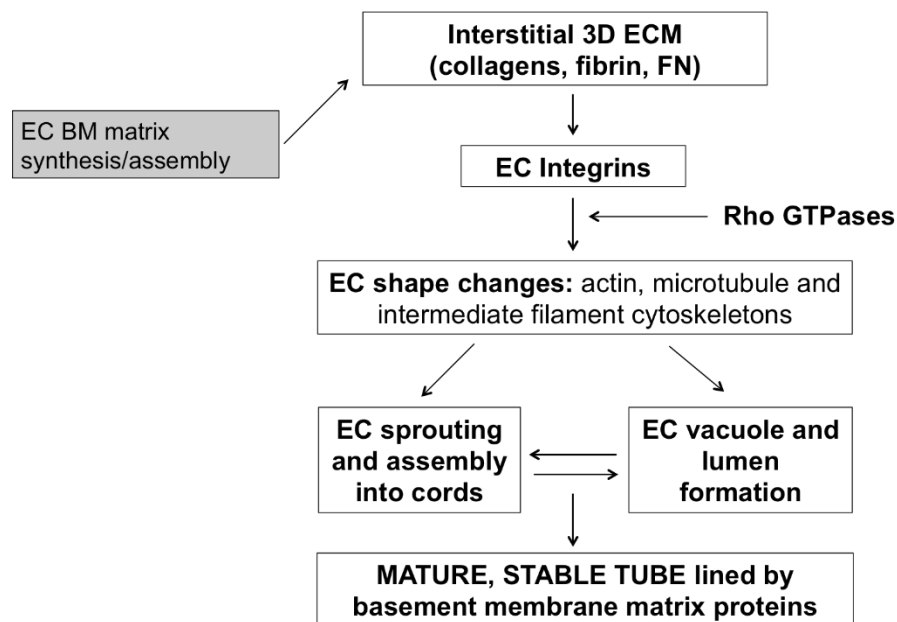
Figure 1.3. The ECM–integrin–cytoskeletal signalling axis (MIC signalling axis) in the capillary tube morphogenesis during angiogenesis.

Molecular regulators of these events are indicated next to where they are thought to intervene during these events. This pathway depends not only on ECs exposure to exogenous ECM environments, conducive for

vascular formation, but also on endogenous synthesis of ECM by ECs. Multiple integrins, as well as a number of ECM environments are permissive for EC morphogenesis. The ability of multiple integrins to regulate this process creates an important integrin signalling redundancy, that may be necessary for blood vessel assembly in different ECM environments. This signalling affects ECs survival, proliferation, migration, shape, and differentiation; all processes that are required during angiogenesis (Adapted from Davis et al., 2002 and Davis et al., 2005)).

Overall, in the endothelium, the switch between quiescence and rapid angiogenic growth is a dynamic process efficiently and tightly coordinated by multiple environmental signals including growth factors, guidance cues and biophysical stimuli – many of which converge on endothelial PI3K signalling pathway.

1.2   PI3K pathway

Phosphoinositide 3-kinases (PI3Ks) are an evolutionary conserved family of enzymes characterised by a dual protein and lipid kinase activity, which regulate a variety of physiological processes in virtually all tissue types (Katso et al., 2001; Fruman et al., 2017). They work as a central mechanism of membrane-to-cytosol communication, which integrate and translate external growth cues (growth factors, cytokines and other cues) into a diverse array of cellular processes (Vanhaesebroeck et al., 2010; Goncalves et al., 2018; Fruman et al., 2017). PI3Ks can be activated through receptor tyrosine kinases (RTKs) and G-protein-coupled receptors (GPCRs) stimulation or through Ras activation; they are recruited at cellular membrane level where they phosphorylate the 3-OH group of membrane phosphatidylinositols (PtdIns) to generate lipid second messengers. These 3-phosphoinositides coordinate the intracellular localisation and activity of multiple effector proteins, that are recruited through specific lipid-binding domains, namely the pleckstrin homology (PH) domain, the phox homology (PX) domain and the FYVE domain (Katso et al., 2001; Vanhaesebroeck et al., 2010). In addition to their catalytic activity, PI3Ks also have scaffolding roles, stabilising the proteins that PI3Ks are associated with and functioning as adaptor proteins in the assembly of protein–protein complexes (Vanhaesebroeck et al., 2005; Hirsch et al., 2009; Gulluni, F. et al., 2017). In these ways, PI3Ks instigate intracellular signalling through a network of downstream effector pathways, regulating an extraordinarily broad range of cellular regulatory processes including cell growth and survival, proliferation, differentiation, motility, metabolism and vesicular trafficking. Overall, PI3Ks facilitate growth by coupling macromolecule biosynthesis with the initiation of cell-cycle progression (Vanhaesebroeck et al., 2012; Goncalves et al., 2018; Vanhaesebroeck et al., 2019).

In mammals, this spectrum of cellular functions is governed by eight catalytic PI3K isoforms that, based on their structural characteristics and lipid substrate preferences, are grouped into three main classes (**Figure 1.4**). In general, class I PI3Ks act in signalling downstream of plasma membrane-bound receptors and small GTPases and phosphorylate the phosphatidylinositol-4,5-bisphosphate (PIP$_2$) to produce phosphatidylinositol 3,4,5-trisphosphate (PIP$_3$). Instead, class II and class III PI3Ks phosphorylate PtdIns producing phosphatidylinositol 3-phosphate (PtdIns3P) to primarily

control membrane trafficking and mostly regulate signalling indirectly (**Figure 1.5**) (Bilanges et al., 2019).

Class I PI3Ks is composed of four catalytic isoforms, namely p110α, p110β, p110γ and p110δ; encoded respectively by the *PIK3CA*, *PIK3CB*, *PIK3CG* and *PIK3CD* genes. p110α and p110β proteins are present in all cell types, whereas p110δ and p110γ are highly enriched in leucocytes (Vanhaesebroeck et al., 2010). Class I PI3Ks form heterodimers in complex with one of the regulatory subunits of the p85 or p101 families, which stabilise the catalytic isoform and modulate the activity and subcellular localisation of the heterodimer complex. Based on the type of regulatory subunit they bind, and their mode of activation, class I is further divided into class IA (p110α, p110β, p110δ), which binds to one of the five p85-type regulatory subunits, and class IB (p110γ), which couples with one of the two related regulatory subunits p101 or p87, that have no homology to p85. Although this initial classification was related to the capacity of being activated through RTKs (class IA) or GPCRs (class IB), recent data indicate that most of class I PI3Ks might be activated by GPCRs; either directly, through Gβγ protein subunits (in the case of p110β and p110γ), or indirectly, through the small GTPases RAS (for p110α, p110δ and p110γ) and RAC1 or CDC42 (p110β), via the Ras-binding domain (RBD) present in all catalytic subunits (Vanhaesebroeck 2010; Bilanges at al., 2019).

Class II is composed of three monomeric lipid kinases PI3K-C2α, PI3K-C2β, and PI3K-C2γ, respectively encoded by PIK3C2A, PIK3C2B, and PIK3C2G; which do not possess a regulatory subunit. PI3K-C2α and PI3KC2β are broadly expressed, while PI3K-C2γ expression is limited to the liver, prostate, and breast (Thorpe et al., 2015). Little is known about their mechanisms of action, specific effectors or functional role in cells; representing the most enigmatic PI3Ks (Falasca et al., 2012). It is likely that these PI3Ks do not act as classic signal transducers downstream of cell surface receptors; instead, they regulate intracellular membrane dynamics and membrane traffic, operating mainly in endocytosis, on early and recycling endosomes as well as on late endosomes/lysosomes (Bilanges et al., 2019).

Finally, Class III PI3Ks comprises the sole catalytic isoform VPS34, encoded by the *PIK3C3* gene, which is ubiquitously expressed. It forms a constitutive heterodimer with the myristoylated [G], membrane-associated VPS15 regulatory subunit. The VPS34-VPS15 dimer is found in distinct multiprotein complexes, which have critical roles in autophagy, various vesicular trafficking events and nutrient signalling (Backer 2016; Vanhaesebroeck

et al., 2010;Bilanges et al., 2019).

In normal cells, PI3K pathway is transiently induced upon growth factors stimulation and is tightly regulated by lipid phosphatases, which remove the phosphate groups added by PI3Ks, effectively antagonising their function. The 5-phosphatase SHIP1 (Src-homology 2 (SH2)-containing inositol phosphatase 1 or INPP5D) can dephosporylate PIP_3 into PIP_2. Whereas, the 3-phosphatase PTEN (Phosphatase and tensin homologue deleted on chromosome 10) removes the 3'-phosphate from both PIP_2 and PIP_3 and the myotubularin from PtdIns(3)P; thus finally terminating PI3K signalling activation.
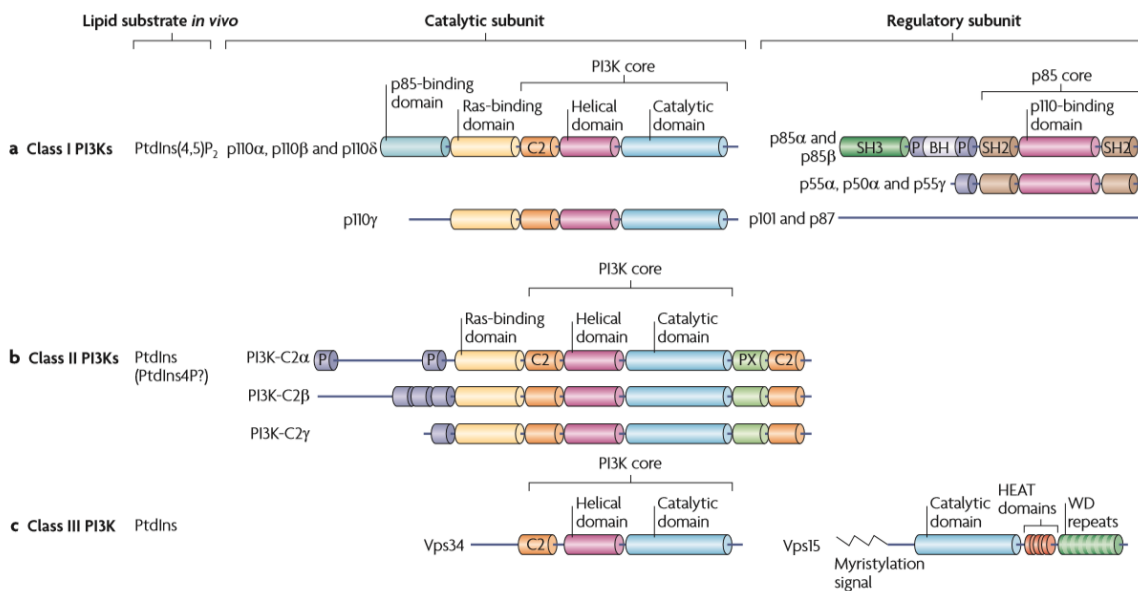
Figure 1.4. PI3Ks family.

PI3Ks are divided into three classes based on their structural and biochemical characteristics. All PI3Ks catalytic subunits have a PI3K core structure, consisting of a helical and a kinase domains and a C2 domain, which likely binds membranes. a) Class I PI3Ks use PtdIns(4,5)P2 as their substrate and exist in complex with a regulatory subunit – either a p85 isoform (for p110α, p110β and p110δ; class IA) or p101 or p87 (for p110γ; class IB). All catalytic subunits have a RBD. All p85 isoforms (p85α, p85β, p55α, p55γ and p50α) have two Src homology 2 (SH2) domains, that bind to phosphorylated YXXM motifs, whereas p101 and p87 lack these domains, do not have homology to other proteins and have no identifiable domains. The roles of the individual p85 subunits are unknown. b) Class II PI3Ks normally use PtdIns as a substrate, but might also use PtdIns-4-phosphate (PtdIns4P) under certain conditions. All the subunits present a RBD domain and have amino- and carboxy-terminal extensions to the PI3K core structure, which could mediate protein–protein interactions. c) Class III PI3K catalytic isoform VSP34 uses PtdIns as a substrate and binds Vps15. Vps15 consists of a catalytic domain (which is thought to be inactive), a HEAT domains (which probably mediate protein–protein interactions) and WD repeats, which have structural and functional characteristics similar to a Gβ subunit (Adapted from (Vanhaesebroeck et al., 2010)).
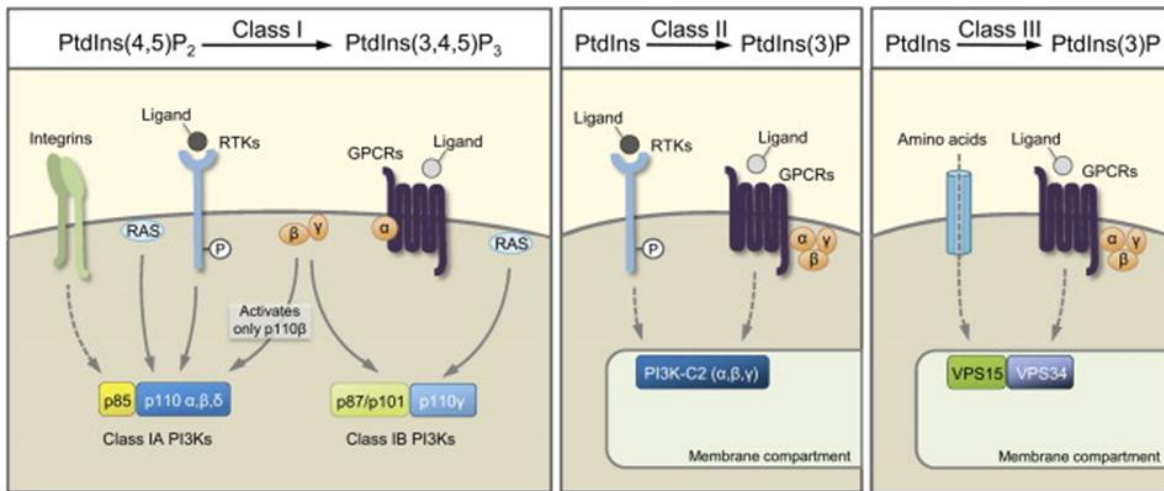
Figure 1.5. Mode of activation of PI3Ks family.

Mammalian PI3Ks are grouped in three classes based on their mode of activation. Class I PI3Ks are activated by several extracellular stimuli. p110α and p110δ are preferentially activated by receptor tyrosine kinases (RTKs), whereas p110β is activated by both RTKs and GPCRs. p110γ isoform exists in complex with the p101 or p87 regulatory subunit, which facilitate activation of p110γ by G-proteins. Class II and Class III PI3Ks are localised in membrane compartments and produce PtdIns(3)P. The signals that activate class II and class III PI3Ks are not yet fully understood, but it has been suggested that class II PI3Ks can be activated by RTKs and GPCRs, while class III can be regulated by GPCRs and nutrient availability (e.g.aminoacids) (Adapted from (Graupera and Potente 2013)).

Given the key role PI3K pathway has in controlling many physiological cell and tissue functions, it has been implicated in several pathologies, including, most prominently, human cancers, inflammation and autoimmunity; with emerging potential roles in metabolic and cardiovascular disorders (Vanhaesebroeck et al., 2010; Vanhaesebroeck et al.,2016; Fruman et al., 2017). Hyperactivation of the PI3K pathway is one of the most frequent events in human cancers and cancer cells frequently contain constitutive elevated amounts of PIP3 levels, due to increased activity of oncogenic signalling proteins residing upstream of PI3K or to mutational activation of PI3K itself (Fruman et al., 2017). Many cancers also exhibit loss of PTEN function, which elevates basal and stimulated PIP_3 abundance by reducing the turnover rate of this second messenger. The high frequency of PI3K pathway alterations in cancers led to the evaluation of the oncogenic mechanisms behind PI3K pathway alterations. *PIK3CA* gene harbours somatic mutations (Samuels et al., 2004); in contrast, mutations in other catalytic isoforms are rare (Samuels et al., 2010; Thorpe et al., 2015). In a meta-analysis of cancer genome sequencing studies, *PIK3CA*

and *PTEN* were found to be the second and third most highly mutated genes in human cancers (Lawrence et al., 2014). Furthermore, the importance of the PI3K in human cell growth is evidenced by the fact that oncogenic *PIK3CA* mutations also occur during development and result in mosaic tissue overgrowth syndromes (PROS), venous malformations and brain malformations associated with severe epilepsy (Kurek et al., 2012).

1.3   PI3K pathway in endothelial angiogenesis

PI3K pathway in angiogenesis has been mostly studied related to the class IA, with different studies in mice being instrumental in delineating the essential functions in vascular development, maintenance and integrity (Lelievre et al., 2005; Graupera et al., 2008; Yuan et al., 2008; Herbert et al., 2009; Nicoli et al., 2012). ECs-specific loss of one of the four p85-regulatory subunits (p85α, p55α, p50α, and p85β) is embryonically lethal due to defects in vessels' integrity; however, each subunit can compensate each other's loss (Yuan et al., 2008).

Although ECs express all class I PI3K isoforms, the sole catalytic p110α subunit, encoded by *PIK3CA* gene, is essential for vascular development and remodelling (Graupera et al., 2008; Herbert et al. 2009; Gambardella). In fact, both genetic inactivation and overactivation of p110α (ubiquitous or ECs-specific), during mouse embryonic development, led to mid-gestation lethality due to severe vessel sprouting and remodelling defects (Graupera et al., 2008; Hare et al 2015; Castel et al., 2016; Berenjeno et al., 2017). In contrast, p110β and p110δ deficient mice are viable, with no evident vascular abnormalities (Graupera et al., 2008). This data is in agreement with the identification of activating *PIK3CA* mutations, and not yet other identified mutant PI3K isoforms, in vascular malformations. Furthermore, the observation that too much and too little activation of p110α leads to embryonic lethality, due to sever vascular defects, suggests that ECs are extremely sensitive to p110α alteration and that its activity needs to be tightly regulated for a correct vascular plexus formation. As p110α-activating mutations in the germline is incompatible with life, this might explain why activating mutations in the *PIK3CA* gene have only been identified somatically and in a mosaic fashion (Castillo et al., 2019).

At the cellular level, p110α exerts its critical endothelial cell-autonomous function by primary regulating ECs migration through the small GTPase RHO-A, which is in turn regulated by the specific GAP ARAP3 upon PIP_3 production (Graupera et al., 2008; Gambardella et al., 2010; Nicoli et al., 2012). Mechanistically, it was recently demonstrated that p110α primary regulates ECs rearrangements and junctional remodelling and stabilisation within the nascent vascular tubes (Angulo et al., 2018). It remains to be understood whether these biological processes are also relevant in the pathogenic endothelium, upon expression of activating mutations of *PIK3CA*. In line with this, defective cell migration causes capillary-venous malformations when ECs are unable to redistribute/rearrange within the vascular network (Laviña et al., 2018). By regulating the junctional morphology of ECs (e.g. adherence junctions), p110α also selectively regulates the barrier function (Cain et al., 2010), thus regulating both angiogenesis and vascular permeability (Serban et al., 2008). Moreover, it was shown that p110α also regulates the venous identity of ECs (Herbert et al. 2009), while arteriogenesis requires inhibition of PI3K signalling (Hong et al., 2006). Furthermore, it has also been demonstrated that ECs-specific loss of p110α in mice resulted in reduced mural cells coverage of the blood vessels, supporting a crucial role for this protein in ECs for recruiting mural cells (Yoshioka K et al., 2012).

The fundamental role of p110α in vascular development is further confirmed by the fact that it is necessary not only for angiogenesis but also for lymphangiogenesis (Stanczuk et al., 2015) and, consequently, in lymphatic malformations (LM) (Boscolo et al., 2015-b). However, the capacity of ECs to respond to upstream signals is different in blood and in lymphatic vessels and understanding how this occurs might shed light into the pathogenic mechanisms of PIK3CA mutations in venous and lymphatic malformations.

Overall, it is not yet known why ECs express this extreme sensitivity to p110α but it can be partially explained by the fact that it is the most active p110 isoform in ECs and is the only class I PI3K isoform directly activated downstream of RTKs (Graupera et al., 2008; Herbert et al., 2009; Nicoli et al., 2012); thus accounting for most of the PIP3 produced in ECs upon RTKs activation (Graupera et al., 2013).

1.3.1   PI3K signalling inputs in ECs

In ECs PI3K signalling pathway can be triggered by multiple, if not all, proangiogenic signals (Soler et al., 2015), including growth factors, guidance cues and biophysical stimuli. Among all the pro-angiogenic factors, vascular endothelial growth factors (VEGFs) and angiopoietins (ANGs), with their receptors tyrosine kinase (RTKs)-VEGFR and TIE specifically expressed in the endothelium, play fundamental roles during angiogenesis. While VEGF receptors regulate endothelial differentiation and initiation of angiogenesis, TIE receptors control later stages in vessel formation, i.e. the stabilization of the initial endothelial sprout and its interaction with subendothelial cells (Eklund and Olsen 2006). In addition, the adhesive protein VE-cadherin and the integrins adhesive receptors play critical roles in ECs during angiogenesis, as briefly described in this section.

1.3.1.1   VEGF/VEGFR, Angiopoietin/TIE2 and VE-Cadherin pathways

A complex and dynamic interplay between VEGF and PI3K signalling exists in the endothelium, however this is not yet well understood. The VEGF family is composed of five ligands (VEGF-A, -B, -C,-D and PIGF) that signal via three receptors (VEGFR1/FLT1, VEGFR2/FLK1 and VEGFR3/FLT4) (Potente et al., 2011). VEGF-A is the best characterised and is commonly referred to as simply VEGF. VEGFR2 has the most important role in VEGF-induced angiogenesis (Ellis and Hicklin, 2008), as it regulates ECs proliferation, migration, differentiation and survival, as well as vessel permeability and dilation (Cébe-Suarez et al 2006). In addition, VEGFR2 forms co-receptor complexes with a number of transmembrane (receptor) proteins, including VEGFR3, VE-cadherin and integrins that cooperatively activate the PI3K signalling axis.

The ANG-TIE system also plays a major role in PI3K activation during vascular morphogenesis and maturation, and is formed by two receptors (TIE1 and TIE2/TEK) and three ligands (ANG1, ANG2 and ANG3) (Augustin et al., 2009). ANG1, expressed by perivascular cells, is an activator of the TIE2 receptor expressed in ECs. ANG1 activates PI3K signalling pathway, leading to vessel maturation and contributing to the maintenance of vascular quiescence. It promotes ECs survival and vessel stabilisation, through the formation of TIE2-TIE2 trans-association complexes at cell junctions (Augustin et al., 2009; Fukuhara et al., 2008; Graupera and Potente, 2013; Saharinen et al., 2008). On the other hand, ANG2 is produced and stored by ECs for rapid release; it is an antagonist of ANG1,

which can disrupt blood vessel formation (Davis et al., 1996; Maisonpierre et al., 1997; Augustin et al., 2009). However, ANG2 can be pro-angiogenic in some circumstances. In the presence of VEGF, ANG2 can promote proliferation and migration of ECs, sprouting and neovascularisation (Asahara et al., 1998; Lobov et al., 2002).

In addition, ANG2 is both an input and an output of PI3K pathway. ANG2 can induce PI3K pathway activation via TIE2 receptor (Papapetropoulos et al., 2000), working as an antagonist of ANG1 and favouring vessel destabilisation (Augustin et al., 2009); whereas, activated PI3K signalling decreases ANG2 expression by inhibiting the Forkhead box O (FOXO)-1 transcriptional activator (Daly et al., 2004; Potente et al., 2005; Daly et al., 2006). In this way, ANG2 acts via an autocrine-loop mechanism to control TIE2-PI3K signalling outputs, through FOXO1 transcription factor.

It has also been demonstrated that the transmembrane adhesive protein VE-cadherin, essential for regulating endothelial barrier function, can directly or indirectly activate PI3Ks to regulate junctional organisation and vessel permeability, during vascular development, by a FOXO1 dependent mechanism (Taddei et al., 2008). It is still debated how VE-cadherin and PI3K assemble at the plasma membrane, but is known that VE-cadherin signals through PI3K as a component of multi-protein complexes at the cell membrane, which involve VEGFR2 and TIE2 receptors (Lampugnani 2012).

1.3.1.2   Role of Integrins in angiogenesis

Growth factors' activation of angiogenesis is dependent on proper ECs-ECM attachment (Brooks et al., 1994). In the absence of matrix attachment cells undergo apoptotic cell death through a process termed *anoikis* (a Greek word for "homelessness"; Frisch et al., 2001). VEGF activation of ECs is dependent on matrix attachment and constitutively active AKT blocks cell detachment–induced apoptosis (Fujio et al., 1999). This suggests that matrix attachment is required for growth factors to activate AKT and maintain ECs viability; and cell attachment/adhesion is mediated mainly through the engagement of ECM with integrin molecules.

Integrins are a family of noncovalently associated heterodimeric cell surface receptors, composed of an α- and β-subunits, which mediate cell-ECM and cell-cell adhesions (Hynes 2007). Currently, 18 α- and 8 β-subunits exist, that combine to form more than 24 different integrins. Integrins are most widely known for their role as adhesion receptors for a variety of ECM proteins, such as fibronectin (FN), vitronectin, collagen,

laminin, von Willebrand factor, fibrinogen, thrombospondin, and osteopontin. Most integrins recognise several ECM proteins and conversely, most matrix proteins bind more than one integrin. When integrins bind to ECM, they become clustered and associate with the actin cytoskeleton through adaptor/signalling molecules, which further promotes integrin clustering and the assembly of actin filaments, leading to the formation of focal adhesion and activation of intracellular signalling (Giancotti et al., 1999). For instance, ECs stimulated with angiogenic growth factors, or those in newly formed vessels, express high levels of $\alpha v\beta 3$ integrin, and antagonists against $\alpha v\beta 3$ or $\alpha v\beta 5$ integrin block the growth factor-induced angiogenesis. It has also been demonstrated that $\alpha v\beta 3$ integrin can associate with VEGF and PDGF receptors, potentiating either VEGF or PDGF signalling respectively (Elicieri 2001).

Also, because several integrin signalling molecules including focal adhesion kinase (FAK), integrin-linked kinase (ILK) and Shc adaptor proteins, have been associated with AKT activation (Frisch et al., 2001), down regulation of AKT activity induced by cell detachment is likely due to the decrease in integrin-dependent AKT activation (Shiojima and Walsh 2002).

Collectively, these findings suggest that integrin signalling, induced by cell attachment ("outside-in" signal), is an important regulator of growth factor–dependent ECs survival and angiogenesis through PI3K-AKT signalling pathway. Furthermore, VEGF-induction of "inside-out" signals has also been shown to activate integrins (Byzova et al., 2000); suggesting that integrin and growth factor signalling are cooperative and synergistic with regard to activation of AKT signalling. In fact, integrin activity in angiogenesis can be modulated either by expression or by intracellular signalling from growth factor or chemokine receptors ("inside-out" signalling), which alter integrin conformation.

Overall, a myriad of (co)-receptor complexes can activate PI3K-dependent endothelial functions, suggesting that distinct combinations of (co)-receptor complexes specify the dynamics of PI3K pathway activation orchestrating ECs functions and responses.

1.3.2   PI3K signal transduction and signalling outputs in ECs

Upon growth factors stimulation, RTK activation stimulates the recruitment of p85 regulatory subunit of PI3K to the membrane and, consequently, activation of the p110 catalytic subunit of PI3K (mainly p110α, also referred as PI3Kα). PI3Kα, in turn, phosphorylates PIP$_2$ lipid to PIP$_3$, that may be metabolised to PI(3,4)P2 by 5-phosphatases SHIP-1 and SHIP-2 (SH2 Domain-Containing Inositol 5'-Phosphatase 1 and 2). Both PI(3,4,5)P3 and PI(3,4)P2 act as second messengers, interacting with the PH domains of a variety of protein effectors, among which the serine/threonine kinase AKT is the most well-known (Vanhaesebroeck et al., 2010; Fruman et al., 2017). There are three AKT isoforms (AKT1, AKT2, and AKT3) and AKT1 is predominantly expressed in ECs, being critical for VEGF-induced angiogenesis (Chen et al., 2005; Lee et al., 2014) and essential to sustain vessel integrity during adulthood (Kerr et al., 2016). AKT translocation at the plasma membrane enables its phosphorylation by phosphoinositide-dependent kinase 1 (PDK1) on Thr308 and by the mammalian target of rapamycin complex 2 (mTORC2) on Ser473, leading to its full activation. Then, AKT phosphorylates a large number of downstream substrates (>100) (including, e.g. mTORC1, eNOS, p21, GSK3, FOXOs), thereby converting upstream PI3K/AKT signals into diverse cellular responses (Manning BD, Cantley 2007) (**Figure 1.6**). A few examples are discussed below.
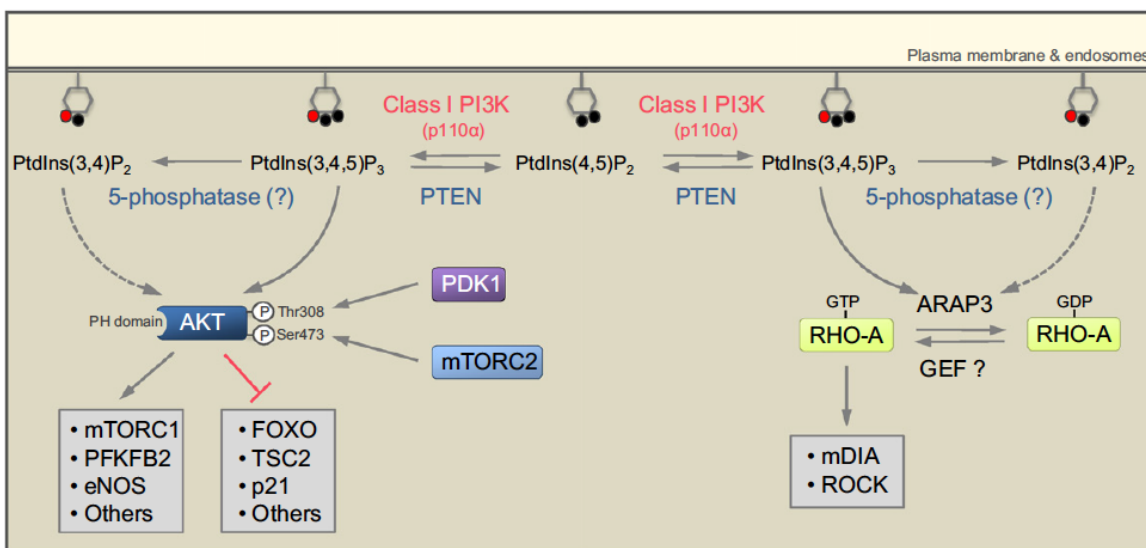
Figure 1.6. Class IA PI3K signalling in ECs.

In ECs, upon stimulation, class IA PI3K (mainly p110α) produces PtdIns(3,4,5)P3 and indirectly PtdIns(3,4)P2, which recruit signalling molecules through their lipid-binding PH domains. AKT is the best studied target that

phosphorylates a network of downstream effectors, which are either activated (e.g.mTORC1,PFKFB2,eNOS) or inhibited (e.g.FOXO,TSC2,p21). ARAP3/RHO-A is another important pathway downstream of PI3K signalling in ECs, requiring PtdIns(3,4,5)P3 for translocation to the cell membrane and catalytic activation. The small GTPase RHO-A cycles from an inactive GDP-bound state to an active GTP-bound state, regulating cell migration through mDIA and ROCK. ARAP3 inhibits RHO-A activity by acting a GTPase activating protein (GAP). The GTPase exchange factor (GEF) that stimulates RHO-A activity in ECs is not known to date. PI3K functions are counter balanced by the 3'-phosphatase PTEN (Adapted from (Graupera and Potente 2013).

AKT enhances protein synthesis and cell growth by leading to the phosphorylation of the mammalian target of rapamycin 1 (mTORC1). Activation of mTORC1 and its substrates, 4E binding protein 1 (4E-BP1) and 70-kDa S6 kinase (S6K1), result in increased cell proliferation (Boutouja et al., 2019). S6K1 contributes to metabolic reprogramming by increasing glycolysis and protein, lipid, and nucleotide biosynthesis (Magnuson et al., 2012), while the eukaryotic initiation factor-4E (eIF4E)-binding proteins (4E-BPs) control cell proliferation and survival (Malka-Mahieu et al., 2017). Keeping the complex PI3K-AKT-mTOR network homeostatically balanced is critical to prevent aberrant cellular proliferation and maintain glucose homeostasis. Endothelial-specific deletion of several components of mTORC has shed light onto the mTOR cell-autonomous role in vessels growth (Fan et al., 2017; Ding et al., 2018). However, this is still insufficient to fully understand how and in which contexts mTOR regulates angiogenesis.

AKT also phosphorylates and activates the endothelial nitric oxide (NO) synthase (eNOS) to produce NO, which can stimulate vasodilation, vascular remodelling and angiogenesis (Manning and Cantley, 2007). Following VEGF activation, AKT phosphorylates eNOS at Ser1177, leading to an increase in eNOS activity and NO production (Fulton et al., 1999; Dimmeler et al., 2000). The same phosphorylation is also required for VEGF-induced ECs migration (Dimmeler et al., 2000). Thus, NO is a regulator of cell migration and angiogenesis, as it is quickly produced downstream of the VEGFR-2/PI3K/AKT axis in ECs (Williams et al., 2000). NO presumably modulates angiogenesis by inducing a vasodilatation-associated expansion of ECs surface, enabling a more proper response of the endothelium to angiogenic and promigratory agents (Lamalice et al., 2007). Furthermore, NO can increase the expression and transcriptional activity of Hypoxia Inducible Factor 1 (HIF-1), thus resulting in the induction of VEGF mRNA (Kasuno et al., 2004). In fact, PI3K-AKT signalling can mediate angiogenesis by direct regulating HIF-1α, which in turn regulates the expression of VEGF and other angiogenic factors to finally promote angiogenesis (Wang et al., 1995; Jiang et al., 2001; Semenza, 2003).

PI3K signalling pathway also drives gene expression programs in the nucleus through FOXO transcription factors, upon AKT-dependent phosphorylation (Oellerich MF and Potente 2012). In the vasculature, FOXOs maintain homeostasis by acting as negative regulator of endothelial angiogenic behavior, with FOXO1 being the most relevant suppressor of endothelial growth, which drives endothelial quiescence (Furuyama et al., 2004; Hosaka et al., 2004; Graupera and Potente 2013). Upon PI3K activation, AKT phosphorylates FOXO isoforms, resulting in their nuclear exclusion and proteasomal degradation and thereby promoting survival, proliferation, migration and angiogenic vessels growth (Daly et al., 2004; Potente et al., 2005; Goettsch et al., 2008). In ECs, FOXO1 regulates the expression of several angiogenesis and vascular remodelling target genes including eNOS (Potente et al., 2005), ANG2 cytokine (ANG1 antagonist) (Daly et al., 2004; Potente et al., 2005; Daly et al., 2006) and pericytes attractant platelet-derived growth factor-B (PDGF-B) (Kim et al., 2000; Daly et al., 2004; Hu et al., 2008). PDGF-B is essential for the recruitment of mural cells (Lindblom et al., 2003), whilst autocrine secretion of ANG2 favours vessel destabilisation (Augustin et al., 2009). As the initiation of ECs sprouting requires vessel destabilisation and pericytes detachment, AKT activity is inversely correlated with PDFG-B and ANG2 levels. Conversely, cell confluence during tube formation induces pericytes recruitment, through a decrease in AKT activity and an increase in PDGF-B levels, ultimately providing stabilisation and maturation of nascent vessels. Recently, FOXO1 emerged as an essential regulator of vascular growth that couples metabolic and proliferative activities in ECs, antagonising c-MYC (Wilhelm et al., 2016). Endothelial-restricted deletion of FOXO1 in mice induces a profound increase in ECs proliferation, which interferes with coordinated sprouting, thereby causing hyperplasia and vessel enlargement. Thus, it is not surprising that endothelial FOXO1-deprived mice die at mid-gestation due to defects in vascular development (Hosaka et al., 2004; Furuyama, T., et al. 2004; Wilhelm et al., 2016).

Finally, some studies have also showed that PI3K signalling pathway regulates angiogenesis by critically regulating components of the actin machinery in the endothelium (Gambardella et al., 2010; Angulo et al., 2018). In particular, it has been demonstrated that this regulation is multifactorial, enabling a fine-tuning of the myosin light chain activity and, in turn, actin contractility. This includes both activation of the RHO-A small GTPase (Graupera et al., 2008; Gambardella et al., 2010) and the myosin light chain phosphatase (MLCP) (Angulo et al., 2018). Together, this highlights that the understanding of the PI3K signalling and function in the endothelium is still in its infancy and the development of new

approaches will allow to elucidate how this signalling pathway governs physiological as well as pathological angiogenesis.

Overall, during angiogenesis, PI3K activation in ECs is mostly linked to AKT activation and to its downstream cellular responses. Sustained AKT1 activation in ECs has been shown to induce the formation of structurally and functionally abnormal blood vessels, with increased permeability due to deficient mural cell coverage, that recapitulate the aberrations of abnormal tumor vessels (Phung et al., 2006).

1.4 Vascular Malformations

As described in previous paragraphs, the generation and expansion of functional blood vessels occur through a series of key morphogenic processes, which, in turn, are controlled by the interactions and ordered effects of numerous angiogenic and antiangiogenic factors. As such, it is not surprising that developmental defects can occur.

Lesions of the vascular system are the most common congenital and neonatal abnormalities (Mulliken et al., 2013). Vascular anomalies are localised defects of the vasculature, mostly due to defects during vasculogenesis or angiogenesis (Cohen 2006), which usually affect a limited number of vessels in a restricted area of the body (Brouillard and Vikkula 2003). The immense phenotypic diversity seen among vascular anomalies makes these lesions difficult to neatly categorize and, historically, different classification systems have been proposed. In 1982 Mulliken and Glowacki (Mulliken and Glowacki 1982) proposed a classification system of vascular anomalies based on endothelial characteristics, subsequently adopted in 1996 by the International Society for the Study of Vascular Anomalies (ISSVA), into proliferative vascular tumours and nonproliferative vascular malformations. At present, the ISSVA classification is based on clinical, radiological, and/or histopathologic features and an online, interactive version is available and regularly updated (http://www.issva.org/classification); it incorporates recent advances in the genetic and pathologic characterisation of these diseases.

Specifically, vascular malformations are a heterogeneous group of diseases affecting a large population (one in 100 individuals) (Mattassi et al., 2009). Vascular malformations are usually present at birth and grow proportionately with the patient. They are usually localised and generally divided according to the type of vessel affected, i.e. capillary, venous, arteriovenous, lymphatic and combined malformations (Mulliken et al., 1982; Mulliken et al., 2013).

1.4.1   Venous Malformations: clinical presentation

Venous Malformations (VM) account for two-thirds of all congenital vascular malformations, representing the most common type of vascular malformations, with an incidence of 1 in 5000 people (Uebelhoer et al., 2012; Seront et al., 2018) and a prevalence of 1% in the general population (Legiehn et al., 2008). They are congenital localised developmental defects occurring during vascular morphogenesis, causing disorganised angiogenesis, and leading to abnormal, tortuous and dysfunctional venous

channels (Hage et al., 2018).

Histologically, VM appear as dedifferentiated and immature vessels, most likely occurred because of an abnormal hyperproliferation of ECs during vascular development (Castillo et al., 2016; Castel et al., 2016). VM are characterised by a thin ECs lining, surrounded by sparse, erratically distributed, vascular mural cells and a disorganised ECM (Dompmartin et al., 2010; Nätynki et al., 2015). The relative lack of supporting mural cells could be linked to alterations in ECs adhesion, SMCs recruitment by chemoattractants, a combination of both, or even other unknown events (Brouillard and Vikkula 2003). Macroscopically, VM appear as soft, compressible, light-to-dark blue lesions in sponge-like configuration, that may occur anywhere in the body (Goines et al., 2018) (**Figure 1.7**). They predominantly occur in cutaneous, subcutaneous and mucosal tissues, but can affect any organ or tissue and can be found in deeper structures, such as muscles and internal organs such intestine (Dompmartin et al., 2010; Mulliken et al., 2013). More than 90% of VM occur sporadically and consist of a unifocal lesion, with patients typically presenting a single isolated lesion. Rarely lesions are multifocal, affecting at least two distinct sites (e.g. Multifocal Venous Malformations (MVM)). Beyond sporadic forms, this multifocality can also be seen in inherited forms that exhibit autosomal dominant transmission, such as Cutaneomucosal venous malformation (VMCM) and Glomuvenous malformation (GVM) (Brouillard et al., 2007; Soblet et al., 2017). In addition, although VM most often occur as a solitary lesion, they can also be observed as a part of more complex vascular anomaly syndromes (e.g. the Klippel–Trenaunay syndrome, the Maffucci syndrome and the Congenital Lipomatous Overgrowth, Vascular malformations, Epidermal nevi, and Skeletal/spinal abnormalities (CLOVES)), or in combination with other capillary and/or lymphatic malformations (CVM, CLVM) (Dompmartin et al., 2010).

Although present at birth, VM are not always clinically evident until later in life; they tend to grow and expand proportionally with the growth of the child and do not regress. Growth is most pronounced during puberty and pregnancy. As VM do not regress but expand proportionally with time, they have a major impact on the quality of life of patients, causing significant morbidity. In particular, they are painful and disfiguring, and many of them lead to bleeding, recurrent infections, thrombosis and organ dysfunction. Symptoms vary depending on the location and size of VM; they may go unnoticed for years prior to presentation, ranging from superficial asymptomatic varicosities to extensive, disfiguring lesions. Recurrent or chronic pain and swelling are often the presenting symptomatology (Hage et al., 2018). VM can also threaten life because of their extension into vital

structures, airway obstruction and neurovascular dysfunction. Unlike other vascular malformations, VM are associated with chronic consumptive coagulopathy (also known as localised intravascular coagulopathy) because of blood stagnation and repetitive cycles of thrombosis and thrombolysis. Approximately 50% of VM patients have elevated D-dimers and some of them have low serum levels of fibrinogen (Hermans et al., 2006; Dompmartin et al., 2008).

Accurate diagnosis has been a limiting factor in VM management (Lee et al., 2015) and it is usually made in early adulthood based on symptoms, clinical findings and imaging data (Behravesh et al., 2016). As the clinical presentation of VM is highly variable, an experienced multidisciplinary team carefully plans the treatment strategy on a case-by-case basis (Dompmartin et al., 2010; Mattila et al., 2015). Due to the poor understanding of the pathological mechanisms underlying the development of VM, therapies have long been limited and primarily based on supportive care, compression therapy and ablation of malformed veins by sclerotherapy alone or in combination with surgery (Burrows et al., 2004; Dompmartin et al., 2010). It is important to note that multiple treatment sessions are usually needed to achieve adequate symptom relief and surgical resection might be unfeasible, due to the size or location of lesions (i.e. extensive and infiltrating). Thus, current treatments are only rarely curative, as malformed veins can seldom be removed or destroyed completely and tend to recanalise and recur (Ali et al., 2017), with patients commonly experiencing a high risk of recurrence and progression of VM.
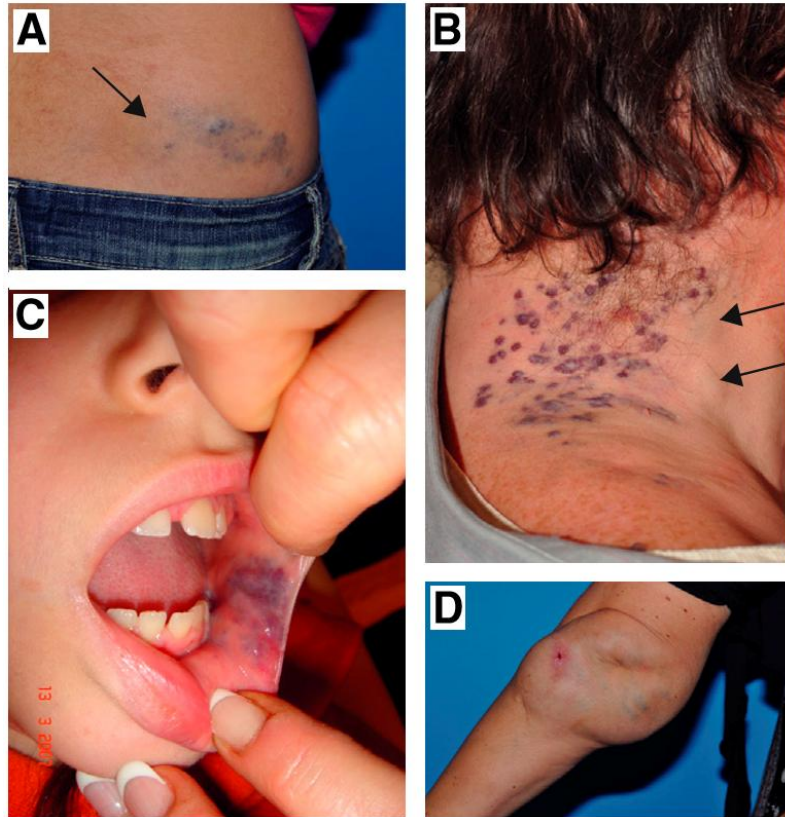
Figure 1.7. Human VM.

Cutaneous (A and B), sub-cutaneous (A and B, arrows; D), mucosal (C), or extended deep into muscles (intra-muscular), joints (intra-articular, (D) or other tissues and organs. (A and B) Skin involvement; (C, D) no skin involvement (Adapted from (Limaye et al., 2015)).

1.4.1.1   Genetic cause of Venous Malformations

The advent of high-throughput and ultra-deep sequencing technologies has led to great progresses in the discovery of the genetic landscape of VM. Around 60% of sporadic venous malformations are caused by somatic gain-of-function mutations in the ECs-specific tyrosine kinase (*TEK*) gene, encoding the TIE2 receptor, resulting in its ligand-independent activation (Limaye et al., 2009). More than 20 different mutations have been described, occurring alone or as double mutations in *cis* (in the same allele); among these, the TIE2-L914F mutation is the most common one in the *TIE2*-mutated sporadic VM (Seront et al., 2019).

TIE2 is the receptor for angiopoietins 1 and 2 (ANG1 and ANG2) and is essential in the regulation of vascular development and maintenance through the PI3K signalling pathway (Augustin et al., 2009). Activating mutations in TIE2 result in enhanced activation of the

downstream PI3K and MAPK signalling pathways (Vikkula et al., 1996; Kontos et al. 1998; Harfouche et al., 2003; Nätynki et al., 2015; Boscolo et al., 2015; Castel et al., 2016); although the exact importance of MAPK in VM pathogenesis and a possible cooperation/crosstalk of PI3K and MAPK signalling pathways in VM is still unclear, as reviewed in Kangas et al., 2018.

Upon ligand binding, TIE2 triggers PI3K signalling pathway, which in ECs is mainly mediated by the PI3Kα (Graupera et al., 2008), encoded by the *PIK3CA* gene.

In line with this, *PIK3CA* gene was identified as a second major gene mutated in VM (Limaye N et al., 2015; Castillo et al., 2016; Castel et al., 2016), with somatic, heterozygous, gain-of-function mutations accounting for about 25-30% of the sporadic cases (reviewed in Castillo et al. 2019). Somatic, gain-of-function mutations in *PIK3CA* are among the most frequently observed oncogenic events in human tumours (Samuels et al., 2010; Zhang Y et al., 2017) and tend to occur in three hotspots affecting highly conserved residues: E542K and E542K mutations in the helical domain and H1047R mutation in the kinase domain, with H1047R being the most common one (Madsen et al., 2019). It is unclear whether these mutations prevail one over the other, but both lead to a constitutive binding of p110α to the plasma membrane by two different independent gain-of-function mechanisms (Zhao et al., 2008; Burke et al., 2012), both of which trigger an over activation of PI3K pathway that is no longer dependent on upstream stimulation by growth factors.

Many cancer studies have shown that these hotspot mutations induce a gain-of-function compared to the wild-type protein and prompt transformation and tumorigenicity (Ikenoue et al., 2005; Samuel et al., 2005). Also, others demonstrated that gain-of-function PI3K signalling affects the synthetic activities of a cell at transcriptional and translational levels, suggesting that these mutations provide a selective growth advantage to the cell (Bader et al., 2005).

Although widely referred to as cancer "drivers", the same mutations have also been identified in non-malignant, albeit often severe, nonhereditary postzygotic overgrowth disorders called PROS, which often exhibit mixed capillary, lymphatic, and venous malformations, and in a variety of vascular malformations such as LM and CLVM (Lindhurst et al. 2012; Hoon et al., 2015; Madsen et al., 2018). The existence of the same *PIK3CA* mutations in both simple (VM, LM) and combined (CLVM) vascular malformations suggests that the type, location and/or severity of the vascular anomaly are likely dependent on when and/or what EC lineage or progenitor cell the mutational event occurs during embryonic development. Although they are believed to occur during

embryogenesis, the timing and origin of these mutations remain unclear and the cellular origin likely involves ECs or an early endothelial cell lineage. This suggests that ECs are extremely sensitive to PI3K signalling pathway, which needs to be tightly regulated for proper vessel formation.

In VM, *PIK3CA* and *TEK* mutations are largely mutually exclusive, all triggering an overactivation of PI3K signalling pathway (**Figure 1.2**). An unusual case has been reported in which both *PIK3CA* and *TEK* mutations have been found in ECs derived from same VM (Goines et al., 2018). Of note, in this specific case, neither *PIK3CA* nor *TEK* mutations were hotspots mutations. Furthermore, TIE2-L914F, TIE2 double mutations or PIK3CA mutations have never been found as inherited, suggesting that they all are lethal in germline (reviewed in Kangas et al., 2018); as already shown for *Pik3ca*[H1047R] using genetic mouse models (Hare et al., 2015; Castel et al., 2016; Berenjeno et al., 2017; di Blasio et al., 2018).

In addition, although gain-of-function somatic mutations in *TIE2* and *PIK3CA* genes reside in a common signalling pathway, some gene-specific effects may be clinically present in unifocal VM. For example, *PIK3CA* mutation-positive VM were noted as deeper lesions, not extending into the skin, in contrast to common *TIE2* mutation-positive VM (Kangas et al., 2018). Also, while ERK1/2 and STAT1 are activated in *TIE2*-mutant ECs, they are not in *PIK3CA*-mutant ECs. Furthermore, AKT activation is higher in *PIK3CA*-mutated ECs compared to *TIE2*-mutant ECs (Timothy et al., 2019). The remaining *TIE2/PIK3CA*-mutation negative VM are likely caused by infrequent mutations in several different genes connected to PI3K and MAPK signalling pathways, as suggested by Castel et al. (Castel et al., 2016).

1.4.1.2   Biology of Venous Malformations

Although the genetic causes of VM are known, we are still at the early beginnings in the understanding of the underlying pathological mechanisms. Nevertheless, the development of *in vitro* and especially *in vivo* models brought great advances into the biological mechanisms that may have a role in the initiation, growth and maintenance of VM lesions. Both genetic- and ECs transplantation-based murine models for VM have been developed, demonstrating that TIE2 or PIK3CA mutations in the ECs compartment are sufficient for VM lesion formation (Boscolo et al., 2015; Castillo et al., 2016; Castel et

al., 2016; di Blasio et al., 2018), identifying the endothelial TIE2-PI3K-AKT axis as a major VM-causing signalling pathway.

A sustained AKT activation induces pathological angiogenesis and increases blood vessels diameter and vessels density in mouse models (Phung et al., 2006; Goines et al., 2018). It has been suggested that an increase in AKT may support ECs survival in SMC-deficient malformed veins (Morris et al., 2005), but the importance of increased resistance to apoptosis for VM has not yet confirmed. Also, activated AKT negatively regulates FOXO1; thus target genes, implicated in vascular morphogenesis and remodelling, such as ANG2 and PDGF-B are downregulated in ECs expressing either TIE2 or PIK3CA mutations (**Figure 1.8**) (Limaye et al., 2015; Castillo et al., 2016; Castel et al., 2016; Uebelhoer M et al., 2013). Although not yet proved mechanistically, the decrease in ANG2 and PDGF-B could explain the defective mural cell coverage characterising the VM lesions.

At the cellular level, cell migration is an ECs function predicted to be influenced by TIE2 (Uebelhoer et al., 2013) and PIK3CA mutations (Castillo et al., 2019); however, migration velocities are not increased based on *in vitro* assays (Soblet et al., 2017; di Blasio et al., 2018).

Recent *in vivo* and *in vitro* studies demonstrated that PIK3CA mutant ECs show enhanced proliferation (Castillo et al., 2016; Castel et al., 2016; Goines et al., 2018; di Blasio 2018) and a reduced expression of arterio-venous specification markers (Eph-B4, Ephrin-B2, and COUP-TFII). This supports the idea of a dedifferentiated or progenitor-like state of these cells. Of note, a characteristic feature of the endothelium in patients and VM mouse-derived lesions is the loss of normal ECs morphology. *In vitro* studies demonstrated that loss of ECM fibronectin (FN) and ECs monolayer morphology are common to both TIE2 and PIK3CA mutations (Limaye N et. al., 2015; Natynki M et al., 2015). FN interacts with and functions as a scaffold for proper assembly of many ECM and BM components (Kostourou et al., 2014). In gene-targeted mouse embryos, lack of FN results in defective morphogenesis, including dilated and malformed vessels, and loss of endothelial–mesenchymal contacts (George et al., 1997). FN also binds endothelial α5β1 integrin and potentiates TIE2 signalling induced by ANG1 (Cascone et al., 2005). This suggests that a decrease in FN may have a role in formation of VM lesions. In addition, transmission electron microscopy (TEM) analysis of VM biopsies, from both patients and mouse transplantations, revealed discontinued endothelium, ECs elongations and disorganised

alignment of cytoskeletal filaments concomitant with consistent abnormalities in perivascular ECM. These include structural changes in the BM and fibrillar collagen matrix, suggesting continuous ECM remodelling (Chen et al., 2014; Natynki et al., 2015). Collectively, these observations suggest that altered ECM and cytoskeleton signalling may have a key role in VM pathogenesis, which could also serve as an easily observable parameter for EC normalisation in *in vitro* studies. Also, these data indicate that the most common TIE2 and PIK3CA variants induce the same VM-causative signalling pathways. The described mechanisms may affect ECs intrinsic functions, ECs–SMCs interactions, venous specification and (indirectly) perivascular ECM remodelling; altogether contributing to lesion formation.

1.4.1.3 Targeted therapies for Venous Malformations

The development of different murine models for VM served as a critical proof-of-concept for the use of targeted therapies in this disease, demonstrating that inhibition of the PI3K–AKT–mTOR pathway can decrease VM. Treatment with the mammalian Target of Rapamycin (mTOR) inhibitor, or a rapamycin derivative (i.e. everolimus), of $Tie2^{L914F}$ (Boscolo et al., 2015) and $Pik3ca^{H1047R}$ mutated ECs in mice (Castillo et al., 2016; di Blasio et al., 2018) diminished lesion growth, reduced ECs proliferation and normalised mural coverage. This vessel normalisation was induced by a strong inhibition of p-AKT(Ser473) through rapamycin-mediated mTORC2 disruption. Indeed, even if Rapamycin is an allosteric inhibitor of mTOR that predominantly inhibits mTORC1, a prolonged treatment with Rapamycin has been shown to disrupt the mTORC2 complex, which is known to directly phosphorylate Ser473 residue of AKT (Sarbassov et al., 2006).

Similarly, the use of the PIK3CA-specific inhibitor alpelisib (BYL719), showed a marked decrease in VM size, blocked ECs proliferation and, unlike Rapamycin, induced apoptosis of the expanded ECs (Castel et al., 2016; Limaye N et al., 2015). In contrast, a TIE2 inhibitor (TIE2-TKI) was unable to inhibit lesion growth in $Tie2^{L914F}$-mutated ECs in mice (Boscolo et al., 2015), likely due to its weak capacity to inhibit the mutated form.

Furthermore, an *in vitro* study that treated HUVECs overexpressing TIE2-L914F or PIK3CA variants with BYL719 demonstrated that, a part of abolishing the induced AKT phosphorylation, restored the ECs monolayer organisation and ECM FN levels, while AKT inhibition (with Rapamycin) did not. It is likely that BYL719 was more effective than

Rapamycin because it blocked more efficiently AKT phosphorylation at both Ser473 and Thr308 (Limaye et al., 2015).

Although the use of either Rapamycin or BYL719 shown to be effective against VM driven by both TIE2 and PIK3CA mutations, the use of BYL719 may provide an advantage over Rapamycin by avoiding the immune-suppressive effects of the mTOR inhibitor while targeting a node in the signalling cascade upstream of mTOR, and thereby mitigating hyperactivation of the PI3K-AKT pathway. In addition, Castel et al. (2016) used BYL719 inhibitors in two different cream formulations, thus allowing topical administration of the inhibitor for treatment of cutaneous VM lesions; potentially abolishing the need for systemic treatments that increase toxicity and off-target effects (i.e. hyperglycemia, nausea, gastrointestinal effects, and fatigue)

At present, such as in a multicentric phase 3 trial on adult and children (VASE, EudraCT Number: 2015-001703-32), most of VM are treated with Rapamycin or its analogues (i.e. everolimus or sirolimus), with success in the quality of life of patients because of halting lesion evolution (Hammer et al., 2018). However, Rapamycin does not cure VM, as not fully disappearance of lesions has been observed (Hammer et al., 2018; Boscolo et al., 2015). Nevertheless, by decreasing VM volume, Rapamycin can render lesions that were initially considered unfeasible more amenable to interventional procedures; thus also playing a role as a pre-treatment before radical interventional procedures of large complicated lesions.

Alternatively, the use of PIK3CA-specific inhibitors currently on clinical trials for cancer (Loibl et al., 2016; Hoste et al., 2018) might be considered a better option. Still these inhibitors are currently used at maximum tolerated doses in cancer patients, inducing signalling feedback loops that can block their effects and make these drugs poorly tolerated by the patients. However, a recent successful study treating PROS patients with the BYL719 inhibitor has given new hope for *PIK3CA*-driven vascular malformations patients (Venot et al., 2018). As such, long-term treatment with low-dose of PIK3CA-inhibitors could normalise aberrant PI3K signalling, avoiding systemic toxicity and be effective in reducing or even eliminating *PIK3CA*-driven vascular malformations. Furthermore, the efficacy of these drugs at low doses is crucial taking into account that these are congenital diseases and most patients are paediatric.

Importantly, all these studies indicate that molecular treatments can be effective against VM and provide support for exploring PIK3CA-targeted therapeutics that can block

and reverse the development of VM, potentially improving the quality of life for patients afflicted by these lesions. In addition, the PIK3CA hotspot mutations found in tumours, provide the rationale for the exploration and repurposing of existing and investigational cancer drugs for VM.

Finally, discoveries of the molecular and cellular abnormalities characterising *PIK3CA*-VM, in parallel with accurate pre-clinical mouse models finely reproducing the aetiology of *PIK3CA*-driven VM, will provide the necessary pre-clinical models for the study of molecular-targeted treatments.
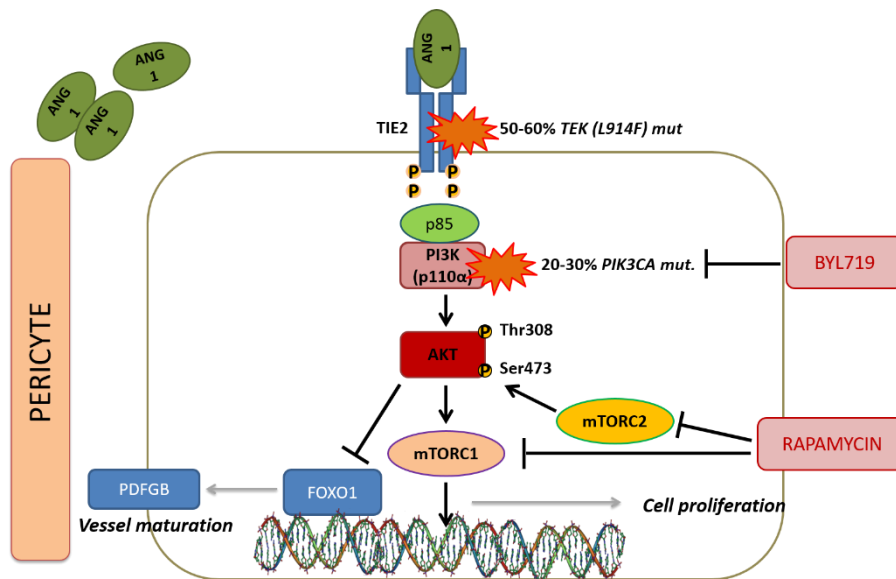
Figure 1.8. PI3K signalling pathway in VM.

Ligand binding of the endothelial TIE2 receptor (e.g. by ANG-1 secreted by pericytes) stimulates the recruitment of the p85 regulatory subunit of PI3K to the cell membrane and the activation of the p110α catalytic subunit of PI3K. PI3K signalling pathway activation phosphorylates AKT on Thr308, leading to a first, partial, activation of AKT. mTORC2 induces a second phosphorylation on Ser473 to fully activate AKT, which is thereby able to activate mTORC1 and its substrates, resulting in cell survival and proliferation. Activated AKT also negatively regulates the transcription factor FOXO1, decreasing levels of pericytes attractant PDGF-B and stimulating pericytes detachment. Orange stars indicate genetic anomalies leading to VM. These TIE2 and PIK3CA mutations result in an excessive and uncontrolled activation of PI3K-AKT signalling pathway, even in confluent cells, leading to abnormal proliferation rate and immature vessels partially caused by inappropriately low PDGF-B levels, causing defective and sparse pericytes coverage. Promising targeted therapies for VM are also indicated. Rapamycin is an allosteric inhibitor of mTOR. It inhibits mTORC1 and disrupts the mTORC2, resulting in decreased activation of AKT, increased levels of PDGF-B, stimulation of pericyte coverage and vessel maturation. This leads to vessel 'normalisation.' BYL719 is a PIK3CA inhibitor that could result in a stronger effect than Rapamycin. PI3K, phosphoinositol 3 kinase; AKT, protein kinase B; mTOR, mammalian Target of Rapamycin.

2   Objective

This thesis is based on the hypothesis that hyperactivation of PI3K signalling pathway plays a key role in the generation and maintenance of VM. Overactivation of PI3K signalling pathway can be induced by activating mutations in upstream receptors (e.g. hotspot mutations in the *TEK* gene, encoding the endothelial tyrosine-protein kinase receptor TIE2, which causes around 60% of sporadic VMs), as well as by activating mutations in the PI3K itself (e.g. *PIK3CA* gene, encoding for PI3Kα isoform, accounting for 25-30% of sporadic VM).

PI3Kα is the only PI3K isoform required for blood vascular development. In addition, it is the most common PI3K isoform found mutated in cancer and hotspot activating mutations are the second most common event in many human tumours (also referred as "oncogenic mutations"), with the H1047R mutation representing the most common one.

Despite the aforementioned discovery of the genetic causes of VM, the impact of PI3K activation in the pathogenesis of VM is still not known.

Thus, the objective of this thesis is to elucidate the impact of the oncogenic PIK3CA-H1047R mutation in ECs, to understand the biological mechanisms involved in the pathogenesis of VM.

To reach this objective we have set up the following specific aims:

1. To unveil the molecular and cellular mechanisms driven by the activating PIK3CA-H1047R mutation in ECs;

2. To generate a robust mouse model of PIK3CA-related VM, in order to explore the biology of PIK3CA mutations and provide a pre-clinical platform to test pharmacologic interventions;

3. To create and characterise a collection of patient-derived primary ECs.

3 Materials and Methods

3.1 Mouse experiments

3.1.1 Mice husbandry and care

All mice analysed in this work were kept in individually ventilated cages and cared under specific pathogen-free (SPF) conditions. All the experimental procedures were performed in accordance with the guidelines and legislations of the Catalan Ministry of Agriculture, Livestock, Fisheries and Food (Catalonia, Spain), following protocols approved by the local Ethics Committees of IDIBELL-CEEA.

3.1.2 Mice lines used

All mice used in this work were backcrossed on a C57BL/6 background for more than 10 generations.

To generate the transgenic mouse line we used in this work, we crossed Pdgfb-iCreER mice into Pik3ca$^{WT/H1047R}$ mice, to induce the *Pik3ca^{H1047R}* expression at the postnatal level, in a heterozygous state and from its endogenous promoter.

❖ **Pdgfb-iCreER mice** express an inducible iCreER recombinase from the endogenous Pdgfb locus allowing the genetic targeting of the vascular endothelium at postnatal level upon 4OH-tamoxifen (4-OHT) administration. In detail, this transgenic mice line expresses a tamoxifen-inducible form of Cre recombinase in vascular ECs by using a phage artificial chromosome (PAC) containing the *Pdgfb* gene. In newborn animals, recombination is achieved in most capillary and small vessel endothelial cells in most organs including the central nervous system. In adult animals, recombination activity is also widespread in capillary beds of skeletal muscle, heart, skin, and gut but not in the central nervous system where only a subpopulation of endothelial cells is labeled. Thus, Pdgfb-iCreER mice are a valuable research tool to manipulate endothelial cells in postnatal mice and study pathological angiogenesis. The derivation of this line has been described in Claxton et al. 2008.

❖ **Pik3ca^{WT/H1047R} mice** harbor one germline *Pik3ca* allele with a conditional H1047R mutation, so these mice are heterozygous for a Cre-inducible knock-in allele of *Pik3ca^{H1047R}*. In detail, an exon-switch strategy inserted loxP sites flanking exon 20 of *Pik3ca gene* and downstream placed a tandem copy of exon 20 containing a CAT→AGG change in codon 1047. Cre–mediated recombination leads to replacement of wild type with mutant exon 20 resulting in p110α-H1047R protein expression at endogenous levels in otherwise normal cells, thus accurately reproducing the scenario of a naturally occurring mutation. The presence of the conditional allele did not affect development. This mice line allows studying the effects of the *Pik3ca^{H1047R}* mutation in the physiologically relevant context of a somatic, heterozygous *Pik3ca* mutation expressed at endogenous levels in otherwise normal cells and tissues. This also circumvents the embryonic lethality exhibited by p110α homozygous mutants (Graupera et al., 2008). The derivation of this line has been described in Kinross et al., 2012.

❖ **Rosa26-CreERT2 mice:** mouse line that ubiquitously expresses the inducible Cre under the Rosa26 promoter**,** enabling temporal control of floxed gene expression by tamoxifen induction in vivo.

3.1.3   Induction of Cre mediated gene activation *in vivo*

3.1.3.1   4-hydroxytamoxifen (4-OHT) preparation

25 mg of 4-OH tamoxifen powder (Sigma, #H7905_25mg) were dissolved in ethanol to obtain a working solution of [10mg/ml]. The solution was aliquot under sterile conditions and stored at -20ºC. Different dilutions were prepared by defreezing and diluting the stored aliquots with sterile phosphate-buffered saline PBS 1X (Sigma #D8537). Remarkably, 4-OH tamoxifen solution needed to be previously homogenized to avoid precipitates.

3.1.3.2   4-hydroxytamoxifen (4-OHT) administration

For postnatal retinal experiments, P1 newborn pups were injected intraperitoneally (IP) with different doses of 4-OHT starting from 25 µg of 4-OHT /pup until the final dose of 0,125 µg/pup was finally established.

For postnatal animal experiments P1 newborn pups were injected intraperitoneally (IP) with 0.5 µg of 4-OHT /pup.

For adult animal experiments 2 mg/day of 4-OHT dissolved in peanut oil were administered for two consecutive days to 6 week-old mice by oral gavage.

3.1.4   Mouse genotyping

3.1.4.1   Tissue digestion

Either ears or tails biopsies collected from adult mice (upon weaning) or newborns pups (upon culling for retina isolation) were lysed with 600 µl of 50 mM NaOH (Sigma). Samples were incubated at 100°C for 15 min and were vortexed and kept at room temperature (RT) until they reached 50-70°C. To neutralize the samples, 100 µl of 1M Tris HCl pH 7.4 (Sigma) were added to each sample. Samples were vortexed, centrifuged at maximum speed for 1 min and kept at 4°C until samples were processed for DNA amplification.

3.1.4.2   PCR

Polymerase chain reactions (PCR) were performed using two different protocols referred as PCR reaction I and PCR reaction II. Primers sequences and PCR conditions are summarized in **Table 3.1.**

PCR reaction I (to a final volume of 25 µl): 1.5 µl DNA sample, 15.875 µl H2O, 2.5 µl 10X Titanium taq reaction buffer, 2.5 µl of 10 M primer pool (forward+reverse), 2.5 µl dNTPs and 0.125 µl 50X titanium taq polymeRASe (Clontech, #K1915- y).

PCR reaction II (to a final volume of 30 µl): 2 µl DNA sample, 15.75 µl H2O, 3 µl MgCl2 15mM (diluted from MgCl2 50 mM Ecogen, #MG-110C), 3 µl of 10X reaction buffer without Mg (Ecogen), 3 µl of 10M primer pool (forward+reverse), 3 µl dNTPs and 0.35 µl Ecotaq DNA polymeRASe (Ecogen, #BT-314106).

Mastercycler (Eppendorf) was used to perform PCRs. The amplified products were run on 2% agarose gel (150V, 70min) and visualised with ethidium bromide (Sigma).

The gel was prepared in TAE buffer 1X from a TAE 50X stock: 242 g Tris base (Sigma), 57.1 ml acetic acid glacial (Panreac) and 100ml EDTA 0.5 M pH8 (Gibco, #15575) in dH$_2$O.

Table 3.1. Primer sequences and PCR conditions for genotyping.

gene	primer sequence	PCR composition	PCR conditions
Pik3ca	**Forward wt allele:** 5´-CACTGCAGGAAGTGTGAAGC-3´ **Reverse wt allele:** 5´-GTGGACAGAAAGGCTGATGC-3´ **Forward mutant allele:** 5'-TTGGTTCCAGCCTGAATAAAGC-3'), 20F (5'-TCCACACCATCAAGCAGCA-3') **Reverse mutant allele:** 5'-GTCCAAGGCTAGAGTCTTTCGG-3'	**PCR reaction I**	95°C, 5 min 95°C, 30 sec 65°C, 30 sec 72°C 1 min 72°C, 2 min for 35 cycles
Pdgfb	**Forward:** 5´-CCAGCCGCCGTCGCAACT-3´ **Reverse:** 5´-GCCGCCGGGATCACTCTCG-3´	**PCR reaction II**	94°C, 4 min 94°C, 30 sec 57.5°C, 45 sec 72°C 1 min 72°C, 5 min for 35 cycles

3.1.5 VM-phenotype assessment in animal experiments

The animals injected at postnatal and adult levels were followed up for 14 and 9 weeks respectively by monitoring animal conditions every two days until the endpoint. This endpoint was determined because it was enough for the assessment of the appearance of vascular defects and because some animals died before the ending of the follow up period for internal hemorrhages. The animals were sacrificed and internally inspected for the presence of vascular defects by focusing mostly in the subcutaneous, mesentery, intestine

and urogenital tract. The tissues presenting vascular defects for high vascularisation (red colour) were surgically isolated and collected, then fixed in 4% PFA and embedded in paraffin. Five µm sections were stained with hematoxylin-eosin using standard histology procedures.

3.1.6 Postnatal mouse retina model, isolation, staining and imaging

3.1.6.1 The postnatal mouse retina: an animal model to study angiogenesis

Despite their anatomical differences, vertebrates share similar developmental programs that give rise to the vascular system and the mouse retina has become an excellent model to study angiogenesis. A remarkable aspect of the retinal vascular system is that its development commences after birth (postnatally), thereby rendering the whole process accessible for various manipulatory strategies. In addition, in contrast to the depth covered by most vascular beds, the retinal vasculature is nearly planar, yet hierarchical and almost stereotypical; features that render it an ideal system in which to evaluate, perturb and/or rescue genetic defects. Thus, because of the feasibility of monitoring and manipulating its entire process, retinal angiogenesis in neonatal mice provides a powerful and robust *in vivo* model that allows investigating various events in angiogenesis, such as endothelial sprouting and the morphogenetic organization of vascular networks (Uemura et al., 2002; Gerhardt et al., 2003; Lu et al., 2004; Stahl et al., 2010). Immediately after birth (P0) and parallel to hyaloid regression, the retinal vascular system starts to develop by sprouting from the optic nerve to form a primitive vascular plexus that reaches the retinal edges at approximately P8. During this first week, retinal vessels extend radially over the superficial layer of the retina to form a two-dimensional vascular structure. Recurrent remodelling and pruning of this primitive plexus (P5-P8) lead to the formation of a hierarchical network structure with the emergence of distinct vessel types, arteries (A) and veins (V) connected by intervening capillary beds. As vascular remodelling commences at the centre of the retina, the retinal vasculature offers concurrent visualization of multiple steps in the angiogenic process, including: sprouting, branching, fusion (in the periphery), remodelling and maturation (towards the centre) (Dorrell and Friedlander 2006; Fruttiger 2007; Stahl et. Al., 2010) (**Figure 3.2**). From P7 onward the superficial retinal vessels start to sprout vertically from the mature region of the superficial plexus into deeper layers (intermediate and deeper), finally leading to the formation of a three-layered vascular

system (**Figure 3.1).** Although the precise mechanisms that control sprouting into the deeper layers are not fully understood (Junge et al., 2009), by the end of the third postnatal week, all three vascular layers are fully mature with multiple interconnecting perpendicular branches between layers; thus forming a three-dimensional network of vessels that spans the entire retina. With this respect, the developmental process of the superficial vascular layer occurring during early postnatal stages (first week) provides a useful model system for analysing the cellular and/or molecular events involved in the formation of the organized vascular architecture. Because of its two-dimensional structure, the superficial vascular network can be illustrated as a whole in flat-mount preparations (**Figure 3.1**); allowing to monitoring the different processes occurring during retinal angiogenesis and thereby providing a unique opportunity to address various issues in vascular biology.

The accessibility and characteristics described above have placed the mouse retina as an excellent and robust model to study the different angiogenic processes during development and disease, because of their spatial separation. In addition, the inducible control of gene using the iCre-LoxP strategy and the easy delivery of drugs in the pups, place the retina as prototypical vascular network for the evaluation of transgenic mice and for pharmacological testing and intervention (Gariano and Gardner 2005; Stahl et al., 2010). In fact, the exploration of this system as a model for vascular-associated disorders has facilitated advancements from pre-clinical to clinical trials in a manner that has not been paralleled by other fields(Kennedy 2006; Dorrell et al., 2007; Ianson et al., 2009).
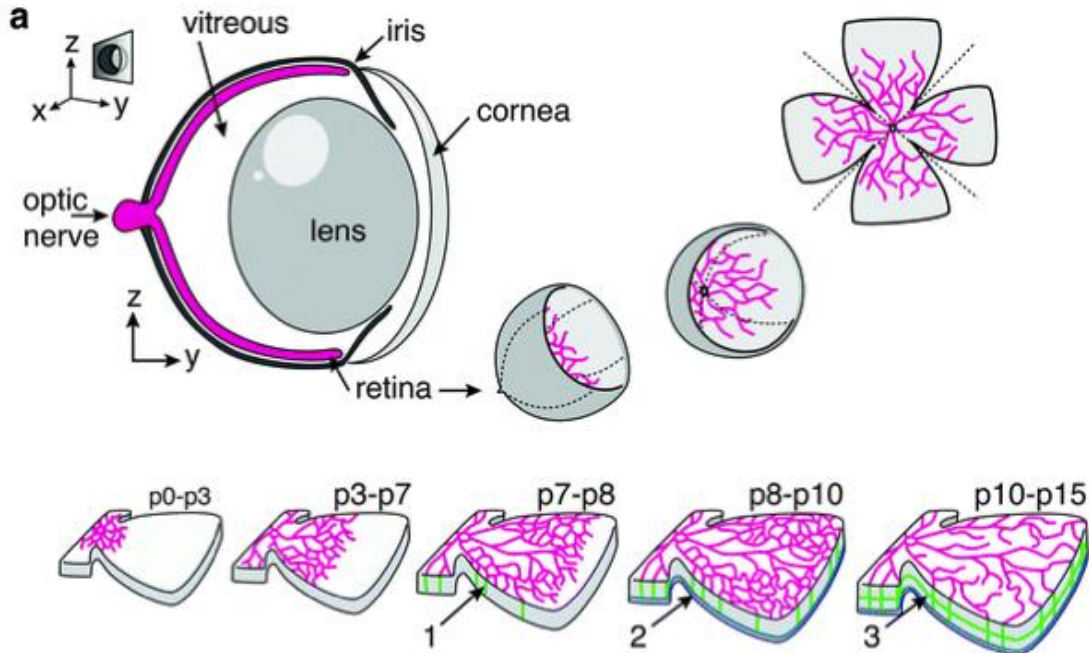
Figure 3.1. The mouse retina: a model system for the study of angiogenesis.

Top: conceptual sketch illustrating the generation of the retina for evaluation of the vasculature. The retina cup is separated from the enucleated eye, clipped to unfold into a clover leaf-like structure, stained for endothelial cells and mounted onto a cover slip for confocal imaging. Bottom: schematic sketch of the developmental stages during retinal angiogenesis. Sprouting is initiated from the optic nerve and proceeds to cover the entire retina around P8, followed by subsequent remodelling and maturation of the superficial plexus. Around P7 vertical sprouting is observed (green) followed by the formation of a second, deep plexus around P8 (blue) and a third, intermediate layer around P10 (green) (Adapted from (Milde et al., 2013)).
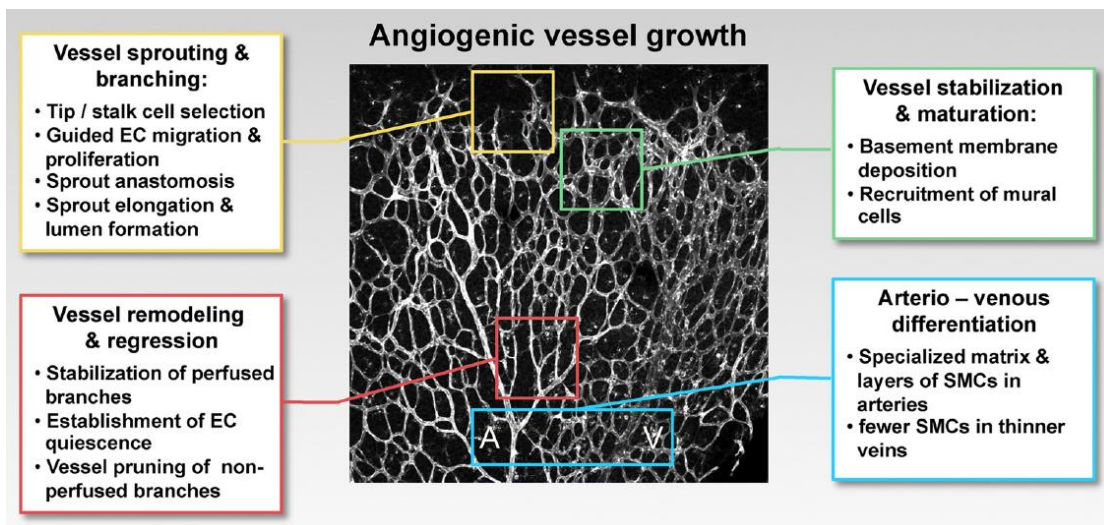
Figure 3.2. The various steps of angiogenic vessel growth in the mouse retina.

63

Principal steps of angiogenic vessel growth that can be simultaneously studied in the mouse retina, illustrated in the mouse retina at postnatal day 6 (P6), stained for an endothelial marker. A indicates artery and V, vein. Specifically, the vasculature extents two-dimensionally and is characterized by an upper front, where ECs grow, proliferate and connect to each other to form a primitive and immature vascular plexus and a lower central front where the vasculature is already more mature, arterio-venous differentiation occurs and the vessels underwent remodelling and regression (Adapted from (Oellerich and Potente 2012)).

3.1.6.2   Retinas isolation

Pups were sacrificed by decapitation and eyes were quickly removed using scissors and forceps. Eyes were fixed in a solution of 4% paraformaldehyde (PFA, Sigma, #15.812-7) in phosphate-buffered saline (PBS) for 1h on ice. Eyes were subsequently washed in PBS followed by dissection of retinas. The procedure of retina isolation was done with the help of a binocular dissecting microscope (Carl Zeiss). Briefly, eyes were collected in a clean culture dish filled with PBS and the cornea was incised with the help of a needle. Using micro-scissors (Fine Science Tools, #15000-10), the cornea was cut and removed. Next, the iris was also removed using two forceps (Fine Science Tools, #11252-00) and the outer layer of the eye, the sclera and the pigmented retina layer started to be separated. The outer layer should be dissected carefully, in small increments, to avoid damaging the retina layer beneath. At this point, the lens and the vitrous humor, which appear as a single jelly-like structure need to be removed. Finally, the hyaloids vessels were carefully detached from the inner side of the eye using fine movements. Isolated retinas were fixed for 1h at 4°C and were kept in PBS at 4°C until they were processed for immunostaining. Procedure details are shown in **Figure 3.3**
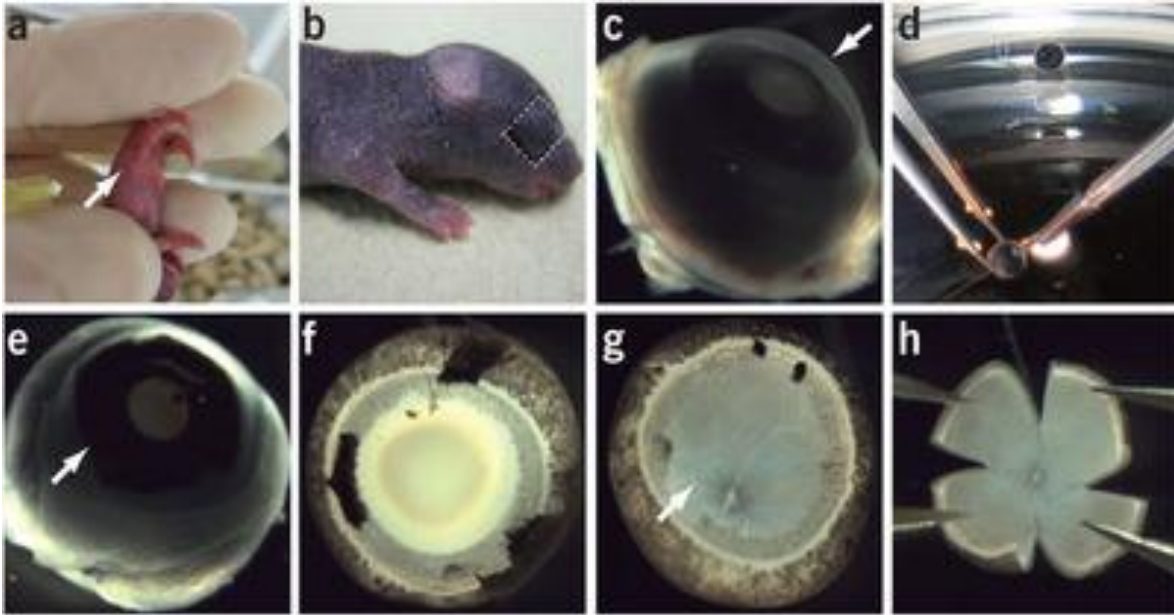
Figure 3.3. Tamoxifen injection, eye isolation and retina dissection in postnatal pups.

a) IP 4-OHT injection in a P1 pup. b) Image showing where to make the incisions around the eye of the pup. c) Dissected eyeball from a p6 pup. Arrow points to the cornea surface. d) Overview of cornea dissection. e) Eyeball without cornea. Arrow indicates dissected cornea. f) Image showing eye without sclera, choroid, cornea layers, pigmented layers and without the iris. g) Dissected eye without lens. Arrow shows hyaloid vessels. h) Retina with four radial incisions. Figure adapted from (Pitulescu et al., 2010).

3.1.6.3 Whole-mount retinas Immunostaining

Retinas were blocked with permeabilization buffer (1% bovine serum albumin (BSA, Sigma), 0.3% Triton X-100 in PBS) ON at 4ºC with gentle rocking. Then, retinas were incubated with primary antibodies in appropriate dilutions (**Table 3.2**) in permeabilization buffer ON at 4°C with gentle rocking. The following day, primary antibodies were removed and retinas were washed 3 times (10 min each) with PBT buffer (0,1% Tween-20 in PBS). Retinas were further incubated 30 min at RT in Pblec buffer (1% Triton X-100, 1 mM CaCl2, 1 mM MgCl2 and 1 mM MnCl2 in PBS pH 6.8) and then they were incubated ON at 4°C or 2h at RT with the appropriate dilution of secondary antibodies (**Table 3.3**). Conjugated isolectin-B4 was added together with the secondary antibodies in the appropriate dilution (**Table 3.3**). Then, retinas were washed 3 times, 10 min each with PBT. All the incubations were done in 2 ml tubes. At the end, between 4-5 incision were made in the retinas to flat mounted them on glass slides using Immu-mount as mounting medium (Thermo Scientific, #9990402).

Table 3.2. List of primary antibodies used for retinas immunostaining.

Antibody	Conj	Host	Dilution	Company	Catalogue#
Erg 1,2,3	-	Rabbit	1:400	Abcam	ab92513
Itga9	-	Rabbit	1:100	Biorbyt Ltd	orb184305

Table 3.3. List of secondary antibodies used for retinas immunostaining.

Antibody	Conj	Dilution	Company	Catalogue#
Goat anti-rabbit	Alexa Fluor 488	1:300	Invitrogen	A11008
Goat anti-rabbit	Alexa Fluor 568	1:300	Invitrogen	A11011
Isolectin GS-IB4	488	1:300	Mol. probes	121411
Isolectin GS-IB4	568	1:300	Mol. probes	121412
Isolectin GS-IB4	647	1:300	Mol. probes	132450

3.1.6.4   EdU proliferation assay in the postnatal retina

EdU is a synthetic analogue of thymidine, and therefore, it can be incorporated into DNA during S phase. The Click-iT EdU Imaging Kit (Invitrogen, #C10340) was used for EdU injection and detection. To determine the number of proliferating ECs in the growing retinal vasculature, P6 mice were injected intraperitoneally with 60 µl of component A from the kit (diluted to 0.5 mg/ml in 50% DMSO: 50% PBS) 2h before they were sacrificed for

retina isolation. Then, the reaction for EdU detection was performed following the manufacturer instructions. Briefly, each pair of retinas were incubated for 1h at RT with gentle rocking in 100 µl of EdU detection solution (8,6 µl)of 10X Click-iT EdU reaction buffer in 77,4 µl of H20 (component D), 4 µl of $CuSO_4$ (component E), 1 µl of 10X azyde-conjugated Alexa-Fluor in 9 µl of H20 (component F) and 0,24 µl of alexa 633 (component B). Retinas were washed twice with PBS and then, they were incubated with permeabilization buffer (1% bovine serum albumin (BSA, Sigma), 0.3% Triton X-100 in PBS) ON at 4ºC with gentle rocking. Thereafter, retinas were incubated in appropriate dilution of Erg 1,2,3 antibody (**Table 3.3**) in permeabilization buffer ON at 4°C with gentle rocking. The day after, retinas were washed 3 times with PBT buffer (0,1% Tween-20 in PBS) at RT, followed by 30 min incubation with Pblec buffer (1% Triton X-100, 1 mM $CaCl_2$, 1 mM $MgCl_2$ and 1 mM $MnCl_2$ in PBS pH 6.8) at RT. Secondary antibody against Erg1,2,3 and isolectin-B4 were incubated ON agitating at 4°C in appropriate dilutions (**Table 3.3**). Retinas were washed 3 times (10 min each) with PBT and finally flat-mounted on glass slides using Immu-mount as mounting medium (Thermo Scientific, #9990402).

3.1.7 Methods used for quantifying vessel features in the postnatal retinas

3.1.7.1 Confocal imaging

Sample imaging was obtained with Leica TCS SP5 confocal microscope, using 4X, 10X and 40X (oil immersion) objectives. Captured images are maximal z-stack projections transformed into .tif file format. Images were processed using Volocity software. Adobe Photoshop CS5 and ImageJ softwares were used for image editing and quantification, respectively. At least six images per retina in the sprouting and in the remodelling areas of at least three samples for each genotype from independent experiments were captured. For quantifications, three independent areas of 10^4 μm^2 were selected from each image taken with 40X objective.

3.1.7.2 Imaging analysis and quantification of postnatal retinal angiogenesis

To study the angiogenic retinal development mouse retinas were collected at P6 and stained for isolectin-B4 (IB4), an EC-marker for blood vessels (Figure 3.4A). We

focused our analysis at P6 before the complete migration arrest has occurred. Specifically, at P6 the retinas vasculature extents two-dimensionally and two areas can be defined: the upper sprouting (or angiogenic) front (SF) where endothelial cells grow, proliferate and connect to each other to form a primitive and immature vascular plexus and a central remodelling plexus areas (RP), in the inner part of the angiogenic front, where the vasculature is already more mature, arterio-venous differentiation occurs and the vessels underwent remodelling and regression (Figure 3.4B).
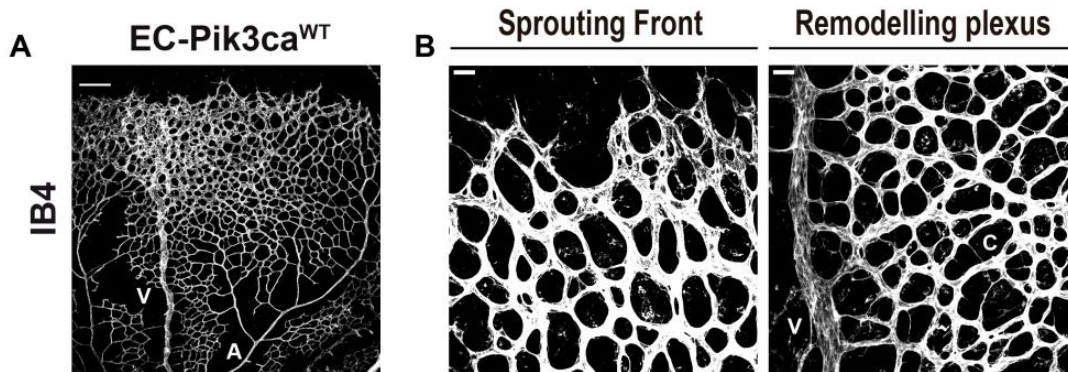
Figure 3.4. Analysis of postnatal retinal angiogenesis.

A. Whole-mount P6 EC-Pik3ca^{WT} retina stained with isolectin-B4 (IB4) to specifically label ECs. B. At P6 the organization of the blood vessel network extents two-dimensionally with 2 areas defined: the upper angiogenic sprouting front where the vessels are sprouting and branching and a remodelling plexus where arterio-venous differentiation occurs and the vessels underwent remodelling and regression. Veins (V), arteries(A) and capillaries(C) are indicated. Scale bars, 150 µm (A), 30 µm (B).

3.1.7.3   VM localization

The localization of isolated malformed vessels (VM) was calculated directly from 10X images of whole-mounted retinas by manually counting the number of the isolated malformed vessels in the remodelling plexus area associated with a vein, an artery or a capillary bed as showed in **Figure 3.5**. Data were represented as % mean. Error bars represent SEM. Six animals per genotype were analysed.
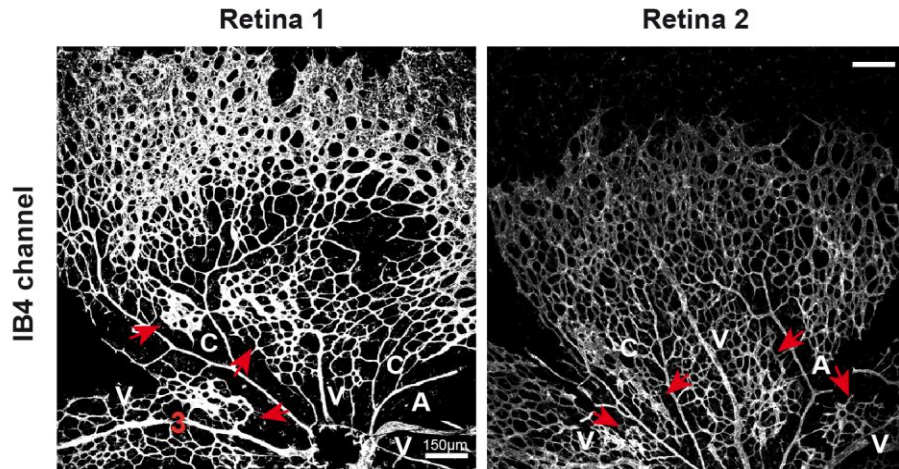
Figure 3.5. Quantification of VMs localization.

3.1.7.4 Quantification of vessel density

The quantification of the retina vascularity or vessel density was done using the Image J software on images of the sprouting front and of the remodelling plexus taken with the 40x objective. The vascularity of the retinas was measured manually from the IB4 channel by adjusting the threshold to select a positive area. The mean percentage of IB4-positive area from the total area (10^4 μm^2) was calculated and results were presented as a fold change between control and mutant groups. Error bars represent SEM.

3.1.7.5 Quantification of ECs number

The quantification of ECs number was done using the Image J software on images of the sprouting front and of the remodelling plexus taken with the 40x objective. The number of endothelial cells was manually counted based on EC-specific nuclei staining (Erg) in 10^4 μm^2 area. The results were presented as mean with SEM error bars.

3.1.7.6 Quantification of ECs proliferation

EdU immunostaining was used to assess the endothelial cell proliferation rate. Fields of 10^4 μm^2 area (**Figure 3.6**, yellow square) were determined in the vascular sprouting front and in remodelling plexus of images taken with the 40x objective from retinas stained for EdU, Erg1,2,3 and isolectin-B4. Both EdU (green) and Erg (red)-positive cells were quantified manually in 10^4 μm^2 areas. The number of Edu+ (green) were divided

by the total number of Erg+ (red) EC nuclei within this visual field of 100x100µm and was represented as % of EdU-positive cells per 10^4 µm^2. The results were presented as mean with SEM error bars.
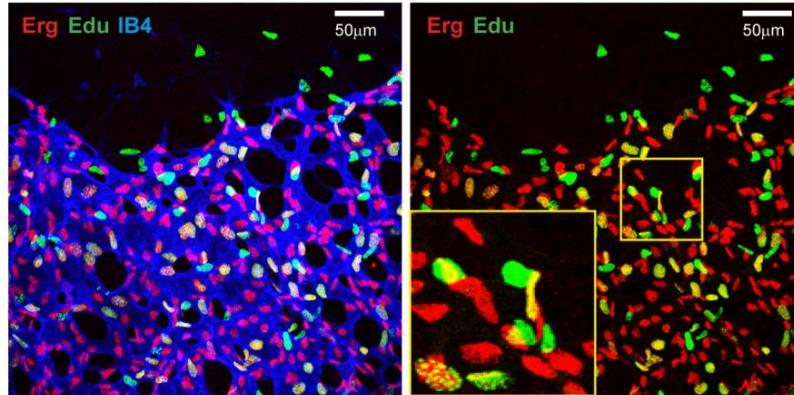
Figure 3.6. Quantification of ECs proliferation.

3.2 *In vitro* experiments

3.2.1   Isolation, culture and treatment of mouse primary cells

3.2.1.1   Tissue digestion and cell selection

The mice were sacrificed by cervical dislocation and their lungs were removed and kept on ice-cold Hank's balanced salt solution (Gibco) containing 1% penicillin/streptomycin (P/S, Gibco). Once in the primary hood, lungs were minced with a scalpel and poured into a 40 μm cell strainer, placed on a 50 ml Falcon tube, to remove blood constituents. Lung pieces were digested in 5ml of of dispase II 4U/ml (Gibco, #17105-041) for 1h at 37ºC. Thereafter, the suspension containing lung pieces was homogenized by pipetting up and down to release single cells from the tissue pieces. Then, DMEM (Lonza, #BE12-604F) containing 10% of sterile inactivated FBS (Gibco, #10270-106) and 1% P/S, later referred to as complete DMEM complete, was added to the cell suspension and the homogenate was filtered through a 40 μm cell strainer placed on a 50ml tube. A pellet containing mouse cells was obtained by centrifugation (5min 1200rpm). The pellet was washed twice with PBS/BSA (PBS containing 0.5% BSA (diluted from PAA, #K11-022), performing a 5 min centrifugation at 1200rpm after every wash. The cell pellet resulting from the last centrifugation was re-suspended in 100μl of PBS/BSA.

First selection

A prepared solution composed by magnetic beads (Dynabeads™ Sheep Anti-Rat IgG, #11035) coated with CD144 antibody (BD Pharmigen, #555289) is used to specifically recognize mouse endothelial cells (mECs) from the lung homogenate. In detail, 8 μl/lung of magnetic beads were placed into a 1.5ml eppendorf and were washed five times with PBS/BSA using a Dynal magnet (Dynal, MCP-S). After the washes, magnetic beads were re-suspended in 8 μl of PBS/BSA and finally 1.25 μl/lung of CD144 antibody (Ab) was added. The mixture of magnetic beads- Ab was incubated 1h at RT by gently shaking. Afterwards, PBS/BSA was added to obtain a final volume of 100 μl for the magnetic beads-Ab mixture. The mixture was transferred to the 100 μl of cell pellet suspension previously obtained and incubation for 1h at RT was performed. The suspension was then washed three times with PBS/BSA using a magnet for cell separation. After the final wash, magnetic beads coupled with ECs were re-suspended in F12 complete medium containing: DMEM F12 (Gibco, #21041-025), supplemented with

20% of inactivated FBS (Gibco, #10270-106), 4 ml of EC growth factor (Promocell, #C-30140) and 1% P/S. The suspension was seeded on a 12-well culture dish pre-coated with 0.5% gelatine (this moment is considered as passage 0 (P0)). The following day, the well was carefully washed twice with PBS/BSA and F12 complete medium was replaced. The medium was changed every second day.

Second selection

Once the cells reached the confluence, they were re-purified by removing the culture medium and incubating the cells for 1h with a solution containing CD144 antibody-coated magnetic beads (prepared as described above in the first selection). After 1h of incubation at RT cells were trypsinized and centrifuged for 5 min at 1200 rpm. The pellet was washed three times with PBS/BSA, re-suspended in 1 ml F12 complete medium and seeded on 12-well culture dishes pre-coated with 0.5% gelatine.

From here on, cells were further cultured on 6-well dishes pre-coated with 0.5% gelatine in F12 complete medium. They were splitted (1:3) following standard procedures always guaranteeing a confluence of at 80-90 % and never exceeding from passage 6. Cells were cultured at 37°C in 5% CO_2 atmosphere.

3.2.1.2   Mouse embryonic fibroblasts (MEFs) culture

MEFs were isolated and kindly provided by the Cell signalling research group (Prof. Bart Vanhaesebroeck), UCL Cancer Institute. MEFs were cultivated in DMEM complete media following standard procedures always guaranteeing a confluence of at 80-90 % and never exceeding from passage 6. Cells were cultured at 37°C in 5% CO_2 atmosphere.

3.2.1.3   Induction of Cre mediated gene activation *in vitro*

3.2.1.3.1   **4-hydroxytamoxifen (4-OHT) preparation**

5 mg of 4-OH tamoxifen powder (Sigma, #H7905_5mg) were dissolved in ethanol to obtain a working solution of [1 mg/ml]. The solution was aliquot under sterile conditions and stored at -20ºC. Remarkably, 4-OH tamoxifen solution needed to be previously homogenized to avoid precipitates.

3.2.1.3.2 **4-hydroxytamoxifen (4-OHT) induction**

In vitro expression of *Pik3ca* ^{H1047R} activating mutation was induced in mECs and MEFs once cells were sufficiently amplified (p3). Cells were splitted (1:3) and treated respectively with F12 complete and DMEM complete medium added with 1µM of 4-OH tamoxifen or ethanol (vehicle) at different time points. Once treated, the cells were harvested and used to perform different experimental studies (without adding any treatment). Procedure is summarized in **Figure 3.7**.
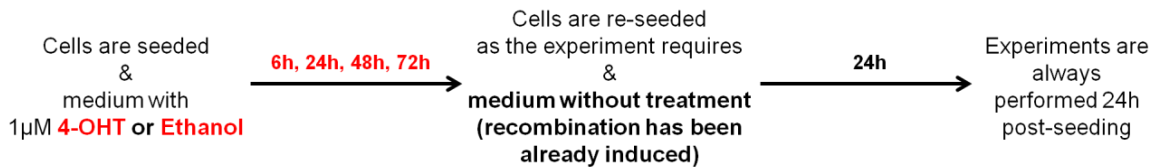
Figure 3.7. Workflow scheme used to induce in vitro expression of the *Pik3ca*^{H1047R} activating mutation.

3.2.2 Isolation and culture of human primary cells

3.2.2.1 Digestion of human biopsies and cell selection

Human primary cells were isolated from patients' surgical resection biopsies from different types of vascular malformations with sizes around to 5 mm^3. Informed consent was obtained from all patients. A dedicated primary hood for human samples was used. To avoid any possible contamination all the material was discarded in a dedicated container with bleach and a double pair of gloves was used for the entire procedure.

Specimens of the VM samples were minced with a scalpel and placed in a 50 ml tube with 5 ml digestion solution composed of HBSS with 4U/ml of dispase II (Gibco, #17105-041) and 0.5 mg collagenase A (Roche, #10103578001). Digestion was carried out at 37°C during 1h and to facilitate tissue digestion sample was gently vortexed time to time during digestion. Then, the suspension was homogenized by pipetting up and down to release single cells from the tissue piece. DMEM complete medium was added to the cell suspension to stop digestion and the suspension was filtered through a 40 µm cell strainer placed on a 50ml tube, to remove indigested and fibrotic tissues. Cell suspension was centrifuged 10' at 800 g and then cell pellet was washed twice with PBS/BSA (PBS containing 0.5% BSA (PAA, #K11-022)) performing a 5 min centrifugation at 1200 rpm

after each wash. The cell pellet resulting from the last centrifugation was re-suspended in 100µl of PBS/BSA.

First selection

Magnetic beads solution was prepared as followed: 16 µl of magnetic beads (Dynabeads™ Pan Mouse IgG, # 11041) were placed into a 1.5 ml eppendorf and were washed five times with PBS/BSA using a Dynal magnet (Dynal, MCP-S). After the last wash, the magnetic beads were re-suspended in 16 µl of PBS/BSA and 2.5 µl of CD31 antibody (Ab, Dako #M0823 (Clone JC70A) were added. The mixture of magnetic beads and CD31 Ab was incubated 1h at RT with gentle shaking. Afterwards, PBS/BSA was added to obtain a final volume of 100 µl for the magnetic beads-Ab mixture. The mixture was transferred to the 100 µl of cell pellet suspension previously obtained to perform 1h incubation at RT. Next, the suspension was added with 800 µl of DMEM complete and placed into the magnet, to separate beads bound-CD31+ ECs from unbounded CD31- cells. The unboud CD31- cells were seeded on a 6-well culture dish pre-coated with 0.5% gelatine (this moment is considered as passage 0 (p0)). Then, the magnet-bound CD31+ cells were washed three times with PBS/BSA using the magnet for cell separation. After the final wash, CD31+ human ECs (hECs) coupled with magnetic beads were re-suspended in EGM-2 (Endothelial Cell Growth Medium-2 BulletKit™ Lonza, #CC-3162) with 1% penicillin/streptomycin, later referred to as complete EGM-2 complete medium. Finally the suspension was seeded on 12-well culture dishes pre-coated with 0.5% gelatine (this moment is considered as passage 0 (p0)). The following day, the wells with the CD31+ and CD31- cells were carefully washed twice with PBS/BSA and replaced with the respective cell medium. The medium was changed every second day.

Second and third selection

Once CD31+ hECs reached 80-90% of confluence, a second purification step was done. Cell culture media was removed and cells were incubated with magnetic beads coated with CD31 Ab (prepared in PBS/BSA as described above in the first selection) for 1h at RT. Then, cells were trypsinized and centrifuged for 5 min at 1200 rpm. Next, cells were washed three times with PBS/BSA, using a magnet to separate hECs bound to beads from other unbounded cell type. After the final wash, ECs coupled with magnetic beads were re-suspended in EGM2 complete medium and seeded on 12-well culture dish pre-coated with 0.5% gelatine in sterile H_2O. The following day, wells were carefully

washed with PBS/BSA and EGM2 complete medium was replaced. A third step of purification was repeated if necessary.

From here on, cells were further cultured on 6-well dishes pre-coated with 0.5% gelatine. CD31+ cells were culture in EGM2 complete medium while CD31- cells were culture in DMEM complete medium; at 37°C in 5% CO_2 atmosphere. CD31+ and CD31-cells were splitted 1:3 and 1:6 respectively, following standard procedures always guaranteeing a confluence of at 80-90 % and never exceeding from passage 5 (p5).

3.2.2.2   Sanger Sequencing of primary hECs

Genomic DNA was extracted from CD31+ and non endothelial cell population CD31− using PureLink™ Genomic DNA Mini Kit (ThermoFisher Scientific, #K182001) following manufacturer instructions and eluting the product into 25 µl of H_2O. DNA quality and quantity were determined using a Nanodrop 2000c Spectrophotometer. 50 ng of DNA was used for PCR using Platinum™ SuperFi™ DNA polymerase (Invitrogen, # 12351010). Primers to amplify TIE2 exon 15 (c.2545C>T (R849W)), 22 (c.3295C>T (R1099*)), 23 (c.3314C>A (T1105N); c.3316A>C (T1106P); c.3324_3334del (E1109Lfs*5) and c.3343G>T (G1115*)); exon 17 (c.2690A>G (Y897C), c.2690A>T (Y897F); c.2740C>T (L914F); c.2752C>T (R918C)) and PIK3CA exons 8 (c.1258T>C (C420R)) 9 (c.1624G>A (E542K) and c.1633G>A (E545K)) and 20 (c.3140A>G (H1047R)) were used at the final concentration of 10 µM and listed in **Table 3.4.** The PCR program is composed by 1 cycle at 98°C for 30 sec, 35 cycles at 98°C 10 sec, 55 °C 15 sec, 72°C for 30sec and 1 cycle at 72°C for 5min. Amplification products were purified using GE Healthcare Purification Kit (GE Healthcare, #10218134) and sequenced at STAB VIDA company. Electropherogram peak results were visualized using SnapGene Viewer Software.

Table 3.4. List of primers used for Sanger sequencing of hECs.

Gene Name	Exon amplified	Forward primer (5'-3')	Reverse primer (5'-3')
Pik3ca	Exon 8 c.1258T>C (C420R)	CTCATGCTTGCTTTGGTTCA	GCCAAAGATTCAAAGCCATT
Pik3ca	Exon 9 c.1624G>A (E542K); c.1633G>A (E545K)	CTGTGAATCCAGAGGGGAAA	ACATGCTGAGATCAGCCAAA
Pik3ca	Exon 20 (c.3140A>G	CATTTGCTCCAAACTGACCA	TGTGTGGAAGATCCAATCCA

	(H1047R)		
Tie2	Exon 15 c.2545C>T (R849W)	GAACCAGCTGTGCAGTTCAA	AGCCTTCCAGGTGATTCTGA
Tie2	Exon 17 c.2690A>G (Y897C),; c.2690A>T (Y897F); c.2740C>T (L914F); c.2752C>T (R918C)	TAGGCAATTTCCACAGCACA	GGCAAACCAGGCTAAGAGAG
Tie2	Exon 22 c.3295C>T (R1099*),	CCTGGGCACATCAGGTATTC	CATGGGCCCTTTAAGAGACA
Tie2	Exon 23 c.3314C>A (T1105N)	AGGTCCCAGGTGTACAGCAC	GGAACCCAGAAGAAGGAACC

3.2.3 RNA extraction and analyses techniques used in primary cells

3.2.3.1 RNA extraction

For gene expression analysis of mECs and MEFs, $1,5 \times 10^5$ cells were seeded on 6-well plates and *in vitro* induced in complete medium for 24 and/or 72h as described above in 3.2.3.2. Plates were then quickly washed with PBS with $Ca^{2+}Mg^{2+}$ (Lonza, # D8537) and stored at -80°C or directly processed. Total RNA was extracted using the RNeasy Plus Kit (Qiagen # 74134) by following manufacturer instruction. RNA was eluted with nuclease free H_2O in a final volume of 40µl and quantified using NanoDrop 1000 (Thermo Scientific). RNA was stored at -80 °C.

3.2.3.2 cDNA synthesis and quantitative Real Time PCR (qRT-PCR) analysis

cDNA was produced from 0.5 µg of RNA using the High Capacity cDNA Reverse Transcription Kit (Applied Biosystems # 4368814) following the protocol recommended by manufacturer. Briefly, 10 µl of reaction mix (**Table 3.5**) was added to 10 µl of sample (0.5 µg RNA plus H_2O up to 10 µl) in a 0.5ml eppendorf; tubes were placed in a thermal cycle with the following program: 25°C 10', 37°C 2h, 85°C 5', 4°C 2∞. The cDNA was diluted 1:10 and stored at -20°C. Quantitative Real Time PCR (qRT-PCR) was performed using

SYBR Green I Master Kit (Roche # 04707516001) in LightCycler 480 Real-Time PCR System. Briefly, 9 µl of reaction mix (5 µl Master mix, 1 µl primers and 3 µl of H_2O) and 1 µl of cDNA diluted 1:10 were used. Different primers were designed in-house using UCSC Genome Browser Website and Primer3web (version 4.1.0) and are listed in **Table 3.6**. Mouse L32 was used as housekeeping gene. PCR program is described in **Table 3.7**. Data analysis was done with the ΔΔCT method.

Table 3.5. Real Time reaction mix composition.

Reagents	Amount for 20 µl reaction
10x RT buffer	2 µl
25X dNTPs mix	0.8 µl
10X Random primers	2 µl
RNase inhibitor	1 µl
Multi Scribe RT	1 µl
Nuclease free H_2O	3.2 µl
Total volume	10 µl

Table 3.6. Primers used for qRT-PCR using SYBR Green I Master Kit.

Name	Forward primer (5'-3')	Reverse primer (5'-3')
mL32	ACCCCAGAGGCATTGACAAC	ATTGTGGACCAGGAACTTGC
Ang2	CCTCGACTACGACGACTCAGT	TCTGCACCACATTCTGTTGGA
Pdgfb	CATCCGCTCCTTTGATGATCTT	GTGCTCGGGTCATGTTCAAGT
Klf10	GCCTGACCTTCAGACAGTCC	TGGCTTGAGCCTTAGGAAGA
Prim1	CTGGGAACACCTGAGGAAAG	TAGGCACAGAAATCCGACCT
Mki67	CATCATTGACCGCTCCTTTA	GCCCTTGGCATACACAAAG
Ccna2	CTTGTAGGCACGGCTGCTAT	AGCCAAGTCAAAAGCAAGGA
Cenpf	GTCAAGCATTTGCACAGCAC	CTCCAGGTGGCAGACTTCTC
Cdkn2b	AAGGACCATTTCTGCCACAG	TCGTGCACAGGTCTGGTAAG
E2f1	ACACAGCTGCAACTGCTTTC	ATGTCTCCTGGCATGAGGTC
Mcm10	ACACAGAAGAGGCTGGCAGT	TCAAGCTCTGCAGAAAAGCA
Cxcr4	ATGGAACCGATCAGTGTGAG	CCGTCATGCTCCTTAGCTTC
Fn1	GGTCCTCTCCTTCCATCTCC	TGCTTCCCATTGTCAAAACA
Ccn1	AGCTCCACCGCTCTGAAAG	GTTCTTGGGGACACAGAGGA
Depdc1b	TGGGTCCTGTCAGCTATGAA	CTGTTTTCAGGAGGCAGGAG
L1cam	GAGCAGGGCACAGCTCTTAG	GACCCGAAAGGTGTAGTGGA

Vcam1	TTGGGAGAGACAAAGCAGAAG	CCATTGAGGGGACTGTCTGT
Cdh5	TGAAAGGAAATGAGTATTTCAGCA	AGACGGGGAAGTTGTCATTG
Pcdh12	GCCTGGTTAGGCTCTCTGTG	TTCCAGGTCAGGTTCTGCTT
Itga2	CCTCACAAACACCTTCAGAGC	ATCATTGCATTGCTGGATCA
Itga4	CAAACCAGACCTGCGAACAG	CAGAAGGCATGACGTAGCAA
Itga5	TGGAAAACATGTCCCCAACT	TTCATCTCCCTGCAGTCCTC
Itgav	GTTCCAAGAGCAGCAAGGAC	CCAATGGAGCTATGGCACTT
Itga6	CGGGATATGCCTCAAGGTTA	ATCTGTCTGGACCGTTTTGG
Itga8	CACGGAGACATTTGGGAGAT	TGGTCTGTGACCCCCATATT
Itga9	TGCTTTCCAGTGTTGACGAG	CCCAGACAGGTGGCTTGTAT
Itgb1	TCCTTCAATTGCTCACCTTG	CCGTCTGGCAATTTGCTATT
Itgb2	TGGAGGATAACATGTACAAGAGGA	GTTGCTGGAGTCGTCAGACA
Itgb3	GGCACCGACAACCACTACTC	ACTGTGGTCCCAGGAATGAG
Itgb4	GGAGGATTCATCCAACATCG	CCGGAGATGCACATTGTATG
Itgb5	GCCAATGAGTACACAGCCTCT	CTTTAGCCCGGATGCTACTG

Table 3.7. qRT-PCR program for SYBR Green.

SYBR green				
Stage 1	**denaturation**			
Cycles	1	Analysis Mode	None	
Target (°C)	Acquisition mode	Hold (hh:mm:ss)	Ramp Rate (°C /s)	Acquisition (per °C)
95	none	00:10:00	4.80	
Stage 2	**annealing**			
Cycles	45	Analysis Mode	Quantification	
Target (°C)	Acquisition mode	Hold (hh:mm:ss)	Ramp Rate (°C /s)	Acquisition (per °C)
95	none	00:00:04	4.80	
62	none	00:00:30	2.00	
72	single	00:00:30	4.80	
Stage 3	**melting**			
Cycles	1	Analysis Mode	Melting Curves	
Target (°C)	Acquisition mode	Hold (hh:mm:ss)	Ramp Rate (°C /s)	Acquisition (per °C)
95	none	00:00:10	4.80	
65	none	00:01:00	2.50	
95	continous		0.11	5

Stage 4	cooling				
Cycles	1	Analysis Mode	None		
Target (°C)	Acquisition mode	Hold (hh:mm:ss)	Ramp Rate (°C /s)	Acquisition (per °C)	
40	none	00:00:20	2.5		

3.2.3.3   RNA sequencing (RNAseq) analysis

RNAseq analysis was performed in collaboration with the Centre Nacional d'Anàlisi Genòmica (CNAG-CRG, Barcelona).

RNA was extracted as described in 3.2.4.1 from four biological samples of mECs, obtained from 2 females and 2 males animals, and treated with 4-OHT and vehicle (EtOH) for 24 hours. Total RNA was quality controlled by Qubit® RNA BR Assay kit (Thermo Fisher Scientific, # Q10211) for quantity and RNA 6000 Nano Assay (Agilent) for integrity. The RNA-Seq libraries were prepared from total RNA using the TruSeq Stranded mRNA Library Prep Kit (Illumina) from total RNA (500 ng). In the mean were generated 59 million paired-end reads for each sample following the manufacturer's protocol. Images analysis, base calling and quality scoring of the run were processed final library was validated on an Agilent 2100 Bioanalyzer with the DNA 7500 assay. The libraries were sequenced using the manufacturer's software Real Time Analysis (1.18.66.3). RNA-seq paired-end reads were mapped against the human reference genome (GRCm38) using STAR version 2.5.3a (Dobin et al., 2013) with ENCODE parameters for long RNA. Annotated genes (gencode version M17) were quantified using RSEM version 1.3.0 with default parameters (Li et al., 2011). Differential expression analysis was performed with DESeq2 version (Love et al., 2014) taking into account that the samples were paired. Principal component analysis was done using the top 500 most variable genes with the 'prcomp' R function and 'ggplot2' R library.

3.2.3.3.1   Gene set enrichment analysis (GSEA)

Gene set enrichment analysis was performed in collaboration with Pujana's Laboratory (IDIBELL, Barcelona). GSEA software and Molecular Signature Database (MSigDB) were used. Mouse gene codes were translated as human homologous ones using MGI reference dataset, keeping only genes described as protein coding ones

(n=14190). In the dataset normalized counts were transformed to pseudocounts adding 1 to avoid null values and then log2 transforming them. For each gene, paired t-test was run. Fold changes between both groups (4-OHT and EtOH) were computed using foldchange method included in gtools R library. Values greater than 1 indicated genes enriched in 4-OHT condition and lower than -1 indicated genes enriched in EtOH condition. Pre-ranked GSEA analysis was performed using previously computed fold changes values by using the c2 curated gene sets. False discovery rate-FDR< 25% and a nominal p-value < 5% were considered for enriched pathways and processes.

The oncogenic PI3K Mutant signature was created by using the gene sets in the following papers (Koren et al., 2015; Van Keymeulen et al., 2015).

3.2.3.3.2 **Bootstrapping analysis**

39 biological processes related to cell-cell and cell-matrix adhesion and cell migration were identified in the GO database (biological processes), from the differential expression analysis. Pujana's Lab applied a bootstrapping method to identify and validate which of these 39 processes resulted enriched of genes differentially expressed. Briefly, gene datasets were obtained from GO database and for each ontology, they checked if the proportion of genes differentially expressed was greater than expected by chance. Concretely they generated 1000 random bootstraps per ontology, by using the significant genes in the ontology, to generate null distributions. Then they compared how many random datasets presented more enriched genes than its original dataset, generating an empirical p-value.

For example, from a total of 23-gene set included in the GO:0001952 signature (regulation of extracellular matrix), pairwise t-test identified 17 genes differentially expressed. The generated random bootstraps presented an average of 4,5 genes differentially expressed (by chance) with a p-value lower than 0,05 and none of the random 1000 bootstraps presented 17 or more differentially enriched genes. This indicated that the process resulted significantly enriched of genes differentially expressed (more than what expected by chance) and present an empirical p-value =0. The same was applied for all the 39 biological processes analysed.

3.2.4 Protein extraction and Western immunoblotting of primary cells (mouse and human)

3.2.4.1 Protein lyses and sample processing

For Western blot analysis 2-hours starvation was performed with cell medium without FBS and growth factors. Next, plates were quickly wash $Ca^{2+}Mg^{2+}$ and stored at -80°C or directly processed. Primary cells were lysed with lysis buffer (150 mM NaCl, 1mM EDTA, 50 mM Tris-HCl pH 7.4 and 1% Triton X-100 in H2O) supplemented with 1mM DTT, 2 mg/ml aprotinin, 1 mM pepstatin A, 1 M leupeptin, 10 g/ml TLCK, 1 mM PMSF, 50 mM NaF, 1 mM NaVO3 and 1 µM okadaic acid (**Table 3.8**). Lysates were collected in a 1.5 ml eppendorf and were kept on ice for 15min. Then, lysates were centrifuged at 4ºC for 15 min at maximum speed. Supernatants were collected in new ice-cold 1.5 ml eppendorfs and kept on ice. Protein content was quantified using the BCA protein assay kit (Pierce # 23225) following the instructions recommended by the manufacturer. Protein samples were then diluted in sample buffer 4X (250 mM Tris-HCl pH 6.8, 40% glycerol, 8% SDS, 0.04% bromophenol blue and 250mM DTT in H2O) in a proportion of 3 volumes of protein sample: 1 volume of 4X SDS sample buffer. Samples were heated at 100ºC for 5 min, spinned for 30sec and stored at -20°C.

Table 3.8. Reagents used to prepare the lysis buffer.

Product	Company-Catalogue #
DL-Dithiothreitol (DTT)	Sigma ; #D0632
Aprotinin	Sigma ; #A6279
Pepstatin A	Sigma ; #P4265
Leupeptin	Sigma ; #L2884
Na-p-tosyl-L-lysine chloromethyl ketone (TLCK)	Sigma ; #T7254
Phenylmethylsulfonylfluoride (PMSF)	Sigma ; #P7626
Sodium fluoride (NaF)	Sigma ; #S7920
Sodium orthovanadate (NaVO3)	Sigma ; #S6508
Okadaic acid	Cayman ChemicalCompany; #10011490

3.2.4.2   Protein electrophoresis and membrane transference

Samples were resolved on 8%, 10% or 12,5% SDS poli-acrylamide gels by using 45-70 μg proteins. SDS-PAGE gels were composed of a stacking part (4% acrylamide, 125mM Tris-HCl pH 6.8, 0.4% SDS, 0.1% ammonium persulfate (APS) and 0.1% tetrametiletilendiamina (TEMED) in H2O) and a resolution part (10% acrylamide, 375mM Tris-HCl pH8.8/0.4% SDS, 0.1% APS and 0.1% TEMED in H2O). Samples were run for 1-2h at 130V with running buffer 1X (25mM Tris, 192 mM glycine and 0.1% SDS in H2O). Thereafter, proteins separated in the acrylamide gels were transferred generally onto PVDF membranes (Roche) previously activated in methanol or nitrocellulose membranes (Roche). Gel to membrane transference was performed at 4ºC at 250 mA for 2h in Transfer buffer 1X (25mM Tris, 192mM glycine and 20% methanol). After transference, membranes were washed for 5min in 1X TBS (For 500mL of TBS 10x: 6g Tris, 43.85 g NaCl, pH7.5) containing 0.05% Tween (referred as TBS-T). Membranes were then incubated for 1h at RT with TBS-T containing 5% of milk. Membranes were washed twice (5min each time) with TBS-T and incubated ON at 4ºC with incubation solution (2% BSA in TBS-T with 0.02% sodium azide) containing the desired primary antibody at the appropriate dilution. **Table 3.9** details primary antibodies used for immunoblotting. The following day, membranes were washed three times (10 min each) with TBST and were incubated for 1h at RT with 5% milk in TBS-T containing the appropriate dilution of secondary antibodies (**Table 3.10**). Upon incubation with secondary antibody, membranes were washed three times (10min each) with TBS-T and protein detection was performed by enhanced chemiluminescence (ECL) following the protocol described in **Table 3.11**. Quantification of band intensities by densitometry was carried out using the Image J software.

Table 3.9. List of primary antibodies used for immunoblotting of primary cells.

Antibody	Host	Company	Dilution	Catalogue #
VE-cadherin	Goat	Santa Cruz	1:200	sc-6458
β-actin	Mouse	ABCAM	1:25000	49900
p-Akt (S473)	Rabbit	Cell Signalling Technology	1:2000	4060

p-AKT(T308)	Rabbit	Cell Signalling Technology	1:500	2965
AKT total	Rabbit	Cell Signalling Technology	1:1000	9272
p-Erk1/2 (Thr202/Tyr204)	Rabbit	Cell Signalling Technology	1:1000	9101
Erk1/2 total	Rabbit	Cell Signalling Technology	1:1000	9102
Itga9	Goat	R&D Systems	1:500	AF3827-SP
VEGFR2	Rabbit	Cell Signalling Technology Santa Cruz	1:1000	2974S
CD31	Goat	Sant Cruz	1:500	Sc-1506

Table 3.10. List of secondary antibodies used for immunoblotting.

Antibody	Host	Company	Dilution	Catalogue #
Anti-Rabbit HRP	Swine	DAKO	1:5000	P 0399
Anti-mouse HRP	Rabbit	DAKO	1:5000	P 0260
Anti-goat HRP	Rabbit	DAKO	1:5000	P 0160

Table 3.11. Protocol for ECL preparation.

Solution A	Solution B
5ml 1M Tris pH8.5 45ml H2O 110µl 90mM coumaric acid (Sigma) 250 µl 250mM luminol (Sigma)	110 µl H2O2 30% 900 µl H2O
*Solutions A and B need to be mixed in a 1:3 ratio	

3.2.5 Proliferation assay for primary ECs

To study cell proliferation EdU assay (Invitrogen, #C10340) was used. EdU (5-ethynyl-2'-deoxyuridine) is a nucleoside analog of thymidine that is incorporated into DNA during active DNA synthesis.

3.2.5.1 Proliferation assay for mECs

Cells were stimulated for 24 hours with 4-OHT and vehicle (EtOH) and then were harvested, counted and 10^5 cells were seeded onto a gelatine pre-coated cover slips and incubated overnight at 37°C in 5% CO_2. The next day, Edu reagent was added directly into the cell culture media for 4 hours at the final cell concentration of [10µm]. The cells were then washed with PBS $Ca^{2+}Mg^{2+}$ and fixed with 4% PFA for 15 minutes at RT. Two more washes with PBS were performed after fixation and thereafter cells were permeabilized with PBS-0.5% Triton X-100 (Sigma, # T8787) for 30 min and washed twice with PBS BSA 3%. EdU incorporated in DNA was immunodetected by incubation for 30 min at RT and cover from light with a Click-iT® reaction cocktail prepared following manufacturer instructions (25 µL Click-iT® reaction cocktail /coverslip). The reaction cocktail was removed and the cover-slips were then washed three times with PBS, adding 1µg/ml of DAPI (4',6-Diamidino-2-Phenylindole, Dihydrochloride Invitrogen, #D1306) in the last one for 10 min. A final wash with PBS was performed before mounting the coverslips on microscope slides using Immu-mount as mounting medium (Thermo Scientific, #9990402). Immunofluorescence was visualized with a Nikon microscope 801 (20x lens). For the analysis the number of EdU positive cells per field was rectified by the total number of cells present in the field (DAPI positive). Three independents experiments with at least three biological samples were used and for each sample 6 photos for conditions (4-OHT and EtOh) were taken. Data were showed as mean with error bars represent SEM.

3.2.5.2 Proliferation assay for hECs

1,5 x 10^5 CD31+ cells were seeded on gelatine pre-coated cover-slips in 6-well plates (3 cover-slip per well) and cultured ON at 37°C in 5% CO_2 atmosphere. The next day, the proliferation was assessed with or without inhibitors treatment by directly adding Edu at the final cell concentration of [10µm] into the cell culture media for 2 hours. The cells were then washed with PBS $Ca^{2+}Mg^{2+}$ and fixed with 4% PFA for 15 minutes at RT.

Then, cell proliferation was assessed as described in the previous paragraph 3.2.5.1. Three independents experiments with two samples were performed and for each sample 6 photos were taken. Data were showed as mean with error bars represent SEM. A statistical upaired t-test was performed.

Inhibitors treatment was performed for 2 hours with BYL-719 (Selleckchem, #S2814), GDC-0941 (Selleckchem, #S1065) and Rapamycin (Selleckchem, #S1039) inhibitors used at a final cell concentration of [1 μM]. DMSO was used as control condition. Three independents experiments with the two samples were performed and for each sample 6 photos were taken. Data were showed as mean with error bars represent SEM. Ordinary One way ANOVA with multiple comparison vs. DMSO was performed.

3.2.6 Wound healing assay for primary ECs (collective cell migration)

In detail, upon 24h-induction with 4-OHT and vehicle (EtOH) collective cell migration capacity of ECs was measured in would healing assay. Briefly, $2.5 \cdot 10^5$ cells were seeded onto gelatin pre-coated 12-well plate and cultured at 37°C in 5% CO_2 atmosphere until confluence. The next day, a 2 hours pre-treatment with [1 mg/mL] of Mytomycin C (Roche, # 10107409001) was performed to minimize the contribution of cell proliferation to gap filling. Then a linear thin-scratch was made with a help of a (yellow) pipette tip, creating a gap ("wound") in a confluent ECs monolayer. Cells were washed with PBS/BSA and new F12 complete cell medium was replaced. Subsequently, images of the cells filling the gap were taken immediately after the scratch (T=0) and a regular time intervals (T7, T18 and T24 hours) with a Nikon Biostation CT (UCL Cancer Institute-Light Microscopy Core Facility). Two different images (areas) for each time points were taken to cover the whole scratch and the scratch area was calculated with ImageJ software. Two independents experiments with four biological samples were performed and data were shown as % of reduction of the gap-area compared to T0. A 2-way ANOVA analysis with multiple comparisons vs. T0 was used.

3.2.7 Inhibitors treatment of primary mECs

10^5 cells were seeded onto gelatine pre-coated 6-well plate and cultured for 48 hours with F12 complete media added with inhibitors. BYL-719 (Selleckchem, #S2814) and Rapamycin (Selleckchem, #S1039) were used at [1 μM] while MK220 (Selleckchem, #S1078) was used at [4 μM] final cell concentration. DMSO was used as control condition.

Upon 48 hours-treatment plates were quickly washed with PBS with $Ca^{2+}Mg^{2+}$(Lonza, #D8537) and stored at -80°C or directly processed for RNA extraction as described in section 3.2.3.1.

3.2.8 Immunofluorescence analysis of primary ECs

3.2.8.1 Immunofluorescence analysis of mECs

Cells were seeded on gelatine pre-coated cover slips in 6-well plates (3 cover-slip per well) and cultured at 37°C in 5% CO_2 atmosphere until desired confluence. Cells were washed once with PBS $Ca^{2+}Mg^{2+}$ and fixed with 4% PFA for 15 minutes at RT. Then, cells were washed three times with PBS and permeabilized in 0.1% Triton X- 100 in PBS for 30min at RT. Next, cells were incubated in blocking solution (3% BSA, 5% goat serum, 0.1% Triton X-100 in PBS) for 1h at RT. Cover-slips were removed from the culturing plate and were incubated in the appropriate dilution of Itgα9 primary antibody (Biorbyt, # orb184305) in blocking solution ON at 4°C in a wet chamber (40μl antibody solution/cover-slip). The following day, coverslips were washed three times (5 min each) with PBS at RT (shaking) and were incubated in the appropriate dilution of anti-rabbit 488 secondary (Molecular Probes, goat anti-rabbit 488 # A-11034) in PBS for 2h at RT in a wet chamber covered from light (40μl antibody solution/cover-slip). Three washes (5 min each) with PBS were performed adding 1μg/ml of DAPI (4',6-Diamidino-2-Phenylindole, Dihydrochloride Invitrogen, #D1306) in the last one for 10 min. A final wash with PBS was performed before mounting the cover-slips on microscope slides using Immu-mount as mounting medium (Thermo Scientific, #9990402).

3.2.8.2 Immunofluorescence analysis of hECs

CD31 + and CD31- human primary cells were seeded on gelatine pre-coated cover slips in 6-well plates (3 cover-slip per well) and cultured at 37°C in 5% CO_2 atmosphere until confluence. The cells were stained following what wrote in the previous paragraph 3.2.8.1, by using the primary antibodies listed in **Table 3.12** and the secondary antibodies listed in **Table 3.13.**

Table 3.12. List of primary antibodies used for primary human cells.

Antibody	Host	Company	Dilution	Catalogue #
Ve-cadherin	Mouse	BD Biosciences	1:50	610252
CD31	Goat	Sant Cruz	1:50	Sc-1506
αSMA	Mouse	Sigma	1:50	C6198
Prox1	Goat	R&D Systems	1:50	AF2727
Itga9	Rabbit	Biorbyt	1:50	Orb 184305

Table 3.13. List of secondary antibodies used for f primary human cells.

Antibody	Host	Company	Dilution	Catalogue #
Anti-Rabbit 488	Swine	DAKO	1:200	P 0399
Anti-mouse HRP	Rabbit	DAKO	1:5000	P 0260
Anti-goat HRP	Rabbit	DAKO	1:5000	P 0160

4 Results

4.1 Unravelling the biology behind *Pik3ca*[H1047R] activating mutation in ECs

4.1.1 Creation of a transgenic mouse line to study the *Pik3ca*[H1047R] activating mutation in ECs

To address objectives 1 and 2, we first aimed to generate a mutant mouse that genetically and specifically activates the expression of *Pik3ca*[H1047R] in ECs. Critically, the expression of *Pik3ca*[H1047R], either in the germline or in ECs during embryonic development is incompatible with life (Hare et al., 2015; di Blasio et al., 2018); thus we generated EC-Pik3ca[H1047R] mice with a conditional endothelium-specific expression of the activating *Pik3ca*[H1047R] mutation.

We took advantage of a tamoxifen-inducible Pdfgb-iCreER transgenic mouse line (Claxton et al., 2008), in which the Cre is only active in ECs after tamoxifen administration, which we crossed with a conditional heterozygous Pik3ca[WT/H1047R] mice (Kinross et al., 2012), bearing one germline *Pik3ca* allele with a conditional H1047R mutation (**Figure 4.1**). In the newly generated EC-Pik3ca[H1047R] mice, one *Pik3ca* allele presents loxP sites flanking wild type exon 20. Downstream is placed a tandem copy of exon 20 incorporating the H1047R (CAT→AGG) mutation. Tamoxifen-inducible Cre excision removes the floxed fragment replacing the wildtype with mutant exon 20, resulting in *Pik3ca*[H1047R] protein expression at endogenous levels in otherwise normal ECs; thus accurately reproducing the scenario of a naturally occurring mutation. This mouse model specifically expresses the *Pik3ca*[H1047R] mutation in ECs in a heterozygous and endogenous way, recapitulating the genetic of the VM disease. In this way, the biological effects of *Pik3ca*[H1047R] expression can be examined both *in vitro* and *in vivo.*
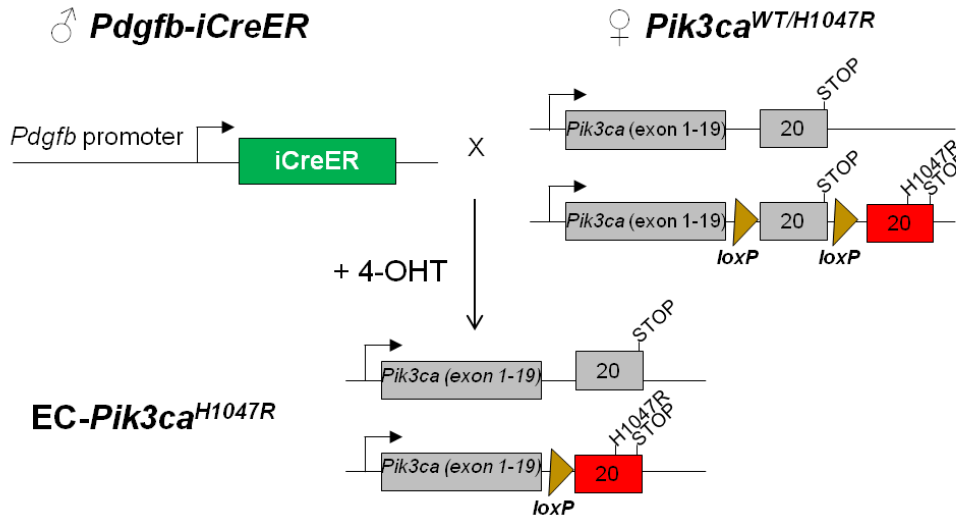
Figure 4.1. A transgenic mouse line to study the _Pik3ca^H1047R_ activating mutation in ECs.

Scheme of the conditional _Pik3ca^H1047R_ allele in EC-PIK3CA^H1047R mice. In the targeted Pik3ca locus, exon 20 is flanked by loxP sites. Endothelial-specific promoter (Pdgfb)-mediated 4-hydroxytamoxifen (4-OHT)-induced Cre excision removes the floxed fragment, activating the conditional mutated _Pik3ca^H1047R_ allele in the targeted endothelial cells.

4.1.2 _Pik3ca^H1047R_ expression in ECs leads to the overactivation of PI3K signalling pathway

Given that very little is known about how _Pik3ca^H1047R_ induces pathogenesis in ECs, we first aimed to study the molecular impact of this mutation _in vitro_. To address this, we chose RNA sequencing analysis. We isolated primary mouse ECs (mECs) from the lungs of EC-Pik3ca^H1047R mice and we confirmed their EC identity by analysing the expression of Ve-cadherin, an endothelial specific junctional marker. We confirmed the knock-in of _Pik3ca^H1047R_ mutation after Cre recombination _in vitro_ by treating mECs with 4-hydroxytamoxifen (4-OHT, the active form of tamoxifen) and vehicle (absolute ethanol, EtOH) at different time points (**Figure 4.2A**), following by assessing p-AKT status. Representative western blot (WB) analysis at 24 hours in **Figure 4.2B** shows that _Pik3ca^H1047R_ activation in ECs induces elevated p-Akt levels at Ser473 and Thr308, indicating the overactivation of PI3K signalling pathway (**Figure 4.2B**). Previous data have identified _Angpt2_ (encoding for Angiopoietin-2, ANG2) and _Pdgfb_ (encoding for platelet-derived growth factor subunit B, PDGF-B) as bona fide transcriptional readouts of PI3K signalling, with both transcripts negatively regulated by PI3K signalling (Uebelhoer et al.,2013; Lymaye et al, 2015; Castel et al.,2016; Castillo et al.,2016). Based on this, we

used *Angpt2* and *Pdgfb* mRNA levels as readouts to define the best time point analysis to study acute transcriptional changes induced by *Pik3ca*^H1047R in ECs (**Figure 4.2C**). Critically, analysis 24-hour post 4-OHT treatment was sufficient to induce a robust activation of PI3K signalling (**Figure 4.2B**) with transcriptional impact (**Figure 4.2C**). Hence, we used 24h post 4-OHT treatment as a reference time point to assess the impact of *Pik3ca*^H1047R expression on the early stage of activation *in vitro*.
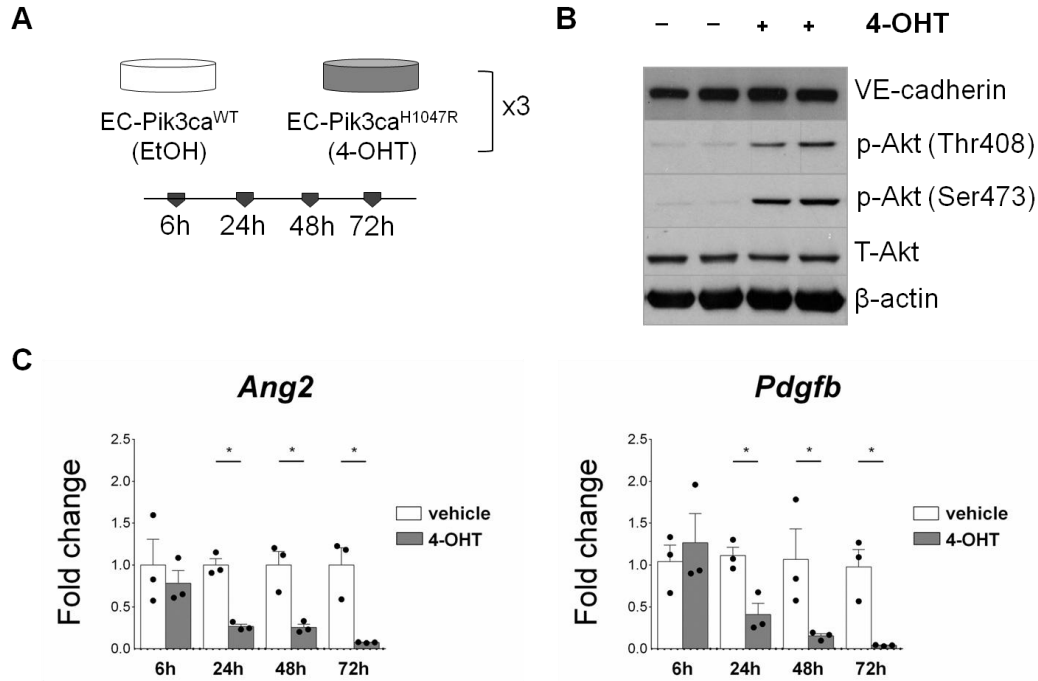
Figure 4.2. *Pik3ca*^H1047R expression leads to overactivation of PI3K signalling pathway in ECs.

A) Schematic representation of the *in vitro* treatment of mECs. Pik3ca^WT/H1047R mECs were isolated, cultured and treated with EtOH (vehicle) and 4-OHT for 6, 24, 48 and 72 hours. B) Analysis of PI3K activation by WB analysis after 24-hour treatment. C) Gene expression levels of *Angpt2* and Pdgfb genes assessed upon treatment at different time points. Data represent mean ± SEM. *p ≤ 0.05 (Mann-Whitney U test), n=3.

4.1.3 A transcriptomic analysis to unveil the biological mechanisms triggered by *Pik3ca*^{H1047R} expression in ECs

To gain insight about the molecular changes occurring upon acute activation of *Pik3ca*^{H1047R} in ECs, we explored the transcriptomic profile of mECs by performing an untargeted RNA sequencing analysis. First, we checked the *Angpt2* and *Pdgfb* mRNA levels (**Figure 4.3A**) in the analysed samples to confirm the expression of the activating *Pik3ca*^{H1047R} mutation in the ECs. Then, a total of 14190 annotated genes in the GRCm38 mouse genome assembly were analysed and a gene-set enrichment analysis (GSEA, Subramanian et al., 2005) was performed.

GSEA analysis on the entire gene-dataset highlighted a significant enrichment in the "Oncogenic PI3K mutant signature" (Koren et al., 2015, Van Keymeulen A et al., 2015, Hutti JE et a., 2012) for *Pik3ca*^{H1047R} mutant ECs (FDR<5% and nominal p-value < 1%, Figure 3B), with 71 up-regulated genes involved in cell cycle and cell proliferation processes. This data was further validated by the Kyoto Encyclopaedia of Genes and Genomes (KEGG) enrichment analysis that indicates an enrichment of genes involved in the control and regulation of the cell cycle (FDR<5% and nominal p-value < 1%, **Figure 4.3B**). These data strongly suggested that *Pik3ca*^{H1047R} expression critically controls and regulates the proliferative behaviour of ECs (di Blasio et al., 2018; Castillo et al., 2016).

Next, we identified 275 differentially expressed genes (DEGs) between *Pik3ca*^{H1047R} (4-OHT) and *Pik3ca*^{WT} (EtOH) mECs (FDR<5% and shrunken log2 fold change (LFC)>1.5) and we screened the biological processes in which the DEGs were involved by using GO database. As expected, PI3K signalling pathway and various processes involved in the cell cycle regulation were highly represented, confirming the previous data (**Figure 4.3C**). Furthermore, 39 biological processes regulating cell-cell and cell-matrix adhesion, as well as cell migration, were significantly represented (FDR<5%, **Figure 4.3C**). Within the identified processes, integrins binding and cell-adhesion-mediated by integrin particularly drawn our attention. In addition, angiogenesis-related processes were highly represented with cell migration involved in sprouting angiogenesis as the most represented one (**Figure 4.3E**). Overall, all the identified signatures were pointing out a potential role for cell adhesion and cell migration as critical biological processes triggered by *Pik3ca*^{H1047R} mutation in ECs.

Next, to support the potential role of these processes, we submitted the 39 identified signatures to a bootstrapping analysis. This bioinformatics analysis compares each

biological signature with 1000 signatures created by chance and verifies if the genes involved are the same or more than expected by chance (blue area, **Figure 4.3D**). Surprisingly, all the 39 biological processes related with adhesion and migration, were enriched of DEGs more than what expected by chance (p value<0.001); validating their role in our context.

To finally underpin the hypothesis that *Pik3ca*[H1047R] expression could affect the adhesion and migration functions of ECs, we individually checked the DEGs in the RNAseq analysis. Two specific genes emerged as strongly modulated: the endothelial Nitric Oxide Synthase (*eNOS*) as the most up regulated and the Chemokine (C-X-C Motif) Receptor 4 (*Cxcr4*) as the most down regulated gene. Since *Cxcr4* has a crucial role in angiogenesis regulation, with the SDF-1/CXCR4 axis playing a role in severe blood vessel abnormalities (Ara T et al., 2005), and eNOS supports ECs migration via integrin dependent mechanisms (Murohara et al., 1999), we deepened our analysis by checking the integrin status. We found that the genes encoding for integrins α- and β- subunits were affected in their expression levels in the *Pik3ca*[H1047R] mutant ECs, with *Itga9* and *Itga8* transcripts significantly deregulated.

Integrins are transmembrane glycoprotein receptors, composed of α and β subunits, and are responsible for cell-cell and cell-matrix interactions. In addition to mediating attachment to their respective extracellular matrix (ECM) ligand(s), they have specialized signalling functions and they can regulate gene expression as well as cell shape, migration, proliferation, and survival. Also, they are crucial in angiogenesis and for vascular integrity and are the major mediators of vascular cell adhesion and migration through the extracellular matrix (Somanath PR et al.2009).

Taken together, these data suggested the hypothesis that expression of *Pik3ca*[H1047R] mutation could modulate ECs adhesion through a specific impact on the integrins profile.
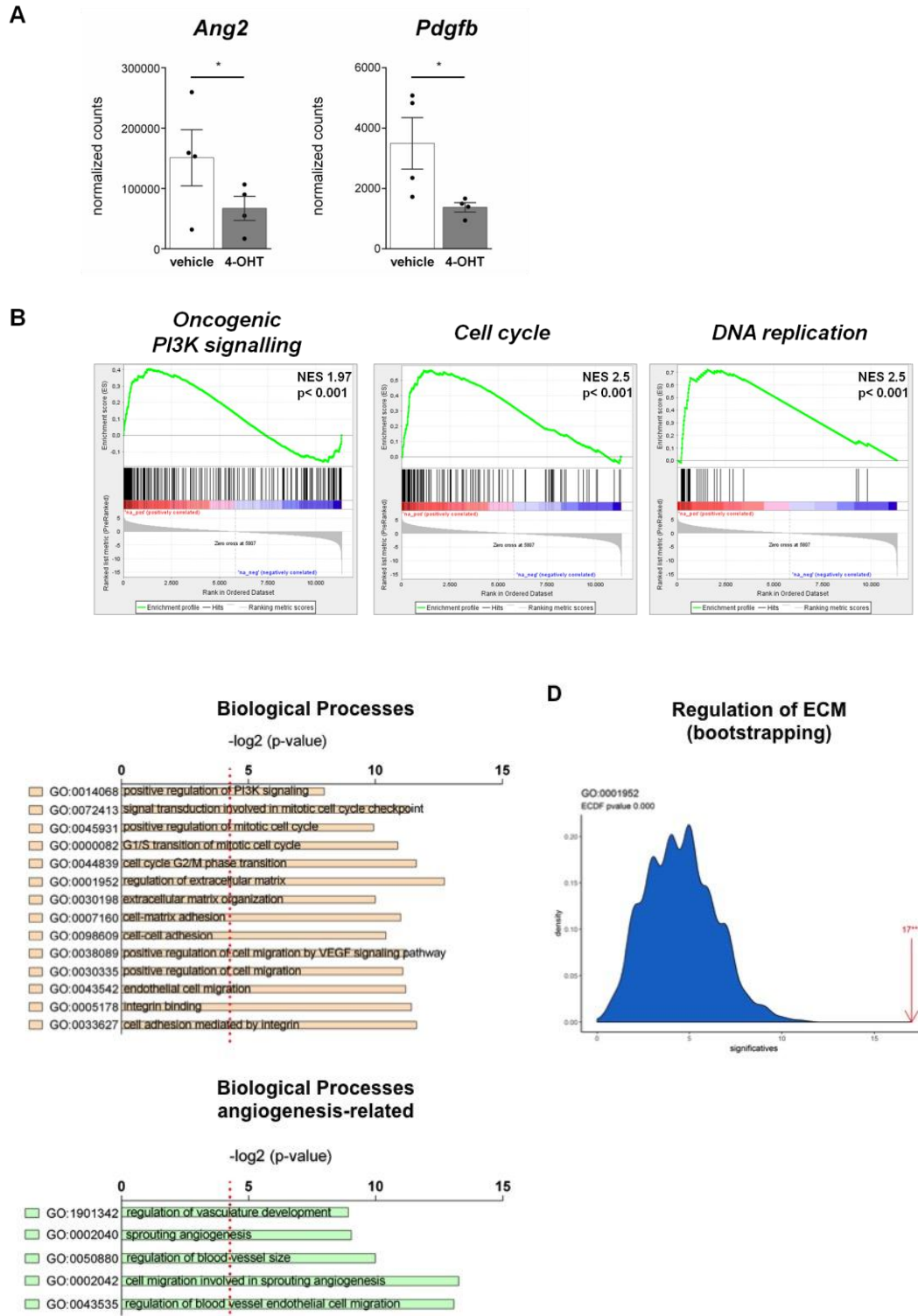
Figure 4.3. *Pik3ca*[H1047R] expression affects the proliferation and adhesion/migration processes of ECs.

A) Gene expression levels of *Angpt2* and Pdgfb genes assessed in the analyzed RNAseq samples. Data represent mean ± SEM. *p ≤ 0.05 (Mann-Whitney U test), n=4. B) GSEA analysis. Top enriched signatures (FDR<5%) in the Pik3ca[H1047R] mECs are shown with the relative normalized enrichment score (NES) and p-

values. C) and E) GO biological processes enriched in Pik3ca^{H1047R} mECs showed with the relative p-adjust values. Red dashed bar show a p-value=0,05. D) Representative image of the process GO:0001952-Regulation of ECM, one out of 39 processes analyzed with a Bootstrapping analysis. Blue area represents the number of random genes (0-10) necessary for a process to be significant. Red arrow indicates that 17 genes changed their values in the dataset, validating the process.

4.1.4 *Pik3ca^{H1047R}* expression affects the proliferation and adhesion molecular signatures of ECs

To validate the proliferation and adhesion signatures, we analysed the expression levels of key genes involved in these functions by RT-qPCR. The proliferative signature was assessed upon 24-hour 4-OHT treatment by looking at key cell cycle and DNA replication genes (**Figure 4.4A**). Mutant *Pik3ca^{H1047R}* mECs up-regulated genes promoting cell cycle progression like *Mcm10, Mki67, E2f1, Klf10* while down-regulated the cyclin-dependent kinase inhibitor *Cdk2nb*.

Next, to validate the adhesion signature, the gene expression profile of a variety of cell adhesion molecules was assessed upon 24- and 72-hour 4-OHT treatment (**Figure 4.4B**). The overall analysis revealed that *Pik3ca*^{H1047R} mutant mECs significantly reduced the expression level of *Cxcr4, Fn1, Ccn1, Vcam1* and *Itga8* genes while strongly increased *Pcdh12, Depdc1b, L1cam, Itga9* and *Itgb2* genes.

These data validated that *Pik3ca^{H1047R}* expression modulates the molecular adhesive profile of ECs in a time dependent manner, with the integrins repertoire particularly affected. This strongly highlights that *Pik3ca*^{H1047R} activating mutation could interfere in the adhesion and migration capacities of ECs.

Among the analysed integrins, *Itga9* mRNA levels were particularly affected by *Pik3ca*^{H1047R} expression over the time, being it the most significantly increased integrin in our specific context. The integrin-α9 (Itgα9) subunit forms a single known heterodimer, α9β1, and is the most recent fibronectin-binding integrin with a role in angiogenesis (Vlahakis NE et al., 2007; Staniszewska I, et al., 2007; Liao YF, et al., 2002; Marcinkiewicz C, et al. 2000). It is a receptor for a number of ECM proteins and plays a role in EC adhesion, facilitating accelerated cell migration (Vlahakis NE et al., 2007). As of now, no deregulation in integrins profiles has been previously identified in the VM-context and we selected itga9 as a potential critical target in mediating the biological effects of *Pik3ca^{H1047R}* expression in mECs.
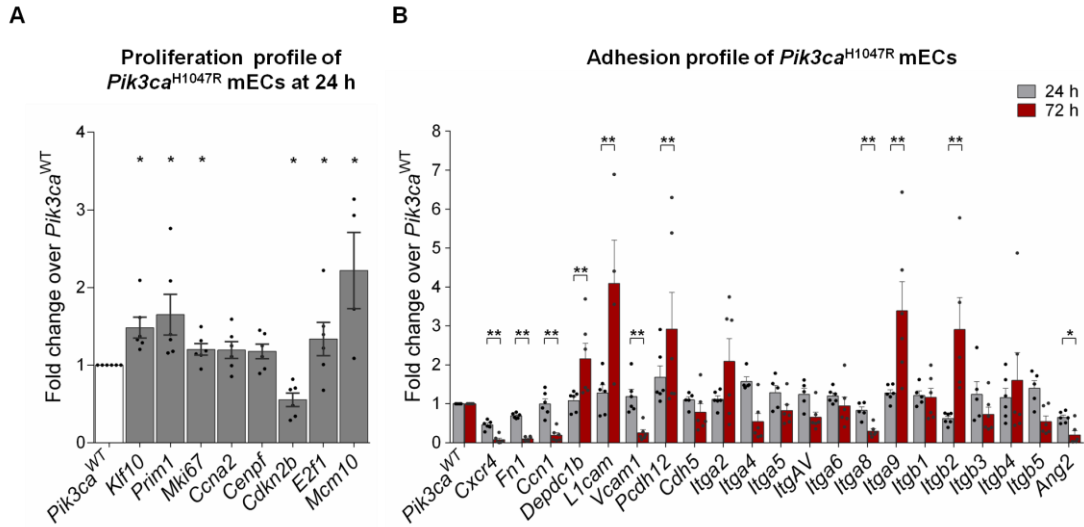
Figure 4.4. *Pik3ca*^{H1047R} expression directly affects the proliferative and adhesive gene expression profiles of ECs.

A) Expression levels of cell cycle genes evaluated upon 24-hour treatment of Pik3ca$^{WT/H1047R}$ mECs. B) Comparison of the expression levels of adhesion genes upon treatment of Pik3ca$^{WT/H1047R}$ mECs at 24 and 72 hours. Data represent mean ± SEM. **p ≤ 0.005, *p ≤ 0.05 (Mann Whitney test), n=6.

4.1.4.1 The molecular changes are rescued by PI3K pathway inhibitors

To confirm that the adhesion molecular signature is PI3K-mediated, we treated mECs with different inhibitors of the PI3K/AKT/mTOR signalling pathway. *Pik3ca*^{H1047R} mECs were treated for 48 hours with BYL-719 (PIK3CA-specific inhibitor), MK-2206 (AKT inhibitor) and Rapamycin (mTOR-inhibitor); DMSO was used as a control. The gene expression level of the putative genes was analysed by RT-qPCR. Interestingly, the expression of all transcripts, previously shown to be up regulated in *Pik3ca*^{H1047R} mutant ECs (DMSO condition, **Figure 4.5A**), were normalized to control levels upon 48-hour treatment with all inhibitors, with higher and comparable efficacy for BYL-719 (PIK3CA-specific) and MK2206 (AKT) inhibitors. In contrast, for the transcripts resulted down regulated in *Pik3ca*^{H1047R} mutant ECs (DMSO condition, **Figure 4.5B**), although a similar tendency in the rescue capacity was observed, no significant results were obtained. These data suggest that *Pik3ca*^{H1047R} expression exerts its critical role by mediating the up regulation of genes expression levels.

A   *Up regulated genes in Pik3ca*^H1047R **mECs**
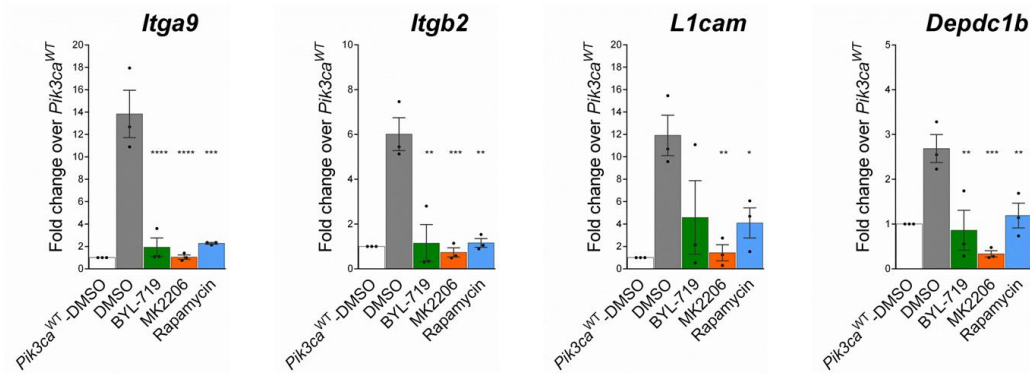
B   *Down regulated genes in Pik3ca*^H1047R **mECs**
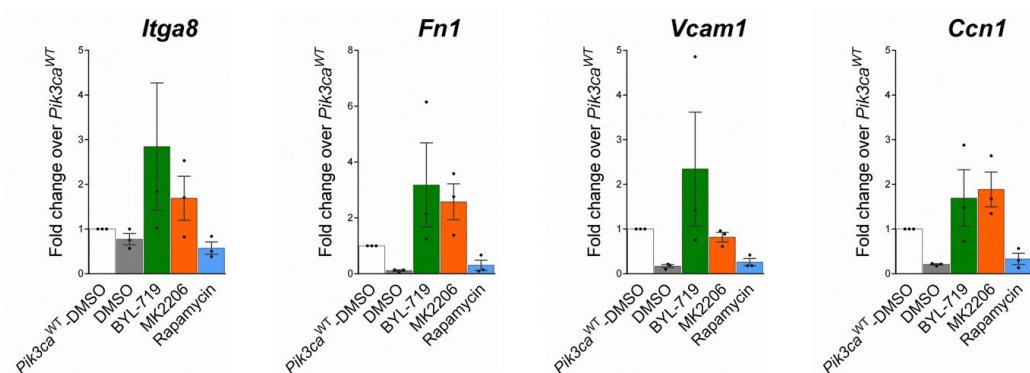
Figure 4.5. The adhesive molecular signature is PI3Kα-mediated and can be rescued with the use of PI3K-AKT-mTOR axis inhibitors.

A) Up regulated and B) down regulated genes upon 24-hour treatment of *Pik3ca*^WT/H1047R mECs. Analyses of gene expression levels were assessed upon 48-hour treatment of *Pik3ca*^H1047R mECs with a PIK3CA-inhibitor (BYL-719), an AKT inhibitor (MK-2206) and mTOR-inhibitor (Rapamycin); DMSO was used as a control. Data represent mean ± SEM, n=3. Two-way ANOVA test vs. DMSO condition has been performed. **** $p<0.0001$ *** $p<0.0005$, ** $p<0,005$, *$p<0,05$.

4.1.4.2   The molecular changes are ECs-specific

Next, a critical question is whether the molecular signature observed is ECs-specific or it also occurs in other cell types. To address this issue, we assessed the expression profile of the putative genes in primary mouse embryonic fibroblasts (MEFs) upon expression of *Pik3ca*^H1047R. These cells were kindly provided by the Cell Signalling research group (Prof. Vanhaesebroeck, UCL Cancer Research) and were isolated from Pik3ca^WT/H1047R mice crossed with Rosa26-CreERT2 mice, expressing *Pik3ca*^H1047R ubiquitously upon 4-OHT-treatment. *In vitro* recombination was verified assessing PI3K signalling pathway activation

by WB analysis (**Figure 4.6A**). The expression profile of adhesion genes was analysed by RT-qPCR after 72-hour treatment with 4-OHT or vehicle (**Figure 4.6B**). The analysis showed that the adhesion molecular profile of MEFs was not affected over the time by the activating *Pik3ca^{H1047R}* mutation. As expected, *Pcdh12* gene was not expressed in MEFs, being it an ECs specific-gene. Only *Itga8* gene showed a tendency in decreasing its level similar to *Pik3ca^{H1047R}* ECs, which might indicate a more general mechanism linked with PI3K signalling that is not ECs related. Critically, the Ct values were comparable between MEFs and ECs. This indicates that these transcripts are expressed at similar levels between both cell types (**Figure 4.6C**).
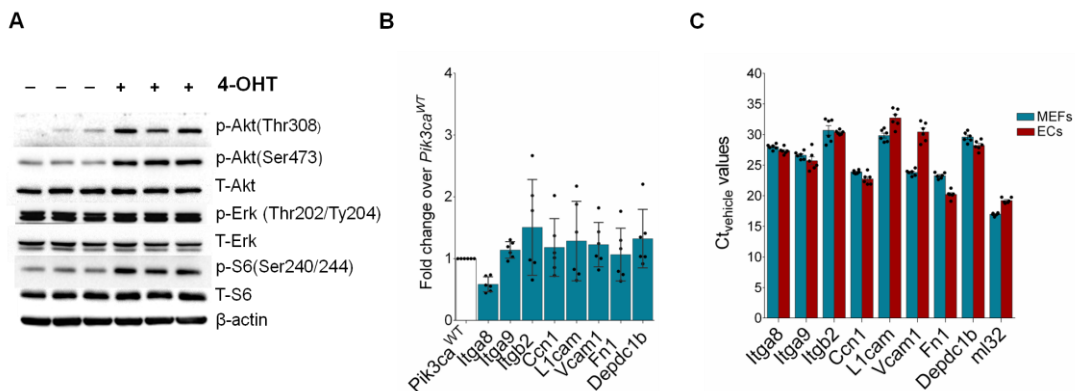
Figure 4.6. Changes in the adhesive molecular profiles are ECs-specific.

A) Assessment of PI3K pathway activation by WB analysis in mouse embryonic fibroblasts (MEFs) upon 24-hour treatment with 4-OHT. B) Gene expression levels of putative genes evaluated upon 72-hour treatment of MEFs, n=6. C) Comparison of Ct values of the putative gene in controls MEFs and ECs.

4.1.5   *Pik3ca^{H1047R}* expression affects Itga9 protein levels and ECs behaviour

Next, we aimed at correlating the molecular signatures with the cellular behaviour of ECs *in vitro*. In detail, since ECs proliferation and migration are early essential events during angiogenesis, and adhesion and migration are integrated cell functions, we hypothesized that a mutant *Pik3ca^{H1047R}* could finally impact the migratory capacity of mECs. Furthermore, as *Itga9* has emerged as potential candidate in mediating the biological effects of *Pik3ca^{H1047R}*, we validated its protein expression levels in Pik3ca^{H1047R} mECs.

97

4.1.5.1 *Pik3ca^{H1047R}* expression increases Itgα9 protein expression

We investigated the up regulation of Itga9 protein in mECs upon 24-hour treatment with 4-OHT/EtOH. First, we assessed Itga9 expression by IF analysis (**Figure 4.7A**), to visualize its subcellular localization. While in control cells Itga9 expression was very low and confined at the cytoplasmic level, in *Pik3ca^{H1047R}* mutant mECs the expression was higher and detectable at both intracellular and membrane level, with some cells expressing it ubiquitously and at the interface of interaction with other cells. Next, we confirmed this overexpression by means of WB analysis in the same experimental setting (**Figure 4.7B**). We observed that only *Pik3ca^{H1047R}* mECs presented increased level of the Itga9 protein, while controls *Pik3ca^{WT}* mECs and MEFs did not. Also, we observed that increased Itga9 protein levels by more than 4-fold changes (**Figure 4.7C**) corresponded with constitutive activation of PI3K signalling pathway, as demonstrated by the increased phosphorylation levels of AKT protein at both Ser438 and Thr308 residues.
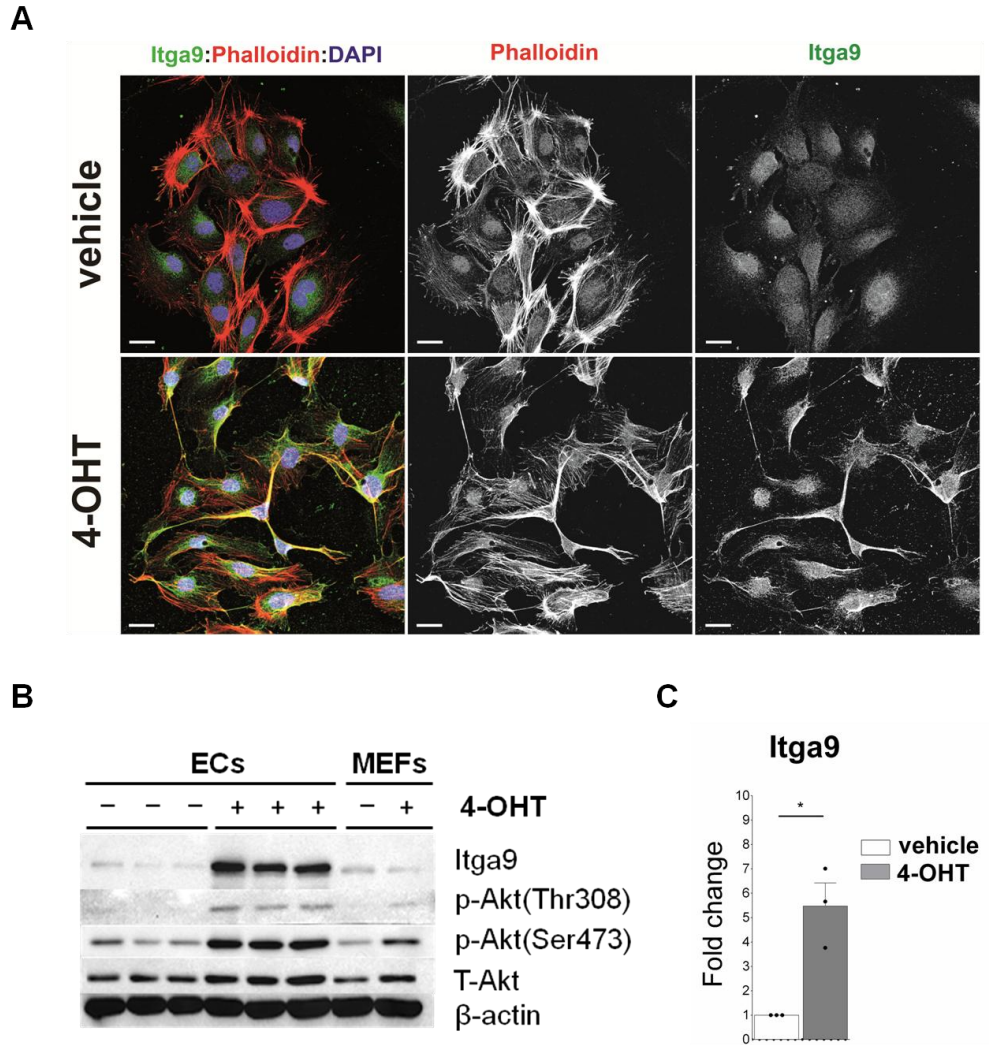
Figure 4.7. Expression of *Pik3ca^{H1047R}* induces Itgα9 overexpression.

A) Representative IF images of Itga9 levels in Pik3caWT (vehicle) and Pik3caH1047R (4-OHT), treated for 24 hours. Anti-Itga9 (green), anti-phalloidin (red). Scale bar 20 μm. B) WB analysis of PI3K pathway activation and Itga9 levels upon 24-hour treatment of mECs and control MEFs. C) Quantification of Itga9 protein levels in Pik3caWT/H1047R mECs.

4.1.5.2 *Pik3ca^{H1047R}* expression increases the proliferation of ECs

Next, we tested the proliferation rate of mECs by using EdU incorporation assays with immunofluorescence (IF) (**Figure 4.8A**) and FACS analyses (**Figure 4.8B**). EdU detects the S-phase of the cell cycle by incorporating the nucleoside analog uridine into newly synthesized DNA. Both analyses showed that mutant *Pik3ca^{H1047R}* mECs (4-OHT treated) exhibited a higher and reproducible proliferation capacity upon early expression (24-hour) of *Pik3ca^{H1047R}* mutation.
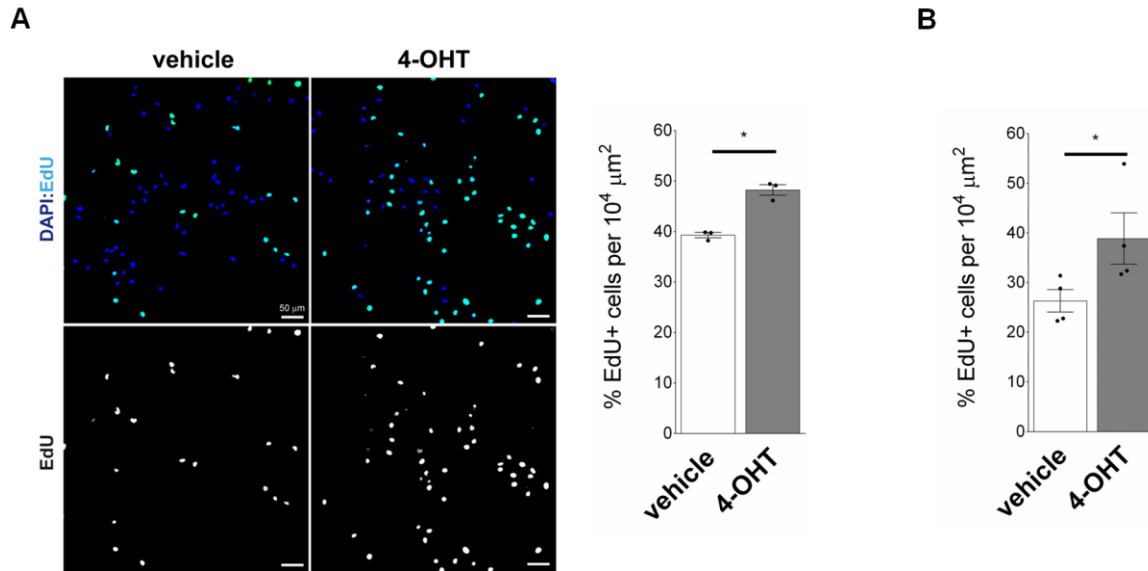
Figure 4.8. Pik3caH1047R expression increases ECs proliferation.

A) Representative IF images of *Pik3ca^WT^* (vehicle) and *Pik3ca^H1047R^* (4-OHT) mECs treated for 24 hours and stained with EdU (light blue) and DAPI (dark blue) with the relative quantification of proliferation rate. Scale bar 50 μm. B) Proliferation rate upon 24 hour treatment of mECs assessed by cytofluorimetric analysis (FACS). Data represent mean ± SEM. (t test), n ≥ 3. * p<0.05.

4.1.5.3 *Pik3ca^H1047R^* expression increases the migration of ECs

Finally, we checked if the migratory capacity of mutant *Pik3ca^H1047R^* mECs was perturbed. Therefore, we performed an *in vitro* wound-healing assay to assess the collective migration property of ECs following 24-hour treatment with 4-OHT/EtOH. The migration capability of the cells was assessed at different time points within 24 hours, revealing that mutant *Pik3ca^H1047R^* mECs migrate faster than control cells (**Figure 4.9B**). This was demonstrated by the increased capacity of these cells in filling the wound already at 17 hours (**Figure 4.9A**). This data demonstrated that *Pik3ca^H1047R^* activation leads to increased migratory capacity of ECs that could be partially explained by the altered molecular adhesive signature of the mutant ECs.
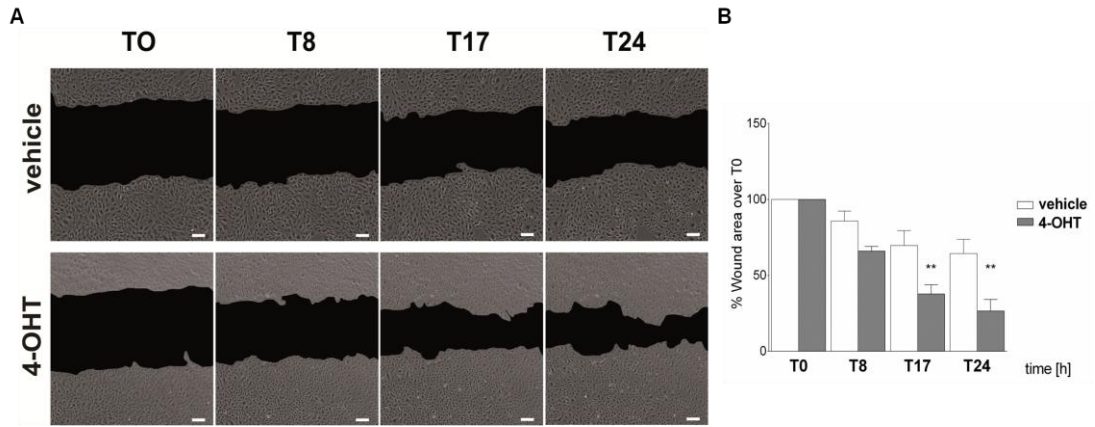
Figure 4.9. *Pik3ca^H1047R* expression increases ECs migration.

A) Representative images of a ECs monolayers at (T0) and at 8, 17 and 24 hours after scratching. Scale bar 250 μm. B) Quantification of cell migration was assessed by two-way ANOVA test of 2 independent experiments.**p< 0,005, n=4.

4.2 Generation of a robust mouse model to explore the biology of PIK3CA-driven VM

The second objective of this thesis was to generate a robust and reproducible mouse model of PIK3CA-driven VM to (1) study the biology of *Pik3ca* pathogenesis in vivo and (2) to provide a pre-clinical platform to test pharmacologic interventions. To this end, we took advantage of EC-Pik3ca^{H1047R} we generated to test three experimental settings, allowing to express the *Pik3ca^{H1047R}* mutation at different stages after birth (**Figure 4.10**).

(A) Postnatal to Postnatal; we used postnatal mouse retina as a biological system. Retinal vasculature develops post birth. This allows us to study the impact of *Pik3ca^{H1047R}* before the onset of vascular development. To achieve that, we induced *Pik3ca^{H1047R}* expression in ECs at postnatal day (P1) followed by harvesting the eyes at P6 (**Figure 4.10A**).

(B) Postnatat to Adult; we aimed to explore which tissues were most susceptible to develop VM upon postnatal induction of *Pik3ca^{H1047R}* expression in ECs. To this end, we administered 4-OHT at P1 followed by culling the animals at 14 weeks of age (**Figure 4.10B**).

(C) Adult to Adult: the expression of *Pik3ca^{H1047R}* was induced in 8-week old mice by administering 2mg/day of tamoxifen (Tx) for 2 consecutive days. The animals were followed up and culled after 9 weeks (**Figure 4.10C**).
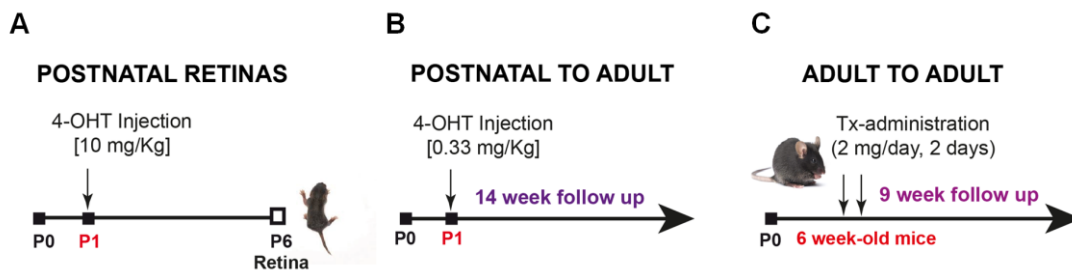
Figure 4.10. Schematic representation of the three experimental settings used to express the *Pik3ca^{H1047R}* activating mutation *in vivo* in EC-Pik3ca^{H1047R} mice at different stages after birth.

Upon several pilot studies, we realized that the postnatal to postnatal model approach (A) provided many advantages (robustness, time, sensitivity, amongst others) compared to B and C. Hence, the following section will just briefly describe the results obtained by applying approach B and C, in favour of the investigation of the postnatal retina exploration (approach A).

4.2.1 *Pik3ca^{H1047R}* expression in the mouse endothelium exhibits different phenotypic vascular defects

4.2.1.1 Early postnatal expression of *Pik3ca^{H1047R}* in mice leads to heterogeneous VM-phenotype (B)

EC-Pik3ca^{H1047R} animals injected at postnatal P1 and culled after 14 weeks, developed subcutaneous vascular lesions mainly in the mesentery and urogenital areas (**Figure 4.11A**). However, a heterogeneous degree of phenotypes was observed between EC-Pik3ca^{H1047R} mice. On a cohort of 7 EC-Pik3ca^{H1047R} analysed animals, one was found dead after 4 weeks (for unclear cause), while the 6 remaining ones presented variable vascular defects, with some presenting a very strong phenotype in terms of size, localization, and expansion of the vascular lesions and others presenting a milder phenotype with only few or no lesions at all (**Figure 4.11B**). Although this model exhibited variable vascular defects, it was not sufficiently robust for our studies.
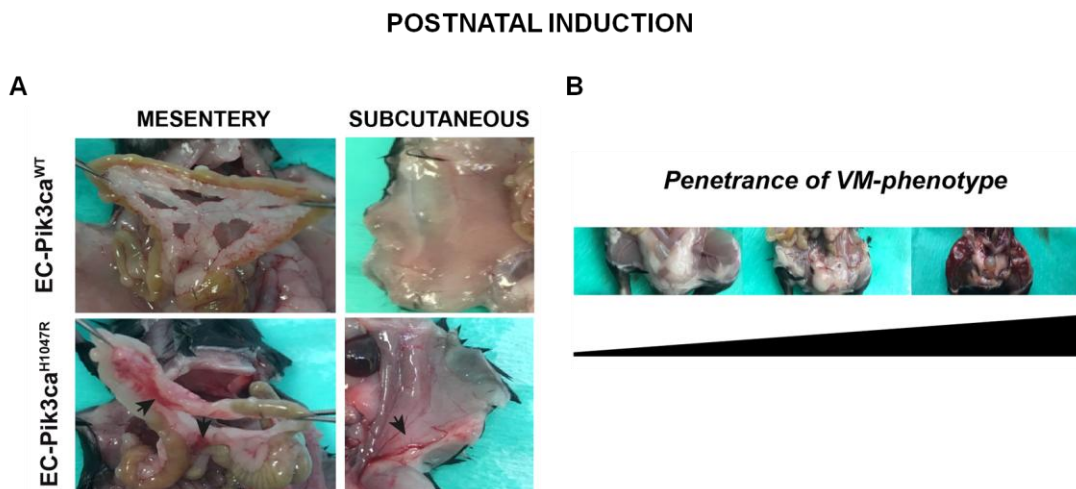
Figure 4.11. Early postnatal expression of *Pik3ca^{H1047R}* in mice.

A) Representative images of the mesentery and subcutaneous tissues in EC- Pik3ca^{WT} and EC-Pik3ca^{H1047R} mice. B) Representative images showing the heterogeneity in the degree of penetrance of vascular defects, from mild (left side) to strong (right side).

4.2.1.2 Adult *Pik3ca*[H1047R] expression in mice leads to localized VM (C)

We then, tried to assess whether vascular lesions induced in adult mice could lead to a more representative phenotype. Interestingly, when the expression of *Pik3ca*[H1047R] mutation was induced in adult mice, we observed the onset of vascular defects in 100% of the cases. Localized vascular lesions were observed in the subcutaneous tissues between the thoracic cage and the neck (**Figure 4.12A**). On a cohort of 7 EC-Pik3ca[H1047R] analysed animals, two died for internal haemorrhages after 8 weeks of follow up.

We decided to perform a histopathological analysis, which confirmed that the lesions were venous malformations with a lymphatic component. Specifically, the vascular lesions were dilated blood filled channels, poorly circumscribed, predominantly thin-walled, irregular, and abnormal sized blood vessels infiltrating normal soft tissues (**Figure 4.12B**). Moreover, the analysis revealed the presence of a malformed lymphatic vessels component, however it was less prominent than the aberrant blood vessels. This is in line with what is seen in human VM, where purely vascular malformations are rare and they usually contain a mixture of vessel types, with some types being pathologically prominent such as the blood vessels in the case of VM (Lowe et al 2012). This model exhibited the capacity of generating always localized vascular lesions; however it requires a long term which is not useful to study and characterize the biology of the disease.
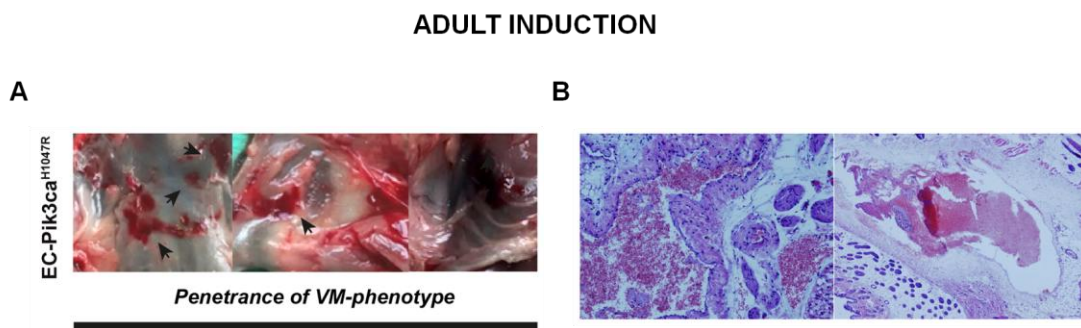
ADULT INDUCTION

Figure 4.12. *Pik3ca*[H1047R] expression in adult mice.

A) Representative images of the vascular lesions localized at the level of the thoracic cage-neck (black arrows) found in all the adult induced EC-Pik3caH1047R mice. B) Representative haematoxylin eosin–stained sections of the EC-Pik3caH1047R mice VM lesions. They appeared as venous malformations showing abnormal, enlarged, and irregular vascular channels similar to human VM.

4.2.1.3 Early *Pik3ca*^{H1047R} expression in the retinal vasculature generates localized vascular defects resembling VM disease (A)

In parallel, we tried to recapitulate the localized VM disease in postnatal retinas, an established experimental model in our lab to study postnatal angiogenesis in a stereotypical manner. Also, mouse retinas have become a state-of-the-art biological system to study vasculature development at high resolution.

Previous data from our lab had showed that endothelial expression of *Pik3ca*^{H1047R} in retinas result in prominent vessel hyperplasia associated with increased ECs proliferation and defective pericyte coverage. Together, this led to the appearance of a vascular bed composed of a single sheet of ECs (Castillo et al., 2016). Of note, this phenotype does not fully recapitulate the etiology of *PIK3CA*-related venous and/or capillary malformations in which enlarge, but distinct hyperplastic vascular channels are the norm.

To better model the disease, we first aimed to study the impact of different doses of 4-OHT (**Figure 4.13A**). We hypothesized that a reasonable (not too many and not too little) number of targeted ECs (which express the *Pik3ca*^{H1047R} mutation upon 4-OHT administration) would lead to the appearance of isolated hyperplastic vascular lesions in venous and/or capillaries locations. To this end, several doses of 4-OHT were injected at P1 EC-Pik3ca^{H1047R} pups, followed by harvesting the eyes at P6. Upon, dissecting and fixing the retinas, we proceeded to stain them with isolectin-B4 (IB4, which binds specifically to the ECs plasma membrane) (**Figure 4.13A**). Critically, the lowest dose [0,05 mg/Kg] emerged as the experimental condition to obtain a reliable and robust phenotype characterized the presence of isolated malformed vessels in the remodelling plexus (**Figure 4.13B-C**). We also noticed a highly proliferative response in the angiogenic sprouting front (**Figure 4.13B-C**).

The appearance of isolated vascular lesions led us to assessed where (which subtype of vessels) the isolated malformed vessels were localized. Interestingly, we observed that all the isolated lesions were appeared, and mainly associated, with a vein (arising within or from a vein) and, in a smaller percentage in the capillary bed (**Figure 4.13D-E**).To note, the lesions were never associated to arteries, thus finely reproducing the human disease.

Taking in account the robustness and reproducibility of the retinas model and the timing it required compared to the generation of adult mice, we decided to use it as *in vivo* model to

translate our *in vitro* findings and study how *Pik3ca^H1047R* expression impacts the biology of vessel malformations.
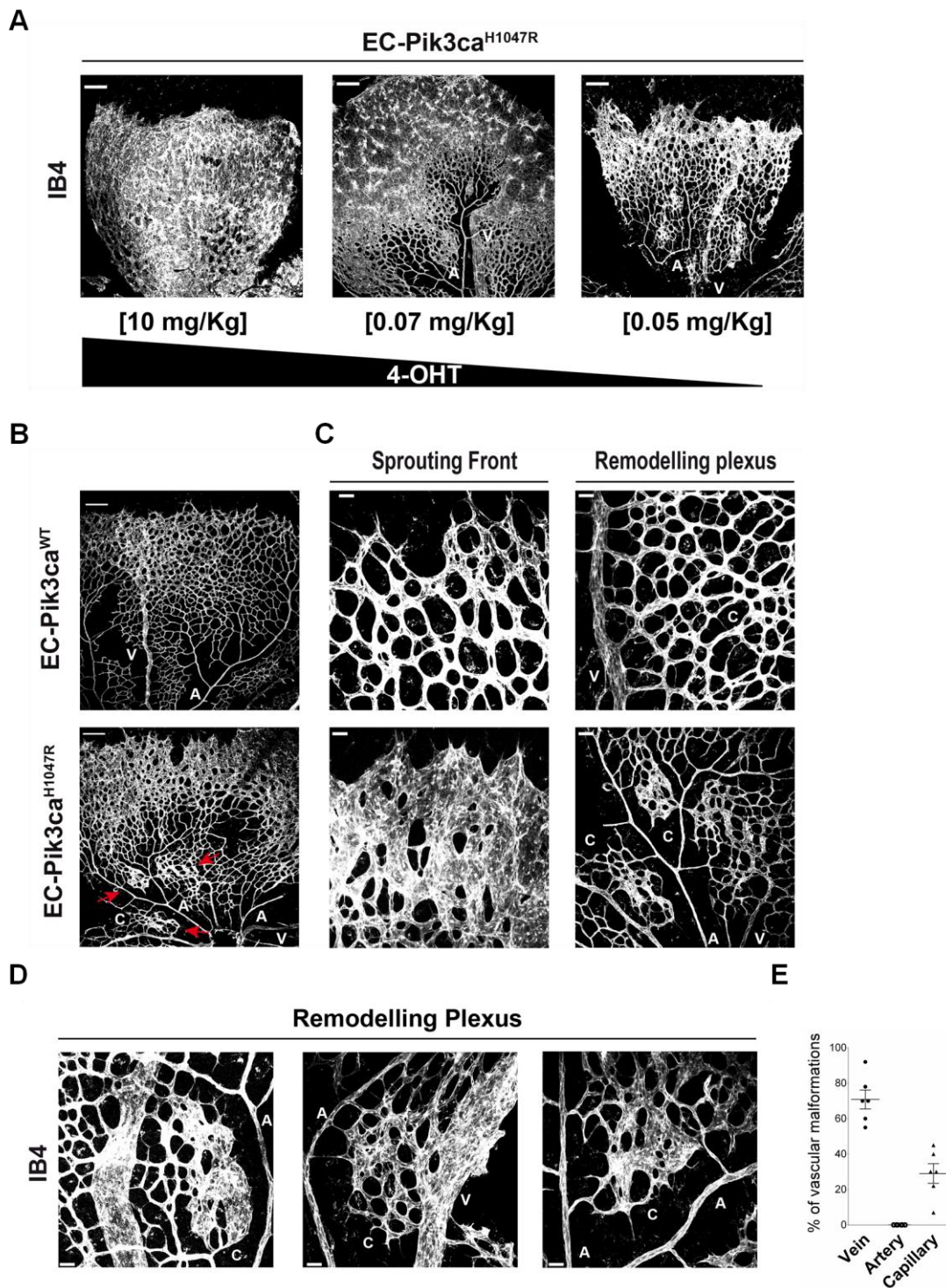
Figure 4.13. *Pik3ca^H1047R* expression in retinal vasculature generates localized vascular defects resembling VM disease.

Representative whole-mount retinas from littermates at P6, stained with Isolectin-B4 (IB4). A) 4-OHT titration to identify a suitable dose reproducing a localized VM-phenotype, n=3 animals/each dose. B) Representative images of EC-Pik3caWT and EC-Pik3caH1047R postnatal retinas vasculature. Red arrows in the EC-Pik3caH1047R retina indicate isolated localized malformed vessels. C) High-magnification images of the sprouting and remodelling areas of EC-Pik3caWT and EC-Pik3caH1047R retinas. Abnormal dilated vessels characterize the sprouting front and the onset of isolated malformed vessels (VM) characterise the remodelling plexus. D) Representative high magnification images of VM localization in EC-pik3caH1047R retinas. E) Quantification of VM localization. Data represents % mean ± SEM (error bars), n=6. Scale bars, 150 µm (A-B), 30 µm (C-D).

4.2.2 *Pik3ca^{H1047R}* expression in retinal vasculature increases ECs proliferation causing localized VM

We started by analysing the degree of vascularity of EC-Pik3ca^{WT} and EC-Pik3ca^{H1047R} retinas. As expected, EC-*Pik3ca*^{H1047R} retinas showed an increased vascularity (or vessel density) in both the sprouting and the remodelling areas, as measured by the IB4-positive area (**Figure 4.14A**). The vascular tubes showed bigger calibre within the whole vascular plexus and the overall area increased by almost 2-fold (**Figure 4.14B**).

Current models of enhanced vessel density involved an increase in the number of ECs (Serra H et al., 2015; Castillo et al., 2016; Hellstrom M. et al, 2007; Tammela T. et al, 2011). In fact, immunostaining of endothelial cell nuclei revealed a significant increase in the total number of ECs in both the sprouting and remodelling areas (**Figure 4.14C**). So, we wondered whether the vascular VM-phenotype observed was a direct consequence of an increased endothelial proliferation rate.
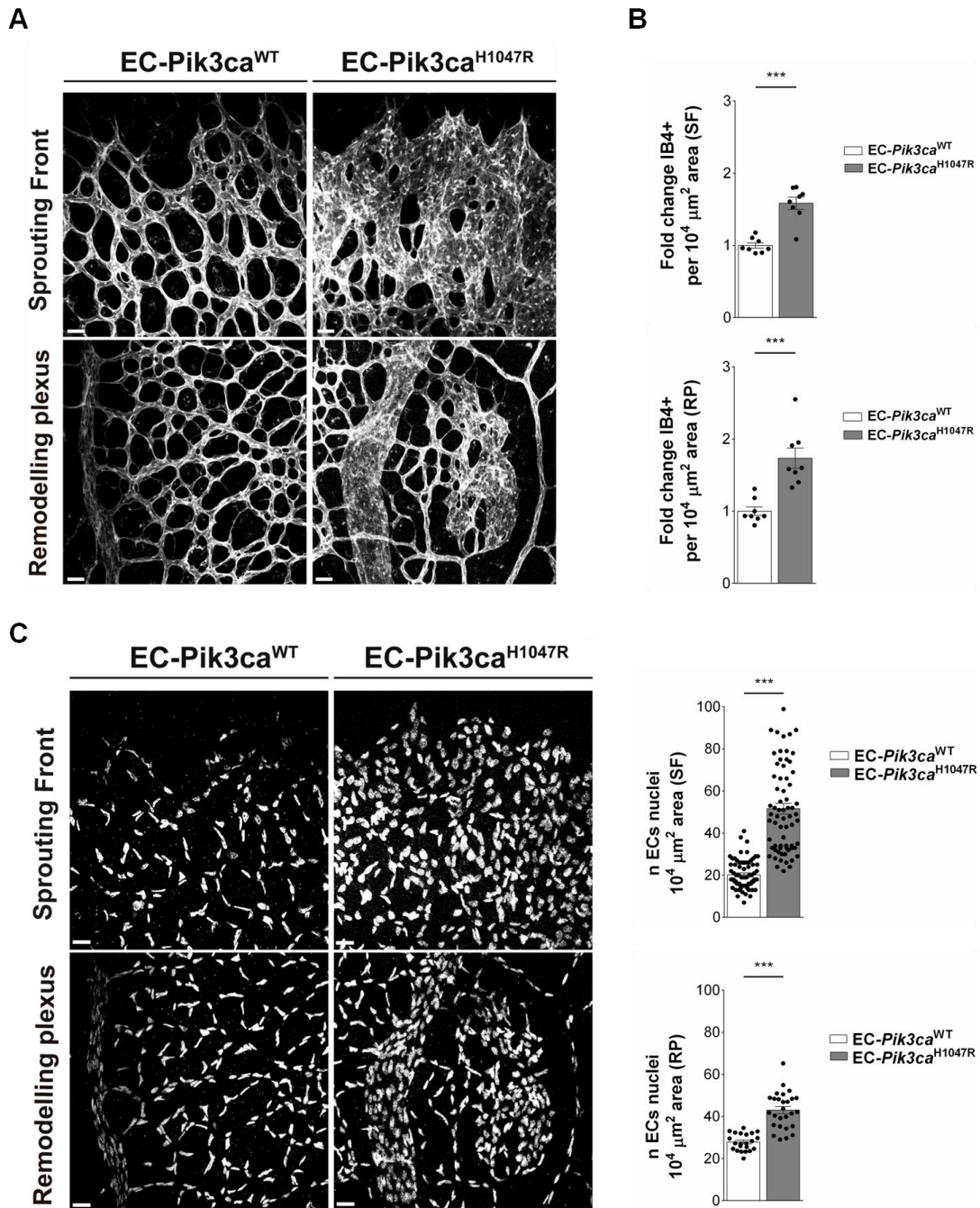
Figure 4.14. *Pik3ca^{H1047R}* **expression regulates retinal vascularity throughout the regulation of ECs number.**

A) Representative images of retinas vascularity in the sprouting and remodelling areas of P6 EC-pik3ca^{WT} and EC-pik3ca^{H1047R} retinas stained with IB4. B) Quantification of retinas vascularity. C) Quantification of endothelial cells number in the sprouting and remodelling areas of P6 EC-pik3ca^{WT} and EC-pik3ca^{H1047R} retinas stained with Erg (endothelial cells nuclei marker). Data represent mean ± SEM. ***P<0.005 (Mann-Whitney U test), n=8 retinas per genotype. Scale bars, 30 µm.

We analysed the proliferation rate of ECs *in vivo* by injecting P6 pups with EdU for two hours. Then we sacrificied the mice and we performed a triple staining of the retinas for EdU, isolectin-B4 and Erg. Although we did not observe differences in the proliferation rate of the sprouting areas between EC-Pik3ca^{WT} and EC-Pik3ca^{H1047R} retinas (**Figure 4.15A**), we observed a high proliferation rate in the remodelling plexus of EC-Pik3ca^{H1047R} retinas compared to the control ones (**Figure 4.15B**).

Altogether, these data confirmed that the mutant *Pik3ca^{H1047R}* directly affects ECs proliferation *in vivo*, increasing the total number of ECs in the vascular network leading to the vessel hyperplasia prototypical of VM disease. Thus, the aberrant proliferative behaviour is the main trigger for the vascular defects observed in the retinal vasculature, causing abnormal vessels in size and shape in the sprouting area and the onset of isolated malformed vessels (VM) in the remodelling area.
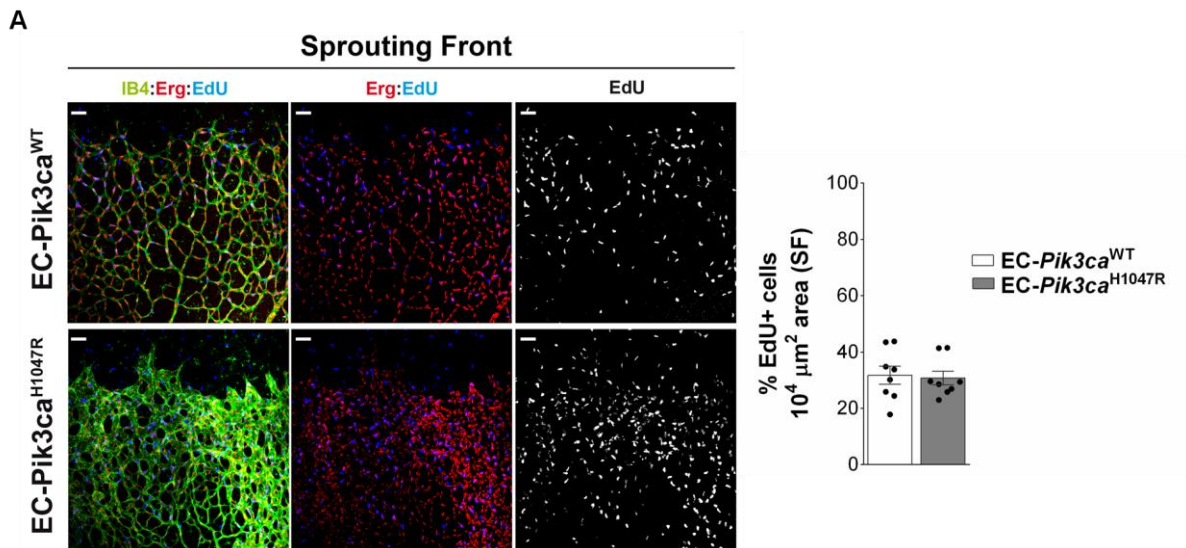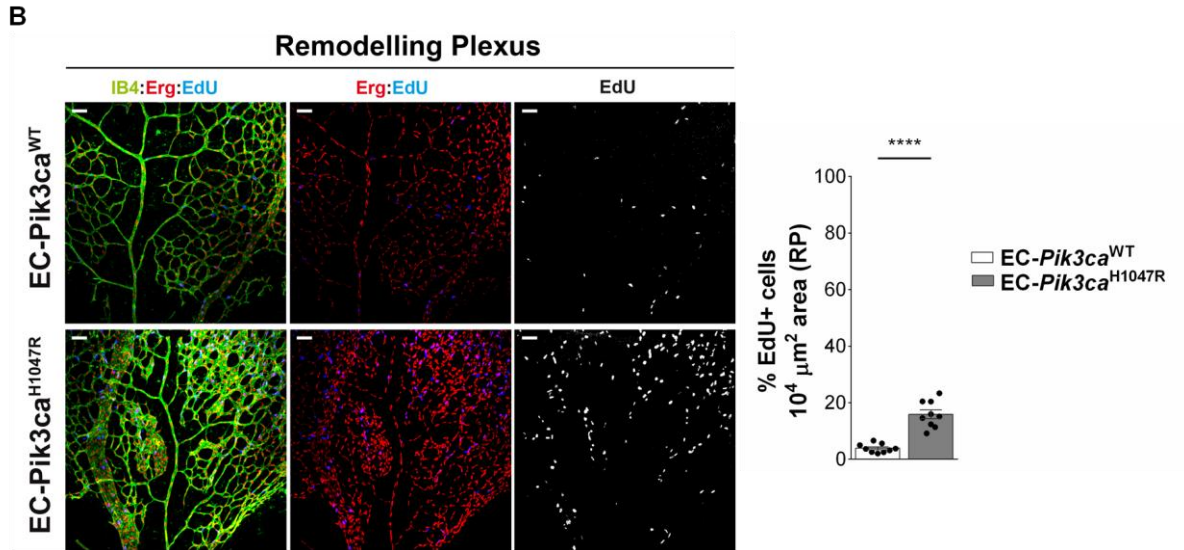
Figure 4.15. *Pik3ca^{H1047R}* **expression primary regulates ECs proliferation** *in vivo* **causing a VM-phenotype.**

Representative images of the A) sprouting and B) remodelling areas of P6 EC-pik3ca^{WT} and EC-pik3ca^{H1047R} retinas stained for Isolectin-B4 (green), Erg (red) and EdU (blue). Both EdU- and Erg-positive cells were quantified and results are presented as a % of EdU-positive cells per 10^4 μm^2 area. Data represent mean ± SEM. ***P<0.005 (Mann-Whitney U test). n= 8 retinas per genotype. Scale bars 50 µm.

4.2.3 *Pik3ca^{H1047R}* expression increases Itga9 levels in retinal vasculature

Next, we assessed if the overexpression of Itga9 protein caused by *Pik3ca^{H1047R}* expression *in vitro* was also occurring *in vivo* and if it was related with the VM-phenotype in the retinal vasculature. By staining mutant and control P6 retinas with Itga9 antibody, we observed that EC-Pik3ca^{WT} retinas showed very low levels in both sprouting and remodelling areas, with only few cells stained punctually (**Figure 4.16A**, red arrows).

Instead, EC-Pik3ca^{H1047R} stained retinas showed increased levels of Itga9 concurrently with the abnormal hyperplastic vessels of the sprouting area (**Figure 4.16B**, islets). Next, when we observed into the remodelling area, we noticed that Itga9 levels were only matching the presence of malformed vessels, whether they were isolated or into enlarged veins (**Figure 4.16C**, red islets).

A

EC-Pik3ca^{WT}

IB4   IB4:Itga9   Itga9

Sprouting Front

Remodelling plexus

B

EC-Pik3ca^H1047R

| IB4 | IB4:Itga9 | Itga9 |

Sprouting Front

C

Remodelling plexus

IB4

IB4:Itga9
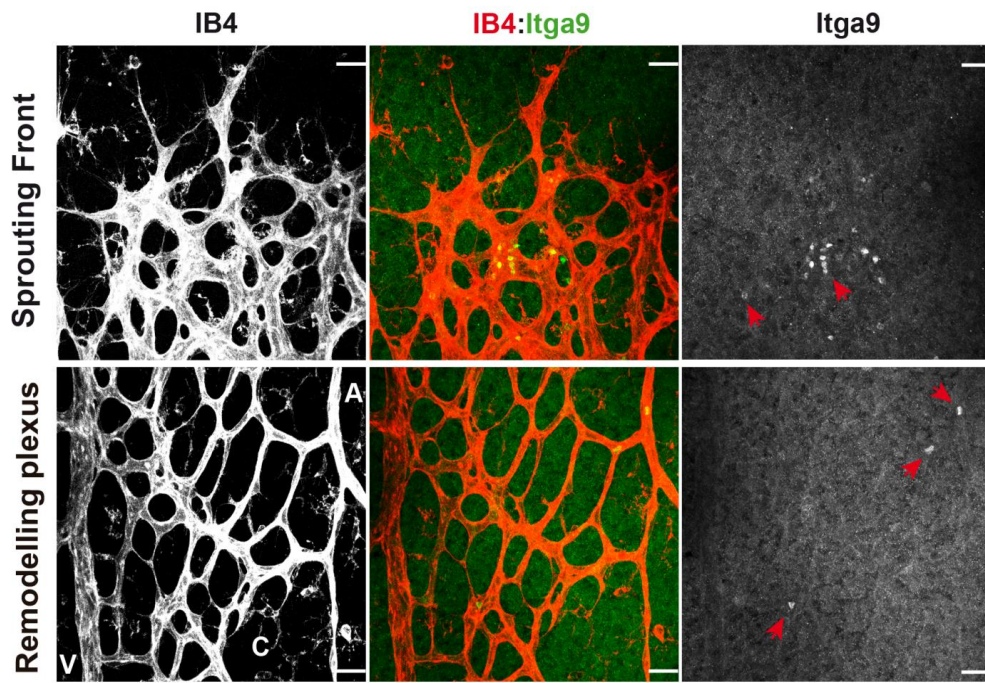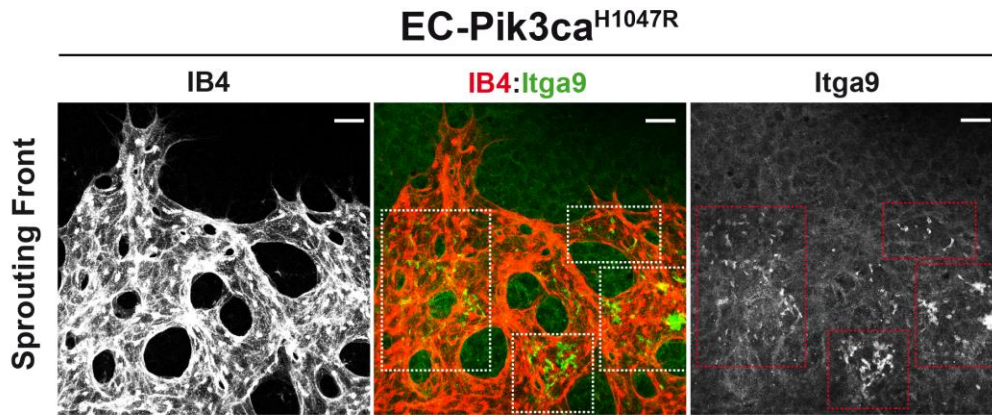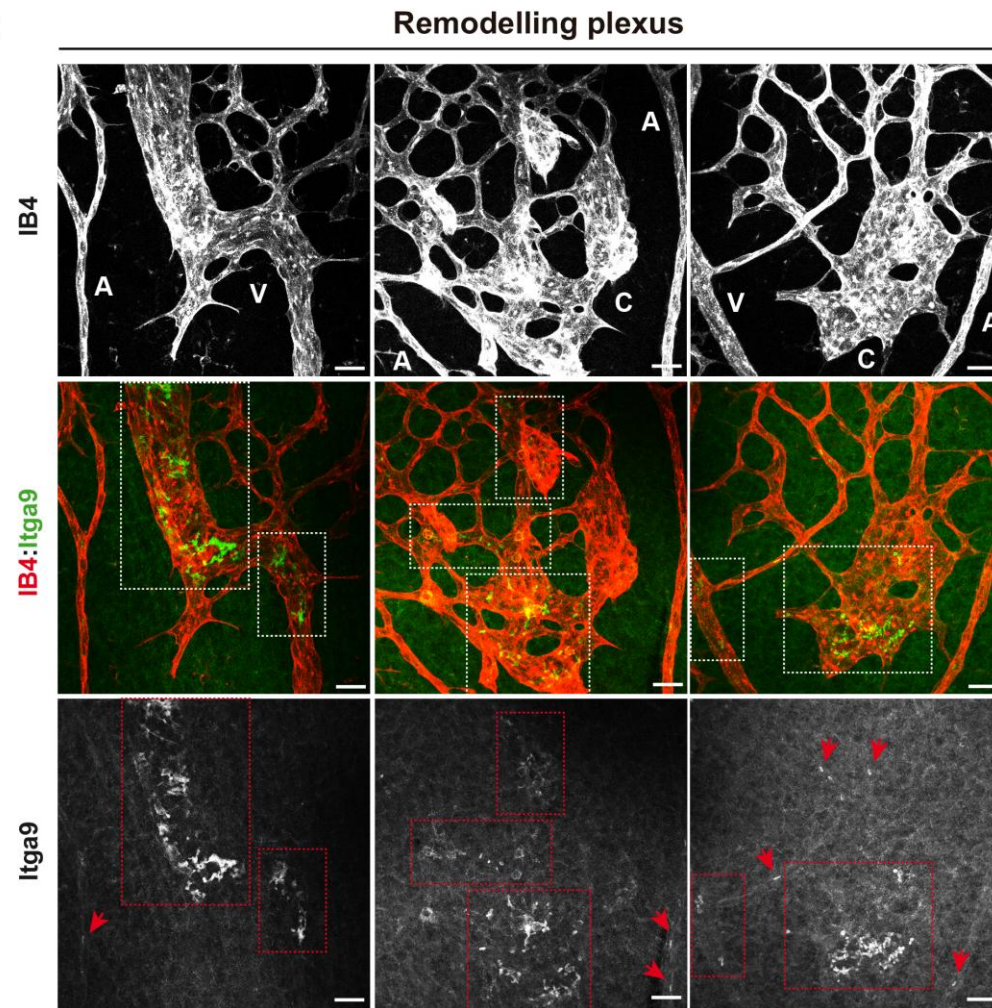
Itga9

Figure 4.16. *Pik3ca^H1047R* expression in mice overexpresses Itga9 in VM.

Representative images of the sprounting and remodelling areas of P6 A) EC-pik3ca^WT and B-C) EC-pik3ca^H1047R retinas stained for IB4 (red) and Itga9 (green). Red arrows show punctual expression of Itga9 by individual cells. Red islets show areas where Itga9 accumulates. White islets show coincidence of Itga9

expression in the malformed vessels. Veins (V), arteries (A) and capillaries (C) are indicated. Scale bars, 20 µm. n ≥ 3 retinas per genotype.

While the current Itga9 staining looks promising at the moment we cannot rule out that the staining is specific. In fact, it is possible that the antibody exhibits cross-reactivity with blood cells and/or proteins (IgG) of the serum. This is a common phenomenon when studying mutants who show an impaired blood flow within malformed vessels, as it occurs in EC-Pik3ca^{H1047R} retinas. This staining warrants further investigation including (i) a better set up of the antibody and/or (ii) the use of a different antibody.

4.3 Patient-derived primary cells to study the biology of VMs

To broaden the translational relevance of the previous data, we investigated if our findings were reflected in patient-derived samples. Thanks to our collaboration with clinicians of the Sant Pau, Sant Joan de Déu and Vall D'Hebron hospitals we have collected surgical resection and biopsies from patients with different type of vascular malformations with the aim of deriving primary human cells.

4.3.1 A new protocol to isolate primary cells from human samples

By taking advantage of the tools available in our laboratory for the isolation of mouse ECs, we tried to set up the isolation of human primary endothelial cells from fresh VM biopsies. Upon several trials, we developed a protocol (**Figure 4.17A**) which allows us to obtain primary human cells from different type of vascular malformations on a routine basis. This protocol allows the isolation of primary human CD31+ endothelial cells (CD31+, hECs) by positive selection as well as the relative CD31- counterpart by negative selection. Morphologically, CD31+ hECs showed the typical cobblestone appearance of the ECs culture while the CD31- cells presented the classical fibroblast-like elongated shape forming a monolayer in cell culture (**Figure 4.17B**).
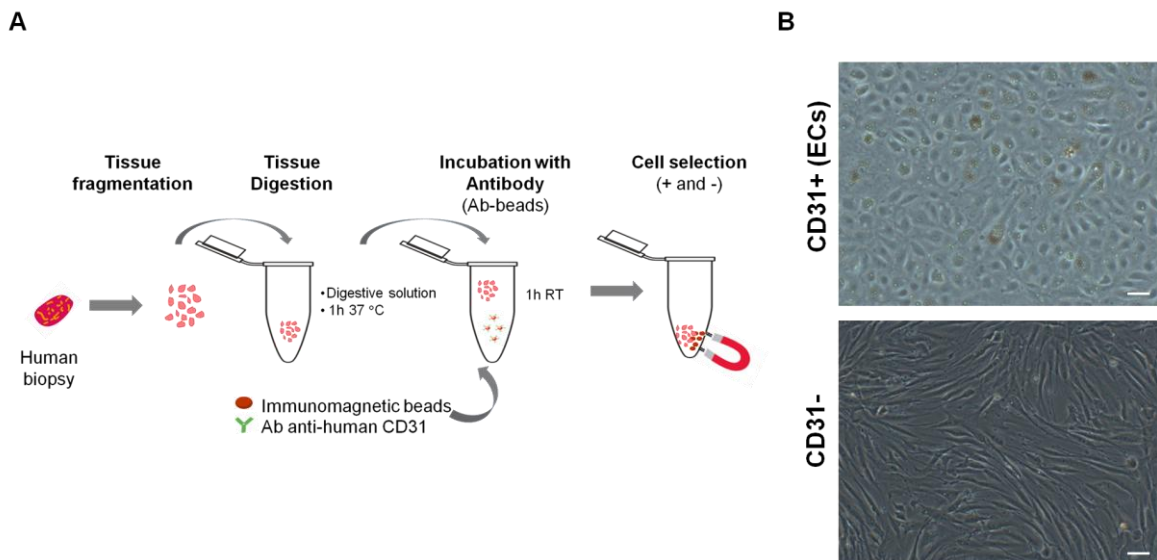
Figure 4.17. Protocol of isolation of primary human cells from vascular malformations biopsies.

A) Schematic representation of the protocol developed for the isolation of human endothelial CD31+ cells and CD31- cells. B) Representative images of CD31+ and CD31- fractions in cell culture. Scale bar 100 µm.

4.3.2 A collection of patient-derided primary human cells to study the biology of VM

Once the protocol of isolation was consolidated, we created a collection of human primary cells derived from patients with different type of vascular malformations (i.e. venous, arteriovenous, capillary and lymphatic). This fundament tool will allow validating and deeply understanding the biology as well as further identifying new mutations responsible for the different human vascular pathologies.

At the completion of this thesis, we successfully isolated CD31+ and CD31- primary cells from 41 patients and the clinical information were collected. Almost 50% of the isolated cells come from patients with Venous Malformations (VM), confirming that VM are the most common type of vascular malformations (**Figure 4.18A**). Since that around 75% of patients with VM have either mutations in *TEK* or *PIK3CA* genes, DNA was extracted directly from the isolated cells and Sanger Sequencing analysis for the main known hot-spot mutations in the TEK and PIK3CA genes (Soblet et al., 2013; Castel et al., 2016; Castillo et al., 2016; Helaers R et al., 2015), frequently associated with vascular anomalies, was performed. In detail, primers amplifying TEK exon 17 (tyrosine kinase domain; c.2690A>G (Y897C), c.2690A>T (Y897F); c.2740C>T (L914F); c.2752C>T (R918C)) and PIK3CA exons 8, 9 (α-helical domain; at sites c.1258T>C (C420R), c.1624G>A (E542K), PIK3CA c.1633G>A (E545K)), and 20 (tyrosine kinase domain; c.3140A>G (H1047R)), were used. As expected, the selected mutations were identified only within the group of VM. TEK^{L914F} mutation was identified in four CD31+ samples, confirming this as the most frequent mutation in our study and in agreement with the literature (Limaye N et al., 2009; Soblet et al., 2013). In addition, *PIK3CA* mutations were identified in two CD31+ samples, one presenting the most frequent oncogenic mutation $PIK3CA^{H1047R}$ and the other one presenting the $PIK3CA^{C420R}$ mutation.

Currently, sequencing analysis did not reveal the simultaneous expression of *TEK* and *PIK3CA* mutations in our primary hECs, confirming the known mutual exclusivity of these mutations. For the remaining VM-derived cells nor *TEK* neither *PIK3CA* mutations were found (**Figure 4.18B**).
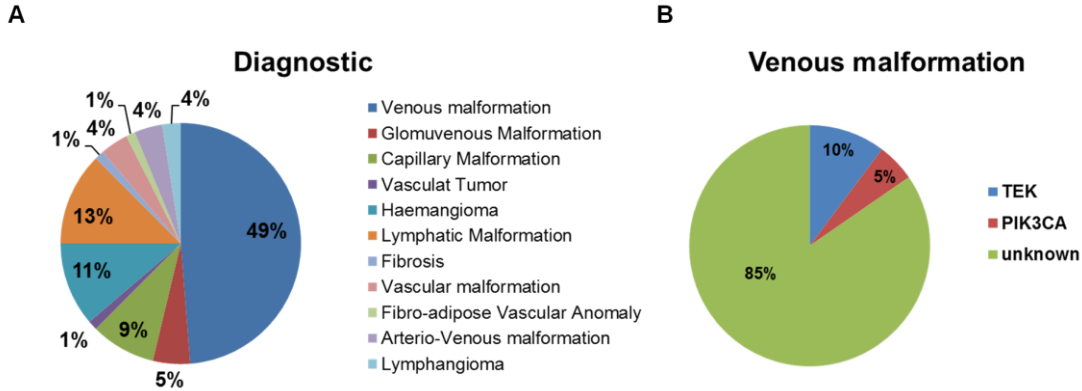
Figure 4.18. Characterization of the collection of primary human cell derived from patients with different type of vascular malformations.

A) Type of vascular malformation of the 38 isolated samples (CD31+ and CD31-) in our collection of primary human cells. B) Percentage of mutations in the TEK and PIK3CA genes within the samples from Venous Malformations.

Next, we took advantage of having identified two CD31+ samples presenting the most common mutation in the *TEK* gene (p.L914F) and in the oncogenic *PIK3CA* mutation (p.H1047R), to perform a thorough characterization of their biology. The CD31+ cells presenting the *TEK*^{L914F} mutation are hereafter referred as VM15 and CD31+ cells presenting the *PIK3CA*^{H1047R} mutation are hereafter referred as VM64.

First, we selected the relative CD31- cells to verify whether they presented the same mutations found in the CD31+ counterpart. As expected, no *TEK*^{L914F} or *PIK3CA*^{H1047R} variants were detected in the CD31- fractions (**Figure 4.19B**), confirming that the identified mutations are only present in the ECs compartment of the vascular malformation. In addition, CD31+ fractions showed a double peak in the analysed variants, indicating the presence of heterozygous mutant cells in the isolated populations (**Figure 4.19A**).

116
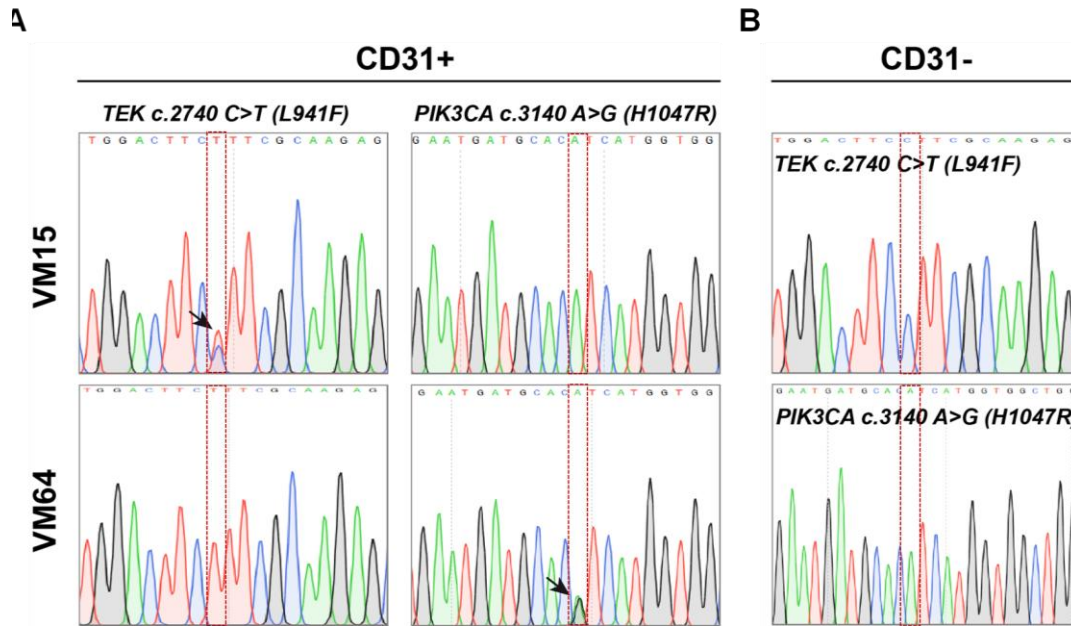
Figure 4.19. Sanger Sequencing analysis for *TEK^L914F* and *PIK3CA^H1047R* mutations.

A) CD31+ cells showed the presence of a mutation (black arrows) at TEK c.2740C > T (p.L914F) for sample VM15 and at PIK3CA c.3140A > G (p.H1047R) for sample VM64. Red islets show localization of the analyzed mutation. No simultaneous expression of TEK and PIK3CA mutations was detected in the same sample, confirming the mutual exclusivity of these two mutations. B) No mutations were identified in the relative CD31-cells of the same patient.

4.3.2.1   Characterization of patient-derived primary human cells

Then, we looked at the expression of ECs-specific markers like CD31 and vascular endothelial (VE)-Cadherin and others by IF analysis (**Figure 4.20**). Human umbilical vein endothelial cells (HUVECs) were used as control of primary human endothelial cells. CD31+ cells clearly expressed CD31 (**Figure 4.20A**) and VE-Cadherin (**Figure 4.20B**), similarly to control HUVECs, and were negative for the expression of smooth muscle alpha actin (αSMA) (**Figure 4.20C**) nor lymphatic marker Prox1 (**Figure 4.20D**).
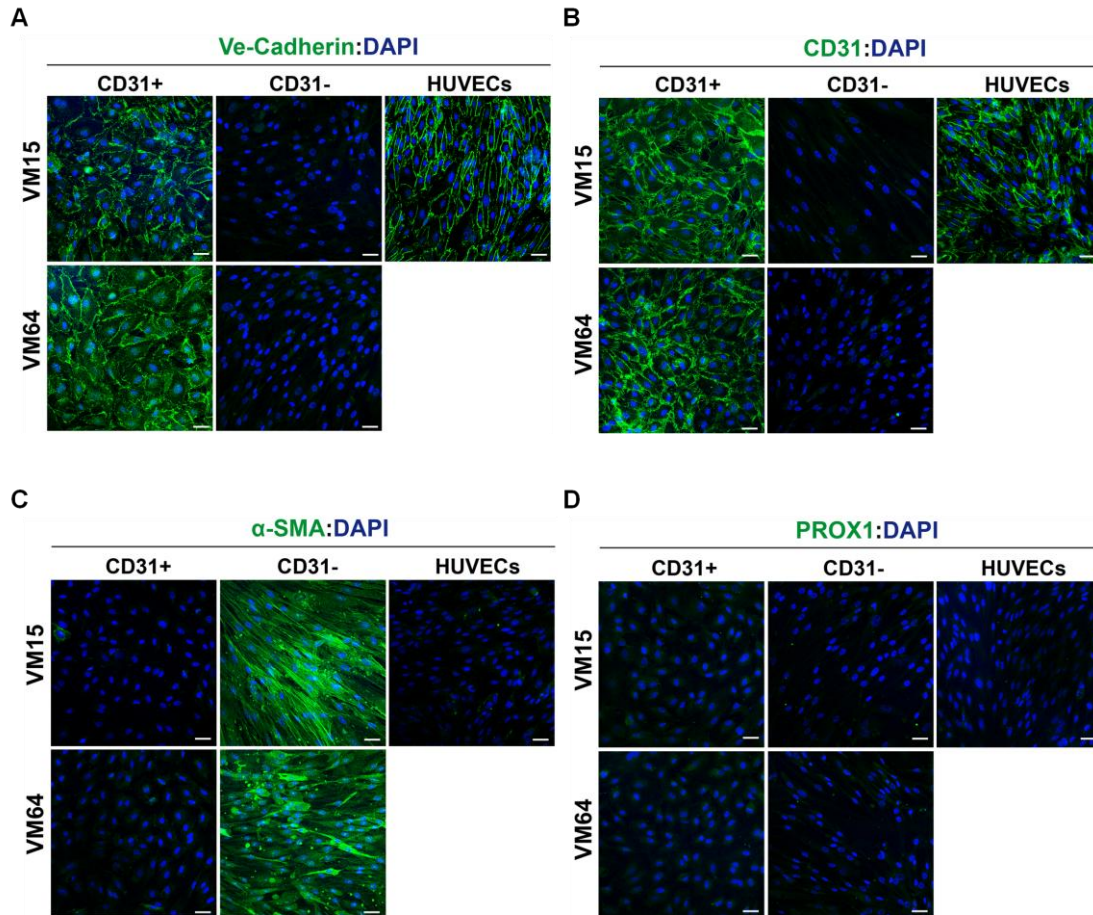
Figure 4.20. Characterization of *TEK^L914F* and *PIK3CA^H1047R* mutant primary human cells.

CD31 + and CD31- fractions immunostained for endothelial and non endothelial markers. Specific markers (green), nuclei (blue). Scale bar 20 µm.

With the aim of further characterise the biology of these cells, we analysed the activation status of the PI3K signalling pathway by WB analysis (**Figure 4.21**). HUVECs and human dermal endothelial cells (HDECs) were used as control cells.

hECs expressing both *PIK3CA^H1047R* (VM64-CD31+) and *TEK^L914F* (VM15-CD31+) mutations showed a constitutive activation of PI3K signalling pathway, demonstrated by elevated p-Akt levels at Ser473 and Thr308, absent or very low in the corresponding CD31- counterparts. *PIK3CA^H1047R* hECs showed a slightly higher activation of PI3K signalling pathway. We also looked at the ERK activation status in the two samples. As expected, ERK activation was higher in the *TEK^L914* mutant hECs when compared to *PIK3CA^H1047R* ones. Finally, we observed that *PIK3CA^H1047R* mutant CD31+ cells presented high VEGFR2 protein levels, which are very low in *TEK^L914F* mutant hECs.
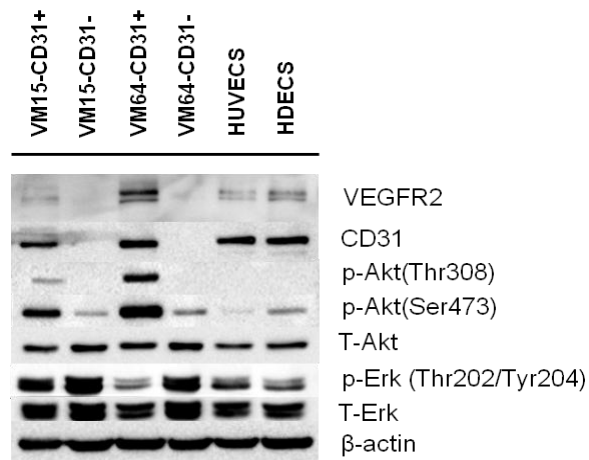
Figure 4.21. PI3K–AKT signalling pathway activation of *TEK^L914^F* and *PIK3CA^H1047R* mutant primary human cells.

Western blot analysis with the indicated antibodies to assess the activation of PI3K signalling pathway in CD31+ and CD31- cells of VM15 (TIE2- p.L914F) and VM64 (PIK3CA p.H1047R) samples. HUVECs and HDECs are controls and β-actin served as loading control.

4.3.2.2 *TEK^L914F^* and *PIK3CA^H1047R^* patient-derived primary human cells exhibit increased proliferation and Itga9 levels

Next, we aimed at validated the biological mechanisms previously identified in mouse ECs also in human cells, with the idea of using the primary human cells as platform for pre-clinical settings. These analyses included both cell proliferation and Itga9 expression in VM15 and VM64 CD31+ cells. The proliferation rate assessed by IF analysis, showed that *PIK3CA^H1047R^* mutant hECs (VM64) presented higher proliferation rate compared to *TEK^L914F^* hECs (VM15) (**Figure 4.22A**). Next, we assessed whether their proliferative capacity was differentially impacted by the treatment with PI3K-mTOR inhibitors. We observed that hECs from both genotypes were sensitive to pan-class I PI3K-inhibitor (GDC-0941) and mTOR-inhibitor (Rapamycin), showing a reduction in the proliferative rate above 15% (**Figure 4.22B**). The proliferation rate was also reduced by the use of the PIK3CA-specific inhibitor (BLY-719), with a proliferation rate around 25-30%, making this inhibitor the less effective in our specific case. Finally, when we compared the two genotypes, we do observe a very comparable behaviour with no differences in the sensitivity to a specific inhibitor, perhaps due to the limited number of biological samples analysed (**Figure 4.22C**).

119
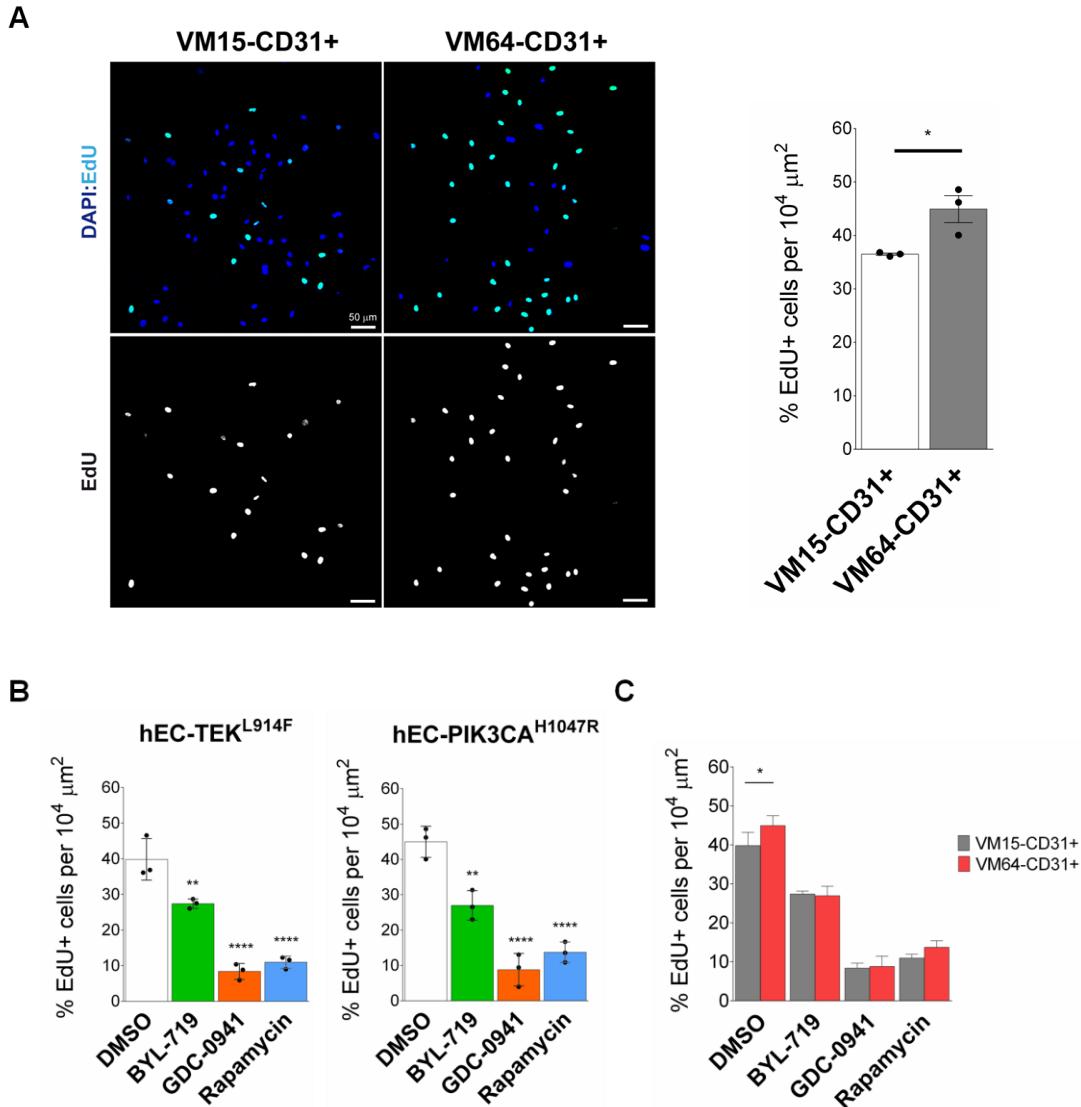
Figure 4.22. Characterization of the proliferation rate in *TEK*[L914F] and *PIK3CA*[H1047R] mutant human primary cells.

A) Assessment of the proliferation rate of VM15 (*TEK*[L914F]) and VM64 (*PIK3CA*[H1047R]) CD31+ cells by IF staining with EdU (light blue) and DAPI (dark blue), scale bar 50 μm. Data represent mean ± SEM of 3 independent replicates.* p<0.05 (Statistical unpaired t test). B) Assessment of the proliferation rate upon the treatment with p110α-specific inhibitor (BLY-719), pan-class I PI3K-inhibitor (GDC-0941) and mTOR-inhibitor (Rapamycin); DMSO was used as a control. Data represent mean ± SEM of 3 independent replicates p****< 0,0001. (Statistical One way ANOVA test). C) Comparison of different inhibitors treatment between the two genotypes. Data represent mean ± SEM of 3 independent replicates.(Statistical 2 way ANOVA test).

Finally, we checked if patients-derived primary cells with a constitutive activation of PI3K signalling pathway were expressing Itga9 protein levels by WB analysis (**Figure 4.23A**). HUVECs and HDECs were used as negative controls. Both *PIK3CA*^{H1047R} (VM64) and *TEK*^{L914F} mutant (VM15) cells expressed solid levels of Itga9, with higher levels in the CD31+ cells compared to CD31- counterpart (**Figure 4.23B**). This evidence confirms the expression of Itga9 protein in patient-derived hECs further confirming the potential role for this integrin in the pathobiology of VM disease.
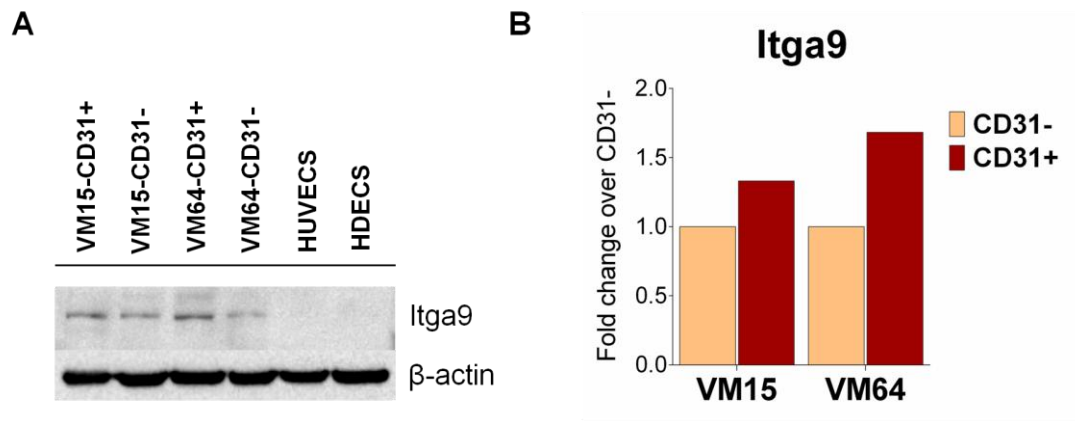
Figure 4.23. Itga9 protein is expressed by primary human cells from Venous Malformations.

A) Western blot analysis and B) quantification of Itga9 protein level in CD31+ and CD31- cells of the VM15 ((*TEK*^{L914F}) and VM64 (*PIK3CA*^{H1047}). HUVECs and HDECs are controls and β-actin served as loading control.

5   Discussion

Venous malformations (VM), the most common type of vascular malformation, are localized defects in vascular morphogenesis characterized by enhanced activation of PI3K signalling pathway. In about 25% of patients, VM are caused by activating mutations in *PIK3CA*. The work presented in this thesis aimed at dissecting the biological mechanisms triggered by the activating PIK3CA-H1047R activating mutation, the most common mutation in the *PIK3CA* gene, in the regulation of ECs behaviour. By developing an innovative approach that combines untargeted transcriptomic analysis with *in vitro* and *in vivo* models, we investigated the biological changes occurring upon early activation of PI3K signalling pathway, to identify key molecular players and cellular processes implicated in the pathogenesis of *PIK3CA*-related VM. In parallel, we set up a new protocol to isolate primary human cells from different type of vascular malformations on a routine basis, allowing the creation of a unique collection of VM-derived cells. These cells are of fundamental importance to investigate, validate and support new biological findings and represent a key pre-clinical tool for transferable research allowing a step towards targeted personalized medicine.

Previous studies demonstrated that both ubiquitous and ECs-specific expression of the *Pik3ca*^H1047R activating mutation in mice is embryonically lethal (Hare et al., 2015; di Blasio et al., 2018). This lethal phenotype is consistent with the observation that genetic evidences of heritable VM with activating mutations in PIK3CA gene have never been reported so far. Consequently, to circumvent the embryonic lethality, we developed a tamoxifen-inducible conditional mouse model (EC-Pik3ca^H1047R) which expresses an endothelium-specific *Pik3ca*^H1047R activating mutation in a heterozygous and endogenous manner, thus reproducing the genetic scenario of VM disease. Furthermore, tamoxifen administration allows the control of *Pik3ca*^H1047R expression in a time-inducible manner, both *in vitro* as well as *in vivo*.

To evaluate the biological effects of the *Pik3ca*^H1047R activating mutation, we first demonstrated that a somatic activating *Pik3ca*^H1047R mutation in ECs compartment is sufficient to generate VM in mice, confirming previous studies (Castillo et al., 2016; Castel et al., 2016). We observed different grades in the penetrance of vascular defects, most likely resulting from different spatial and temporal mosaic acquisition of the mutation in ECs. Specifically, we observed that the expression of *Pik3ca*^H1047R mutation in newborn

animals led to a variable degree of vascular defects, ranging from very mild to extended vascular lesions; suggesting that a reasonable amount of targeted cells is required for a lesion to appear. On the other hand, adult *Pik3ca*^{H1047R} expression always generated localized vascular defects that histologically resemble the human VM-biopsies. Although these pilot studies display some limitations, they have provided important biological information about *Pik3ca*-driven VM. In particular, they suggested that i) a threshold proportion of targeted cells in a specific angiogenic context (e.g. growth) is required for a lesion to appear and ii) the severity of the disease (phenotype) could depend on the period of emergence of mutation. This further supports why during development, early expression of *PIK3CA*^{H1047R} is not compatible with life and is consistent with the lack of reported human hereditary VM driven by *PIK3CA* mutations (Hare et al., 2015). In addition, the identification of the same oncogenic *PIK3CA* mutations in different types of vascular malformations other than VM, such as lymphatic malformations (LM) or combined capillary lymphatic venous malformations (CLVM) further indicates that the type, location and/or severity of the vascular anomaly are likely dependent on when and/or what ECs lineage or progenitor cells the mutational event occurs during development. Although they are believed to occur during embryogenesis, the timing and origin of these mutations remain undefined and the cellular origin likely involves ECs or an early endothelial cell progenitor. Nevertheless, altogether these set of evidence highlight that ECs are extremely sensitive to PI3K signalling pathway and that its activity needs to be tightly regulated for a correct vascular development.

Given that very little is known about how PIK3CA-H1047R mutation induces pathogenesis in ECs, we first aimed at studying the impact of this mutation during angiogenesis. To accurately determine the biological role of *Pik3ca*^{H1047R} in angiogenesis, we chose the retinal vascular tissue as our principal model to mimic the VM disease. This is a state-of-the-art biological system to study vasculature development at high resolution, as it develops a stereotypical vascular pattern in a well-defined sequence of events during the first week after birth in mice. The simultaneous vascular sprouting at the periphery and the remodelling and maturation at the centre of the postanatal retina, allow for the study of the various steps of vessel formation and maturation in a single preparation. Specifically, we induced the expression of *Pik3ca*^{H1047R} at postnatal day 1 (P1) and then we harvested the retinas at P6, when the spreading of the inner vascular plexus proceeds from the optic nerve to the peripheral margins of the retina, allowing to study the formation of the superficial vascular plexus.

Fundamental studies from our lab demonstrated that PI3Kα, encoded by PIK3CA gene, is the only PI3K isoform essential during vascular development and remodelling (Graupera et al., 2008) and that it critically regulates the collective cell migration during angiogenesis (Angulo et al., 2018). Moreover, we demonstrated that endothelial expression of *Pik3ca^{H1047R}* in postnatal retinas results in hyperplastic vessels associated with increased ECs proliferation and defective pericyte coverage (Castillo et al., 2016). However, this phenotype does not fully recapitulate the aetiology of *PIK3CA*-related VM in which enlarged, but distinct hyperplastic vascular channels are present.

To better model the disease we first studied the impact of different 4OH-tamoxifen doses on the VM phenotype. Following what was previously suggested, we started by considering that a reasonable number of targeted cells (not too many and not too little) would lead to the appearance of isolated hyperplastic vascular lesions. So we titrated several 4OH-tamoxifen doses until we found the proper one that recapitulated the different features of VM disease. These included increased sprouting activity, enhanced vessel density and diameter and profound changes in the remodelling and maturation area, where the appearance of distincts localized hyperplastic malformed vessels occurred. These *in vivo* data indicated that early endothelial *Pik3ca^{H1047R}* expression in mice strongly impacts the correct vascular development not only by interfering during sprouting angiogenesis, leading to the formation of abnormal vessels in size and shape, but also in remodelling and maturation processes, when nascent vessels mature to become stable and functional, causing the onset of localized venous-capillary malformations.

The remodelling and maturation steps require critical endothelial cell-cell and cell-matrix interactions to form firm endothelial cell–cell junctions, to recruit supporting mural cells and to guide the deposition of the ECM. The above mentioned *in vivo* evidence is further supported by the fact that, histologically, human VM appear as dedifferentiated and immature vessels, characterized by the lack of supporting mural cells and a disorganized ECM (Dompmartin et al., 2010; Nätynki et al., 2015; Lymaye et al.2015). Although not yet identified, these features could be linked to alterations in ECs adhesion, mural cells recruitment by chemoattractants, a combination of both or even other unknown events (Brouillard and Vikkula 2003).

To investigate at deeper molecular and cellular levels the biological impact of the PIK3CA-H1047R activating mutation in the endothelium we moved to *in vitro* studies. Our data show that PI3K signalling in ECs is a potent inducer of transcriptional changes. This is interesting, as the molecular signature identified offers a novel way to address

fluctuations in PI3K signalling at least in these cells. At the moment it is unclear through which transcriptional factor *Pik3ca* regulates transcriptional changes. FOX proteins are a subgroup of the Forkhead family of transcription factors. Specifically, members of class 'O' (FoxO) share the characteristic of being negatively regulated by PI3K/AKT signalling pathway. Amongst the FoxO members, FoxO1 sustains ECs quiescence during vascular development (Wilhelm et al., 2016). Hence, it is tempting to speculate that the *Pik3ca*-related transcriptional program is regulated by FoxO1.

We thoroughly analysed the transcriptomic profile of acutely regulated *Pik3ca^{H1047R}* mutant ECs by performing an untargeted RNA sequencing followed by a bioinformatic analysis. This analysis firstly confirmed the oncogenic nature of the mutation, which mainly triggers the expression of genes involved in the control and regulation of the cell cycle, finally leading to enhanced ECs proliferation, both *in vitro* as well as *in vivo*. This data is in line with recent published studies (Castillo et al., 2016; Castel et al., 2016; di Blasio L et al., 2018) and has been further validated in primary human VM-derived ECs, where *PIK3CA^{H1047R}* mutant ECs showed a proliferative advantage compared to ECs bearing the most common *TIE2^{L914F}* mutation. Subsequently, we demonstrated that this aberrant hyperproliferative behaviour of ECs *in vivo* is responsible for the increased vessel density and diameter in the sprouting front, as well as for the formation of isolated hyperplastic vessels in the remodelling area of P6 postnatal retinas.

Then, we demonstrated that these isolated malformed vessels were specifically localized in veins and in capillaries to a less extent, but never in the arteries, supporting the venous identity of the malformed vessels and correctly reproducing the human VM disease context. The crucial role exerted by the hyperproliferative state of ECs in the generation of localized VM only in the venous and capillaries compartments is further supported by the fact that ECs proliferation in mouse retinas is reported to peak at P5 (Franco et al., 2015) and occurs predominantly in veins and capillaries (Ehling et al., 2013; Laviña et al., 2018). Moreover, p110α physiologically regulates the venous identity of ECs (Herbert et al. 2009), while arteriogenesis requires PI3K inhibition (Hong et al., 2006); overall confirming the role for *Pik3ca^{H1047R}* mutation in targeting venous and capillary ECs.

From a clinical perspective, this data is extremely interesting because it suggests a causative role for the oncogenic hyperproliferative behaviour of ECs in interfering with the overall vascular development and remodelling. So far, VM have always been considered as nonproliferative lesions (Mulliken and Glowacki 1982; Enjolras 1997, Enjolras and

Mulliken 1997; Enjolras et al., 2007; Wassef et al., 2015), in agreement with the idea that the vasculature primarily expands during embryonic development and remains quiescent in adulthood. This suggested that the presence of the mutation in only ECs is not sufficient to result in high proliferative vascular lesions, and thereby angiogenic growth factor signals are required to promote proliferation. Here, we demonstrate that *Pik3ca*-driven VM are localized proliferative lesions caused by somatic and mosaic expression of *Pik3ca*[H1047R] activating mutation. A further support of this assumption can be easily found by considering the "oncogenic" nature of this mutation, which implies that it confers a selective growth advantage (Strattonet al., 2009). However, murine cancer models demonstrate that activating *Pik3ca* mutations require cooperating genetic lesions to induce and maintain cancer (Robinson et al., 2012; Green et al., 2015; Van Keymeulen et al., 2015). This could partially explain why *PIK3CA*-vascular malformations are not yet considered as vascular tumours.

Following the analysis of the expression profiling of *Pik3ca*[H1047R] mutant ECs, we found that the preponderance of differentially regulated transcripts in Gene Ontology (GO) categories favours cell adhesion and cell migration processes as strongly affected by the H1047R activating mutation. Targeted validation of individual genes by RT-qPCR demonstrated that acute expression of *Pik3ca*[H1047R] *in vitro* strongly impacts the gene expression of several adhesive molecules in ECs, such as the vascular cell adhesion molecule 1 (*Vcam1*), the cellular communication network factor 1 (*Ccn1*) and the protocadherin 12 (*Pcdh12*). The function of the latter *Pcdh12* gene, which encodes for the cellular adhesion protein VE-cad2, is undetermined but may play an important role in cell-cell interactions at inter-endothelial junctions, acting as a regulator of cell migration, probably via increasing cell-cell adhesion clustering at intercellular junctions (Bouillot et al., 2011). Following the lead of an altered adhesive signature, we interestingly observed a strong dysregulation in the expression of the integrin repertoire. Integrins are cell adhesion receptors that mediate cell-cell and cell-matrix interactions (van der Flier and Sonnenberg 2001; Hynes 2002). They are heterodimeric transmembrane receptors composed of α- and β- subunits, which play essential roles in developmental processes that involve close interactions between cells and their surrounding ECM. Their extracellular domains bind to the ECM molecules while the cytoplasmic domains associate with the actin cytoskeleton and affiliated proteins, thereby providing a link between the external and internal environment of the cell (Geiger et al., 2001) and a physical anchor between cell cytoskeleton and ECM. Integrins are crucial in angiogenesis and for vascular integrity as

127

they are the major mediators of vascular cell adhesion and migration through the ECM (Somanath PR et al.2009). In addition to mediating binding to their respective ECM ligand(s), they have specialized signalling functions and they can regulate gene expression as well as cell shape, migration, proliferation and survival. Moreover, ECM-integrin binding is not only required for transducing signals from the matrix to cells but this interaction also initiates responses that allow the cells to organize and remodel the matrix (Leiss et al., 2008). Furthermore, it is important to note that integrin–ECM adhesions are not static unchangeable structures and that dynamic remodelling of the ECM by ECs is critical for vascular morphogenesis (Davis and Senger 2005; Cseh et al., 2010). In this way, integrins receptors and their cognate ECM components, such as FN, play critical roles in the development of the blood vasculature (Hynes, 2007).

We validated the identified molecular changes in the adhesive integrins profile by demonstrating that they i) are cumulative in time ii) are specific of ECs and iii) could be rescued by the use of PI3K inhibitors. These molecular data suggested that the adhesive capacity of ECs expressing the oncogenic $Pik3ca^{H1047R}$ activating mutation is strongly affected. To support this statement, adhesive assays by using different ECM substrates including FN, vitronectin, laminin and collagen are currently ongoing to assess the impaired adhesive capacity of ECs upon acute and sustained expression of $Pik3ca^{H1047R}$.

Nevertheless, an altered ECs adhesive capacity can be referred towards both cells, like other ECs or mural cells, as well as to substrates, such as components of the ECM. Indeed, defective pericyte coverage and a disorganized ECM are prototypical characteristics of VM disease and are features strictly associated to vessel remodelling and maturation. The lack of appropriate pericytes associations makes the vessels less stable, thus allowing abnormally high levels of degeneration to occur and ultimately leading to excessive remodelling and abnormal vascular patterns. By confirming that P$ik3ca^{H1047R}$ activation in ECs reduces $Angpt2$ and $Pdgfb$ mRNA levels, we supported our previous study in which EC-Pik3ca^{H1047R} postnatal retinas showed reduced $Pdgfb$ production and defective pericyte coverage (Castillo et al., 2016). In addition, integrins have been recently shown to act as non-canonical receptors for the angiopoietin-2 (ANG2) growth factor, an important regulator of vascular homeostasis (Hakanpaa et al., 2015). In this study Hakanpaa and colleagues showed that ANG2 binding to FN-receptor integrin $\alpha 5 \beta 1$ activates the integrin, leading to destabilized endothelial cell–cell junctions and altered FN fibrillogenesis. Thus, we can speculate that decreased autocrine ANG2 levels,

together with altered integrins profile and signalling, could cooperate to promote changes in ECs cytoskeleton, matrix adhesion and cell junctions that may lead to an alteration in cell–cell adhesion and integrity of EC-monolayer, which may predispose vessels to endothelial destabilization. Furthermore, the activation state of integrins regulates the capacity of cells to assemble a FN matrix (Wu et al., 1995).

Here, we demonstrated that early as well as sustained expression of *Pik3ca*^{H1047R} in ECs strongly decreases the expression of endothelial FN, a key ECM protein, suggesting that it may have a central role in the formation of VM lesions. The loss of ECM FN in culture has been previously reported by other studies, in both TIE2-VM mutations (Nätynki et al.2015; Iymaye et al., 2015) and in PIK3CA-VM variants (Iymaye et al., 2015), and has been associated with disrupted ECs-characteristic monolayer morphology. In particular, ECs secrete FN as a soluble dimer that is then reorganized into a fibrillar network outside of the cell. In this bioactive fibrillar form, FN provides important mechanical and chemical cues necessary for endowing ECs with a sense of polarity during vascular tubulogenesis (George et al., 1997; Zhou et al., 2008; Zovein et al., 2010). Moreover, FN interacts with and functions as a scaffold for proper assembly of many ECM and BM components (Kostourou and Papalazarou 2014), representing the most essential ECM protein for angiogenesis and vascular development (Astrof and Hynes 2009). In gene-targeted mouse embryos, lack of FN results in defective morphogenesis, including dilated and malformed vessels, and loss of endothelial–mural contacts (George et al., 1997). Furthermore, it has been demonstrated that FN also binds the endothelial integrin α5β1 to potentiate TIE2 signalling induced by angiopoietin-1 (Cascone et al., 2005).

Overall, vascular development and morphogenesis is a very complex and tightly regulated process, with mounting evidence that highlight the fundamental requirement for a coordinated activity of growth factors and integrin–ECM signalling pathways in establishing and maintaining a normal functioning of vascular network. Here, we postulate that *Pik3ca*^{H1047R} mutation might interfere/destabilize vessel development and morphogenesis either directly, by affecting the adhesion property of ECs to its microenvironment, including cells and ECM proteins, and indirectly, by regulating the composition and/or organization of the ECM itself; suggesting a continuous ECM remodelling. In detail, our data suggest that the adhesion capacity of ECs is affected during constitutive PI3K pathway activation and support a linked mechanism between PI3K and Integrins pathways.

Among the analysed α- and β- integrins subunits, we found that integrin-α9 (Itgα9) is the most upregulated integrin upon *Pik3ca^{H1047R}* expression in ECs. The α9 subunit, by forming a single known heterodimer α9β1, is the most recent FN-binding integrin with a role in angiogenesis (Vlahakis NE et al., 2007; Staniszewska I, et al., 2007; Liao YF, et al., 2002; Marcinkiewicz C, et al. 2000). It is a receptor for a number of ECM proteins and plays a role in ECs adhesion and facilitates accelerated cell migration (Vlahakis NE et al., 2007). Furthermore, it has been implicated in diverse biological functions including lymphangiogenesis, lymphatic valve morphogenesis and tumorigenesis (Gupta SK and Vlahakis NE, 2010). As of now, no deregulation in integrins profiles has been previously identified in the VM context and only one study mentioned a role for Itgα9 as a candidate gene for valve defects underlie human lymphedema (Bazigou et al., 2009). At the cellular level we observed that only mouse ECs, and not murine embryonic fibroblasts (MEFs), increased their Itgα9 protein levels upon early expression of *Pik3ca^{H1047R}*, presenting a shift of its subcellular localization from the cytoplasm to the membrane level.

This increase has also been observed in the EC-Pik3ca^{H1047R} postnatal retinas, where Itgα9 accumulates in the hyperplastic dilated vessels of the sprouting front and in the localized malformed vessels of the remodelling area. Although this *in vivo* Itgα9 staining looks promising, we cannot rule out that the EC-Pik3ca^{H1047R} retinas staining is specific. In fact, it is possible that the antibody used in our study exhibits cross-reactivity with IgG proteins of the serum and/or with blood cells; a common phenomenon when studying mutants who show an impaired blood flow within malformed vessels. We are currently validating our results by using a novel anti-α9 antibody to confirm its increased levels upon *Pik3ca^{H1047R}* expression. However, to further support the role of Itgα9 protein in VM context we checked its expression level in patients derived VM-cells. While we did not observe Itgα9 protein levels in HUVECs and HDECs control cells, we observed that human VM-cells with a constitutive PI3K pathway activation, caused either by *PIK3CA^{H1047R}* or *TIE2^{L914F}* mutations, express Itgα9 protein levels, with solid and higher levels in endothelial CD31+ cells compared to CD31- counterpart. Altogether, these data strongly support a critical role for Itgα9 in the pathogenesis of VM. Specifically, we speculate that Itgα9, by interacting with its ligand FN-EIIIA (Bazigou et al., 2009), may directly regulate FN fibril assembly, interfering with the formation and deposition of ECM in newly formed vessels. To fully validate this statement, future studies assessing the FN fibril assembly status *in vitro* as well as *in vivo* will be of fundamental importance.

Interestingly, it has been demonstrated that FN, through the activation of PI3K pathway, mediates cell migration (Stenzel et al., 2011). As transmembrane receptors, integrins are responsible for transducing and modulating dynamic interactions between the extracellular environment and actin cytoskeleton, ultimately influencing cell functions such as adhesion and migration. Indeed, adhesion and migration are integrated cellular functions and are early essential events during sprouting of new blood vessels from the existing vasculature (Ausprunk and Folkman 1997). To migrate, vascular ECs require adhesion to ECM and integrins are considered the main mediators of adhesion force generation during cell migration (Schmidt and Friedl 2010).

We demonstrated that $Pik3ca^{H1047R}$ expression interferes with the migratory capacity of ECs, inducing ECs to migrate faster. This evidence has been further supported by the transcriptomic analysis, which revealed that endothelial nitric oxide (NO) synthase (eNOS) is the transcript most upregulated upon $Pik3ca^{H1047R}$ activation in ECs. AKT phosphorylation of eNOS at Ser1177 leads to increase in eNOS activity and NO production (Fulton et al., 1999; Dimmeler et al., 2000), which can stimulate vasodilation, vascular remodelling and angiogenesis (Manning and Cantley, 2007). The same phosphorylation is also required for VEGF-induced ECs migration (Dimmeler et al., 2000). Furthermore, eNOS supports ECs migration, at least partly, via integrin-dependent mechanisms (Murohara et al., 1999). Therefore, a possible explanation for the formation of abnormal vessel structures during vessels development and morphogenesis could rely on the fact that increased Itgα9 expression in ECs could cause an aberrant adhesion and migration of ECs that incorrectly distribute within the vascular network. In line with this concept, a very recent study by Laviña and colleagues describes that defective cell migration causes severe capillary-venous malformations when ECs are unable to redistribute within the vascular tree (Laviña et al., 2018). In fact, newly formed sprouts are highly dynamic, with ECs interchanging their relative position within the vascular network (Jakobsson et al., 2010; Arima et al., 2011; Bentley et al., 2014; Phng et al., 2015). This collective cell migration across the vascular tubes relies on ECs rearrangement that occurs through the reorganization of cell–cell junctional contacts; thereby allowing the modification of cell−cell adhesion strengths (Millán et al., 2010; Huveneers et al., 2012; Lenard et al., 2013; Bentley et al., 2014). This suggests that a tight regulation of endothelial cell movement, beyond tip cells, is necessary for an adequate patterning of the vascular plexus and that aberrant junctional remodelling are indicative of defects in cell rearrangements (Sauteur et al., 2014). Our lab recently demonstrated that PI3Kα signalling

critically regulates junctional remodelling and cell rearrangement in ECs by controlling actin dynamics (Angulo et al., 2018).

Overall, this thesis demonstrates that the activating *Pik3ca*^{H1047R} mutation alters the integrins expression prolife of ECs and given that aberrant adhesion of ECs to the ECM compromises the formation of stable adherent junctions *in vivo* (Fraccaroli et al., 2015), we can speculate that the upregulation of Itgα9 could promote aberrant adhesion of ECs to the ECM, promoting changes in the ECs cytoskeleton and in the junctional remodelling that might finally affect ECs rearrangement. These changes can affect the collective ECs migration across the newly formed vascular network by inducing ECs to migrate faster. In this way, aberrant ECs could fail to properly remodel and stabilize new cell-cell contacts upon anastomosis, causing localized remodelling defects that lead ECs to grow in aberrant malformed vessels. Specifically, we postulate that VM build up by the local crowding of ECs, which are unable to properly distribute within the vascular network. This speculation implies that *Pik3ca*^{H1047R} expression specifically interferes with ECs actin cytoskeleton, influencing the shape and regulating focal adhesions and junctional status of ECs. Future studies are directed to confirm these statements.

Overall, our work shows for the first time a key role for integrins in VM pathogenesis, demonstrating a link between integrins and PI3K signalling pathways in the regulation of ECs behaviour. Collectively, our findings indicate that a constitutive activation of PI3K signalling in ECs leads to both an increase of proliferative and migratory capacities. We demonstrated that oncogenic *Pik3ca*^{H1047R} mutation affects the adhesive molecular profiles of ECs, with a particular role for the integrins repertoire. We propose that this aberrant integrins adhesive capacity of ECs drives aberrant interaction of ECs to their surrounding environment, including supporting mural cells and ECM interaction and organization. Furthermore, we demonstrated that oncogenic *Pik3ca*^{H1047R} mutation decreases endogenous FN level produced by ECs, which might regulate accelerated ECs migration. We propose Itgα9 as a key mediator for the described aberrant ECs behaviour. Altogether, our findings provide guidance for the development of novel targeted therapies that could be used in combination with PI3K inhibitors.

Furthermore, my thesis has been instrumental in developing murine and human pre-clinical systems that can be used in combination to obtain complementary pre-clinical biological information. Current PIK3CA mutation-based models include a patient-derived EC xenograft (Goines et al., 2018) and murine models with transgenic expression of

Pik3ca^{H1047R} in the embryonic mesoderm or in VE-Cadherin$^+$ cells (Castillo et al., 2016; Castel et al., 2016; di Blasio et al., 2018), recapitulating a mixed vascular disease instead of a specific venous phenotype.

Here, we developed a mouse model that reproduces the genetic and phenotypic characteristics of VM disease in a more precise fashion, recapitulating the scenario of a naturally occurring somatic mutation in ECs and providing the necessary pre-clinical mouse model to study specific molecular-targeted treatments for VM. Furthermore, by inducing the expression of the somatic mutation in different timeframes, we were able to obtain diverse phenotypes burdens, reflecting the heterogeneous human VM phenotypes. Hence, this mouse model permits the modelling of a more comprehensive *PIK3CA*-driven VM disease, allowing the performance of diverse pre-clinical trials according to different VM-phenotypes. In addition, this mouse model could also be further exploited to obtain additional fundamental biological information; e.g. it could be crossed with an mTmG reporter mouse line to define the amount and distribution of targeted ECs triggering the development of VM lesions. Taken together, our evidences highlight the capability of our mouse model to efficiently recreate the *in vivo* context of VM disease, including the complex and dynamic interplay between cells and their microenvironment, which can better help in confirming drugs' efficacy.

In addition, we developed an efficient protocol of isolation to obtain patients' derived primary cells from different type of vascular malformations. This protocol allows to isolate the main cellular components of vascular malformations, represented by CD31+ and CD31- cells, which we used to progressively validate the biological statements generated during this thesis's work.

Overall, these primary cells represent an enormous window of opportunities for the fundamental understanding of venous and vascular malformations pathogenesis. They represent a key tool to explore the comprehensive genetic landscape of venous and vascular diseases, that could inform and direct future classification and stratification systems, allowing both more precise diagnoses and clinical management and, more importantly, the development of targeted therapeutic opportunities.

We are currently creating a collection of patient derived primary cells, which represents a unique and reliable pre-clinical platform to explore VM patients' genetic background and heterogeneity. In this way, human cells will reflect different cellular

susceptibility when testing the differential therapeutic efficacy of various compounds or when testing the efficacy of additional compounds in targeting the specific mutated protein(s); thus enabling the development of personalized treatment options for VM patients in the presence of different *TIE2* or *PIK3CA* mutations. Finally, as recently described by Goines and colleagues (Goines at al., 2018), these cells could also be injected into immune-deficient mice to create an artificial xenograft model that allows to study the relationship between VM-blood vessels characteristics and the mutation type injected, to study the pathology of VM disease on a patient-to-patient basis.

6   Conclusions

1. We have set up novel *in vitro* and *in vivo* models of PI3K-driven VM, which are necessary for the study of their biology as well as the development of molecular targeted therapies;

2. We have set up a unique protocol for the isolation and culture of patient-derived cells from VM. With this, we have demonstrated that mutations are only present in the ECs lineage from these lesions;

3. With our novel mouse model for PI3K-driven VM we have demonstrated that VM arise from ECs-specific somatic mutation in *Pik3ca* and only occur in veins and capillaries. The amount of mutant ECs define the severity of the VM-phenotype;

4. *Pik3ca^{H1047R}* expression induces transcriptomic changes that lead to the reprogramming of adhesion molecular signature, with a particular role for the integrins repertoire. Among these, Integrin-α9 is the most upregulated in ECs;

5. At the cellular level, *Pik3ca^{H1047R}* expression leads to enhanced proliferation and migration of ECs, which might drive aberrant ECs behaviour during vascular development and morphogenesis causing VM.

7   References

Adams RH and Alitalo K. (2007). Molecular regulation of angiogenesis and lymphangiogenesis.*Nat Rev Mol Cell Biol.*8(6): p. 464-78.

Adams DM, Trenor CC, Hammill AM, Vinks AA, Patel MN, Chaudry G et al. (2016). Efficacy and safety of sirolimus in the treatment of complicated vascular anomalies. *Pediatrics* 137:e20153257.

Ali S, Mitchell S. (2017). Outcomes of venous malformation sclerotherapy: a review of study methodology and long-term results. *Semin Intervent Radiol.*34:288–93.

Ara T, Tokoyoda K, Okamoto R, Koni PA, Nagasawa T. (2005). The role of CXCL12 in the organ-specific process of artery formation. *Blood.*15: 105(8):3155-61.

Arima S, Nishiyama K, Ko T, Arima Y, Hakozaki Y, Sugihara K, Koseki H, Uchijima Y, Kurihara Y, Kurihara H.(2011). Angiogenic morphogenesis driven by dynamic and heterogeneous collective endothelial cell movement. *Development.* 138(21):4763-76.

Asahara T, Chen D, Takahashi T, Fujikawa K, Kearney M, Magner M, Yancopoulos GD, Isner JM. (1998). Tie2 receptor ligands, angiopoietin-1 and angiopoietin-2, modulate VEGF-induced postnatal neovascularization. *Circ Res.* 83(3):233-40.

Astrof S and Hynes RO. (2009). Fibronectins in vascular morphogenesis. *Angiogenesis.*12,165-175.

Augustin HG, Koh GY, Thurston G, Alitalo K. (2009). Control of vascular morphogenesis and homeostasis through the angiopoietin-Tie system. *Nat Rev Mol Cell Biol.*10(3):165-77.

Ausprunk DH, Folkman J. (1997). Migration and proliferation of endothelial cells in preformed and newly formed blood vessels during tumor angiogenesis. *Microvasc Res.*14(1):53-65.

Backer JM. (2008). The regulation and function of Class III PI3Ks: novel roles for Vps34. *Biochem J.*410:1–17.

Backer, J.M. (2016). The intricate regulation and complex functions of the Class III phosphoinositide 3-kinase Vps34. Biochem. J. 473, 2251–2271.

Bader AG, Kang S, Zhao L, Vogt PK. (2005). Oncogenic PI3K deregulates transcription and translation. *Nat Rev Cancer.*5(12):921-9.

Bazigou E, Xie S, Chen C, Weston A, Miura N, Sorokin L, Adams R, Muro AF, Sheppard D, Makinen T. (2009). Integrin-alpha9 is required for fibronectin matrix assembly during lymphatic valve morphogenesis. *Dev Cell.* 17(2):175-86.

Behravesh S, Yakes W, Gupta N, Naidu S, Chong BW, Khademhosseini A et al. (2016). Venous malformations: clinical diagnosis and treatment. *Cardiovasc Diagn Ther.* 6:557–69.

Bentley K, Franco CA, Philippides A, Blanco R, Dierkes M, Gebala V, Stanchi F, Jones M, Aspalter IM, Cagna G, Weström S, Claesson-Welsh L, Vestweber D, Gerhardt H. (2014). The role of differential VE-cadherin dynamics in cell rearrangement during angiogenesis. *Nat Cell Biol.* 16(4):309-21.

Berenjeno IM et al. (2017). Oncogenic PIK3CA induces centrosome amplification and tolerance to genome doubling. *Nat Commun.* 8(1):1773.

Bilanges B, Posor Y, Vanhaesebroeck B. (2019). PI3K isoforms in cell signalling and vesicle trafficking. *Nat Rev Mol Cell Biol.* 20(9):515-534.

Boscolo E, Limaye N, Huang L, Kang KT, Soblet J, Uebelhoer M, Mendola A, Natynki M, Seront E, Dupont S, Hammer J, Legrand C, Brugnara C, Eklund L, Vikkula M, Bischoff J, Boon LM. (2015). Rapamycin improves TIE2-mutated venous malformation in murine model and human subjects. J *Clin Invest.*125 (9):3491-504.

Boscolo E, Coma S, Luks VL, et al. (2015-b). AKT hyper-phosphorylation associated with PI3K mutations in lymphatic endothelial cells from a patient with lymphatic malformation. *Angiogenesis.* 18:151–162.

Bouillot S, Tillet E, Carmona G, Prandini MH, Gauchez AS, Hoffmann P, Alfaidy N, Cand F, Huber P. (2011). Protocadherin-12 cleavage is a regulated process mediated by ADAM10 protein: evidence of shedding up-regulation in pre-eclampsia. *J Biol Chem.* 286(17):15195-204.

Brooks PC, Clark RA, Cheresh DA. (1994). Requirement of vascular integrin $\alpha v \beta 3$ for angiogenesis. *Science.* 264:569–571.

Brouillard P, Vikkula M. (2003). Vascular malformations: localized defects in vascular morphogenesis. *Clin Genet.* 63(5):340-51.

Brouillard P, Vikkula M.(2007). Genetic causes of vascular malformations. *Hum Mol Genet.* 2007. 16 Spec No. 2:R140-9.

Burke JE, Perisic O, Masson GR, et al. (2012). Oncogenic mutations mimic and enhance dynamic events in the natural activation of phosphoinositide 3-kinase p110alpha (PIK3CA). *Proc Natl Acad Sci U S A.* 109:15259–15264.

Burke, J.E., and Williams, R.L. (2015). Synergy in activating class I PI3Ks.*Trends Biochem. Sci.* 40, 88–100.

Burrows PE, Mason KP. (2004). Percutaneous treatment of low flow vascular malformations. *J Vasc Interv Radiol.*15(5):431–445.

Boutouja F, Stiehm CM, Platta HW. (2019). mTOR: a cellular regulator interface in health and disease. Cells. 8(1):18.

Byzova TV, Goldman CK, Pampori N, Thomas KA, Bett A, Shattil SJ,Plow EF. (2000). A mechanism for modulation of cellular responses to VEGF: activation of the integrins. *Mol Cell.* 6:851–860.

Cain RJ, Vanhaesebroeck B, Ridley AJ. (2010). The PI3K p110alpha isoform regulates endothelial adherens junctions via Pyk2 and Rac1. *J Cell Biol.* 188(6):863-76.

Carmeliet, P. (2003). Angiogenesis in health and disease. *Nat. Med.* 9,653–660.

Carmeliet P, Jain RK. (2011). Principles and mechanisms of vessel normalization for cancer and other angiogenic diseases. *Nat Rev Drug Discov.* 10(6):417-27.

Cascone I, Napione L, Maniero F, Serini G, Bussolino F. (2005). Stable interaction between alpha5beta1 integrin and Tie2 tyrosine kinase receptor regulates endothelial cell response to Ang-1. J. Cell Biol., 170, 993–1004.

Castel P, Carmona FJ, Grego-Bessa J, Berger MF, Viale A, Anderson KV, Bague S, Scaltriti M, Antonescu CR, Baselga E, Baselga J. (2016). Somatic PIK3CA mutations as a driver of sporadic venous malformations. *Sci Transl Med.* 30; 8(332):332ra42.

Castillo SD, Tzouanacou E, Zaw-Thin M, Berenjeno IM, Parker VE, Chivite I, Milà-Guasch M, Pearce W, Solomon I, Angulo-Urarte A, Figueiredo AM, Dewhurst RE, Knox R, Clark GR8, Scudamore CL, Badar A, Kalber TL, Foster J, Stuckey DJ, David AL, Phillips WA, Lythgoe MF, Wilson V, Semple RK, Sebire NJ, Kinsler VA, Graupera M, Vanhaesebroeck B. (2016). Somatic activating mutations in Pik3ca cause sporadic venous malformations in mice and humans. *Sci Transl Med.*30; 8 (332):332ra43.

Castillo SD, Baselga E, Graupera M. (2019). PIK3CA mutations in vascular malformations. *Curr Opin Hematol.*;26(3):170-178.

Cébe-Suarez S, Zehnder-Fjällman A, Ballmer-Hofer K. (2006). The role of VEGF receptors in angiogenesis; complex partnerships.*Cell Mol Life Sci.* 63(5):601-15.

Chen J, Somanath PR, Razorenova O, Chen WS, Hay N, Bornstein P, Byzova TV. (2005). Akt1 regulates pathological angiogenesis, vascular maturation and permeability in vivo. *Nat Med.* 11:1188–1196.

Chen G, Ren J-G, Zhang W, Sun Y-F, Wang F-Q, Li R-F et al. (2014). Disorganized vascular structures in sporadic venous malformations:a possible correlation with balancing effect between Tie2 and TGF-b. Sci Rep.4:5457.

Claxton, V. Kostourou, S. Jadeja, P. Chambon, K. Hodivala-Dilke, M. Fruttiger. (2008).Efficient, inducible Cre-recombinase activation in vascular endothelium. *Genesis* 46, 74–80.

Cohen MM Jr. (2006). Vascular update: morphogenesis, tumors, malformations, and molecular dimensions. *Am J Med Genet.*140(19):2013–38.

Cseh B, Fernandez-Sauze ., Grall D, Schaub S, Doma E, Van Obberghen-Schilling E. (2010). Autocrine fibronectin directs matrix assembly and crosstalk between cell-matrix and cell-cell adhesion in vascular endothelial cells. *J. Cell. Sci.* 123,3989–3999.

Daly C, Wong V, Burova E, Wei Y, Zabski S, Griffiths J, Lai KM, Lin HC, Ioffe E, Yancopoulos GD, Rudge JS. (2004). Angiopoietin-1 modulates endothelial cell function and gene expression via the transcription factor FKHR (FOXO1). *Genes Dev.*18(9):1060-71.

Daly C, Pasnikowski E, Burova E, Wong V, Aldrich TH, Griffiths J, Ioffe E, Daly TJ, Fandl JP, Papadopoulos N, McDonald DM, Thurston G, Yancopoulos GD, Rudge JS. (2006). Angiopoietin-2 functions as an autocrine protective factor in stressed endothelial cells. *Proc Natl Acad Sci U S A.*103(42):15491-6.

Davis S, Aldrich TH, Jones PF, Acheson A, Compton DL, Jain V, Ryan TE, Bruno J, Radziejewski C, Maisonpierre PC, Yancopoulos GD. (1996). Isolation of angiopoietin-1, a ligand for the TIE2 receptor, by secretion-trap expression cloning. *Cell.* 87(7):1161-9.

Davis GE, Bayless KJ, Mavila A. (2002). Molecular basis of endothelial cell morphogenesis in three-dimensional extracellular matrices. Anat Rec. 268(3):252-75.

Davis GE, Senger DR. (2005). Endothelial extracellular matrix: biosynthesis, remodeling, and functions during vascular morphogenesis and neovessel stabilization. *Circ Res.* 97(11):1093-107.

Dbouk HA. (2016). Venous malformations: PIK3CA mutations guide new treatments. *Oncotarget.* 2;7(31):48852-48853.

di Blasio L, Puliafito A, Gagliardi PA, Comunanza V, Somale D, Chiaverina G, Bussolino F, Primo L. (2018). PI3K/mTOR inhibition promotes the regression of experimental vascular malformations driven by PIK3CA-activating mutations. *Cell Death Dis.*19;9(2):45.

Dimmeler S, Fleming I, Fisslthaler B, Hermann C, Busse R, Zeiher AM. (1999). Activation of nitric oxide synthase in endothelial cells by Akt-dependent phosphorylation. *Nature.* 399:601–605.

Dimmeler S, Dernbach E, Zeiher AM. (2000). Phosphorylation of the endothelial nitric oxide synthase at ser-1177 is required for VEGF-induced endothelial cell migration. *FEBS Lett.*477:258–262.

Ding Y, Shan L, Nai W, Lin X, Zhou L, Dong X, Wu H, Xiao M, Zhou X, Wang L, Li T, Fu Y, Lin Y, Jia C, Dai M, Bai. (2018). DEPTOR Deficiency-Mediated mTORc1 Hyperactivation in Vascular Endothelial Cells Promotes Angiogenesis. *Cell Physiol Biochem.* 46(2): p. 520-531

Dobin A, Davis CA, Schlesinger F, Drenkow J, Zaleski C, Jha S, Batut P, Chaisson M, Gingeras TR. (2013). STAR: ultrafast universal RNA-seq aligner. *Bioinformatics.* 29(1):15-21.

Dompmartin A et al. (2008). Association of localized intravascular coagulopathy with venous malformations. *Arch Dermatol.* 144(7): 873–877.

Dompmartin, A., Vikkula, L. M. Boon. (2010). Venous malformation: Update on aetiopathogenesis, diagnosis and management. *Phlebology* 25, 224–235.

Dorrell MI, Friedlander M. (2006). Mechanisms of endothelial cell guidance and vascular patterning in the developing mouse retina. *Prog Retin Eye Res.* 25(3):277-95.

Dorrell MI, Aguilar E, Scheppke L, Barnett FH, Friedlander M. (2007). Combination angiostatic therapy completely inhibits ocular and tumor angiogenesis. *Proc Natl Acad Sci U S A.* 104(3):967-72.

Eble, J.A., and Niland, S. (2009). The extracellular matrix of blood vessels. *Curr. Pharm. Des.* 15, 1385–1400.

Ehling M, Adams S, Benedito R and Adams RH. (2013). Notch controls retinal blood vessel maturation and quiescence. *Development.*140, 3051-3061.

Eilken HM. and Adams RH. (2010). Dynamics of endothelial cell behavior in sprouting angiogenesis. *Curr. Opin. Cell Biol. 22*, 617–625.

Eklund L, Olsen BR. (2006). Tie receptors and their angiopoietin ligands are context-dependent regulators of vascular remodeling. *Exp Cell Res.* 312(5):630-41.

Eliceiri BP. (2001). Integrin and growth factor receptor crosstalk. *Circ Res.* 89:1104–1110.

Ellis LM, Hicklin DJ. (2008). VEGF-targeted therapy: mechanisms of anti-tumour activity. *Nat Rev Cancer.* 8(8):579-91.

Enjolras O. (1997). Classification and management of the various superficial vascular anomalies: hemangiomas and vascular malformations. *J Dermatol.* 24(11):701–710.

Enjolras O and Mulliken JB (1997). Vascular tumors and vascular malformations (new issues). Adv Dermatol. 13:375–423.

Enjolras O, Wassef M, Chapot R. (2007). Color Atlas of Vascular Tumors and Vascular Malformations. Cambridge University Press; 2007.

Falasca M, Maffucci T. (2012). Regulation and cellular functions of class II phosphoinositide 3-kinases. *Biochem J.* 443(3):587-601.

Fan W, Han D, Sun Z, Ma S, Gao L, Chen J, Li X, Li X, Fan M, Li C, Hu D, Wang Y, Cao F. (2017). Endothelial deletion of mTORC1 protects against hindlimb ischemia in diabetic mice via activation of autophagy, attenuation of oxidative stress and alleviation of inflammation. *Free Radic Biol Med.* 108:725-740.

Folkman, J. (2007). Angiogenesis: an organizing principle for drug discovery? *Nat. Rev. Drug Discov.* 6, 273–286.

Fraccaroli A, Pitter B, Taha AA, Seebach J, Huveneers S, Kirsch J, Casaroli-Marano RP, Zahler S, Pohl U, Gerhardt H, Schnittler HJ, Montanez E. (2015). Endothelial alpha-

parvin controls integrity of developing vasculature and is required for maintenance of cell-cell junctions. *Circ Res.* . 19;117(1):29-40.

Franco CA, Jones ML, Bernabeu MO, Geudens I, Mathivet T, Rosa A, Lopes FM, Lima AP, Ragab A, Collins RT, Phng LK, Coveney PV, Gerhardt H. (2015). Dynamic endothelial cell rearrangements drive developmental vessel regression. *PLoS Biol.* 13(5):e1002163.

Frisch SM, Screaton RA. (2001). Anoikis mechanisms. *Curr Opin Cell Biol.*13:555–562.

Fruman DA, Chiu H, Hopkins BD, Bagrodia S, Cantley LC, Abraham RT. (2017). The PI3K Pathway in Human Disease. *Cell.* 170(4):605-635.

Fruttiger M. (2007). Development of the retinal vasculature. *Angiogenesis.*10(2):77-88.

Fujio Y, Walsh K. (1999). Akt mediates cytoprotection of endothelial cells by vascular endothelial growth factor in an anchorage-dependent manner.*J Biol Chem.* 274:16349–16354

Fukuhara S, Sako K, Minami T, Noda K, Kim HZ, Kodama T, Shibuya M, Takakura N, Koh GY, Mochizuki N. (2008). Differential function of Tie2 at cell-cell contacts and cell-substratum contacts regulated by angiopoietin-1*. Nat Cell Biol.* 10(5):513-26.

Fukumura D, Gohongi T, Kadambi A, Izumi Y, Ang J, Yun CO, Buerk DG, Huang PL, Jain RK. (2001). Predominant role of endothelial nitric oxide synthase in vascular endothelial growth factor-induced angiogenesis and vascular permeability. *Proc Natl Acad Sci U S A.* 98(5): 2604-9.

Fulton D, Gratton JP, McCabe TJ, Fontana J, Fujio Y, Walsh K, Franke TF, Papapetropoulos A, Sessa WC. (1999). Regulation of endothelium-derived nitric oxide production by the protein kinase Akt. Nature. 399:597–601.

Furuyama T, Kitayama K, Shimoda Y, Ogawa M, Sone K, Yoshida-Araki K, Hisatsune H, Nishikawa S, Nakayama K, Nakayama K, Ikeda K, Motoyama N, Mori N. (2004). Abnormal angiogenesis in Foxo1 (Fkhr)-deficient mice. *J Biol Chem.* 279(33):34741-9.

Gambardella L, Hemberger M, Hughes B, Zudaire E, Andrews S, Vermeren S. (2010). PI3K signaling through the dual GTPase-activating protein ARAP3 is essential for developmental angiogenesis. *Sci Signal.* 3(145):ra76.

Gariano RF, Gardner TW. (2005). Retinal angiogenesis in development and disease. *Nature.* 438(7070):960-6.

George EL, Baldwin HS, Hynes RO. (1997). Fibronectins are essential for heart and blood vessel morphogenesis but are dispensable for initial specification of precursor cells. Blood, 90, 3073–3081.

Gerhardt H, Golding M, Fruttiger M, Ruhrberg C, Lundkvist A, Abramsson A, Jeltsch M, Mitchell C, Alitalo K, Shima D, Betsholtz C. (2003). VEGF guides angiogenic sprouting utilizing endothelial tip cell filopodia. *J Cell Biol. 2003.*161(6):1163-77.

Giancotti FG, Ruoslahti E. (1999). Integrin signaling. *Science.* 285:1028–1032.

Goettsch W, Gryczka C, Korff T, Ernst E, Goettsch C, Seebach J, Schnittler HJ, Augustin HG, Morawietz H. (2008). Flow-dependent regulation of angiopoietin-2. *J Cell Physiol.* 214(2):491-503.

Goines J, Li X, Cai Y, et al. (2018). A xenograft model for venous malformation. *Angiogenesis*; 21:725–735.

Goncalves MD, Hopkins BD, Cantley LC. (2018). Phosphatidylinositol 3-Kinase, Growth Disorders, and Cancer. *N Engl J Med.* 379(21):2052-2062.

Graupera M, Guillermet-Guibert J, Foukas LC, Phng LK, Cain RJ, Salpekar A, Pearce W, Meek S, Millan J, Cutillas PR, Smith AJ, Ridley AJ, Ruhrberg C, Gerhardt H, Vanhaesebroeck B. (2008). Angiogenesis selectively requires the p110alpha isoform of PI3K to control endothelial cell migration. *Nature.* 453(7195): 662-6.

Graupera M, Potente M. (2013). Regulation of angiogenesis by PI3K signaling networks. *Exp Cell Res.* 15;319(9):1348-55.

Green S, Trejo CL, McMahon M. (2015). PIK3CA(H1047R) Accelerates and Enhances KRAS(G12D)-Driven Lung Tumorigenesis. *Cancer Res.* 75(24):5378-91.

Gulluni, F. et al. (2017). Mitotic spindle assembly and genomic stability in breast cancer require PI3K- C2α scaffolding function. *Cancer Cell* 32, 444–459.

Gupta SK, Vlahakis NE. (2010) Integrin alpha9beta1: Unique signaling pathways reveal diverse biological roles. *Cell Adh Migr.*4 (2):194-8.

Hage AN, Chick JFB , Srinivasa RN, Bundy JJ, Chauhan NR, Acord M, Gemmete JJ. (2018). Treatment of Venous Malformations: The Data, Where We Are, and How It Is Done. *Tech Vasc Interv Radiol.* 21(2):45-54.

Hammer J, Seront E, Duez S, et al. (2018). Sirolimus is efficacious in treatment for extensive and/or complex slow-flow vascular malformations: a monocentric prospective phase II study. *Orphanet J Rare Dis.* 13:191.

Hakanpaa L, Sipila T, Leppanen VM, Gautam P, Nurmi H, Jacquemet G, Eklund L, Ivaska J, Alitalo K, Saharinen P. (2015). Endothelial destabilization by angiopoietin-2 via integrin β1 activation. *Nat Commun.* 6:5962.

Hare LM, Schwarz Q2, Wiszniak S2, Gurung R3, Montgomery KG4, Mitchell CA3, Phillips WA. (2015). Heterozygous expression of the oncogenic Pik3ca(H1047R) mutation during murine development results in fatal embryonic and extraembryonic defects. *Dev Biol.* 404(1):14-26.

Harfouche R, Gratton JP, Yancopoulos GD, Noseda M, Karsan A, Hussain SN. (2003). Angiopoietin-1 activates both anti- and proapoptotic mitogen-activated protein kinases. *FASEB J.* 17(11):1523-5.

Helaers R, Eklund L, Boon LM, Vikkula M (2015). Somatic activating PIK3CA mutations cause venous malformation. Am J Hum Genet 97(6): 914–92.

Hellstrom, M. et al. (2007). Dll4 signalling through Notch1 regulates formation of tip cells during angiogenesis. *Nature* 445, 776–780.

Herbert SP, Huisken J, Kim TN, Feldman ME, Houseman BT, Wang RA, Shokat KM, Stainier DY. (2009). Arterial-venous segregation by selective cell sprouting: an alternative mode of blood vessel formation. *Science.* 326(5950):294-8.

Hermans C, Dessomme B, Lambert C, Deneys V.(2006). Venous malformations and coagulopathy. *Ann Chir Plast Esthet.* 51(4-5):388-93.

Hirsch, E., Braccini, L., Ciraolo, E., Morello, F. & Perino, A. (2009). Twice upon a time: PI3K's secret double life exposed. *Trends Biochem. Sci.* 34, 244–248.

Hoon Chul Kang, Seung Tae Baek, Saera Song, Joseph G. Gleeson. (2015), Clinical and genetic aspects of the segmental overgrowth spectrum due to somatic mutations in PIK3CA. *J Pediatr.*167(5):957-62.

Hong CC, Peterson QP, Hong JY, Peterson RT. (2006). Artery/vein specification is governed by opposing phosphatidylinositol-3 kinase and MAP kinase/ERK signaling. *Curr Biol.* 16(13):1366-72.

Hosaka T, Biggs WH 3rd, Tieu D, Boyer AD, Varki NM, Cavenee WK, Arden KC.(2004). Disruption of forkhead transcription factor (FOXO) family members in mice reveals their functional diversification. *Proc Natl Acad Sci U S A.* 101(9):2975-80.

Hoste G,Slembrouck L,Jongen L,et al. (2018). Unexpected benefit from alpelisib and fulvestrant in a woman with highly pretreated ER-positive, HER2-negative PIK3CA mutant metastatic breast cancer. *Clin Drug Investig;* 38:1071–1075.

Hu HT, Huang YH, Chang YA, et al. (2008). Tie2-R849W mutant in venous malformations chronically activates a functional STAT1 to modulate gene expression. *J Invest Dermatol.*128:2325–2333.

Hutti JE, Pfefferle AD, Russell SC, Sircar M, Perou CM, Baldwin AS. (2012). Oncogenic PI3K mutations lead to NF-κB-dependent cytokine expression following growth factor deprivation. *Cancer Res.*1:72(13):3260-9.

Huveneers S, Oldenburg J, Spanjaard E, van der Krogt G, Grigoriev I, Akhmanova A, Rehmann H, de Rooij J. (2012). Vinculin associates with endothelial VE-cadherin junctions to control force-dependent remodeling. *J Cell Biol.* 196(5):641-52.

Hynes RO. (1992). Integrins: versatility, modulation, and signaling in cell adhesion. *Cell.* 69:11–25.

Hynes RO. (2002). Integrins: bidirectional, allosteric signaling machines. *Cell.* 110(6):673-87.

Hynes RO. (2007). Cell-matrix adhesion in vascular development. *J Thromb Haemost.* 5(suppl 1):32–40.

Iason S. Mantagos, Deborah K. Vanderveen, Lois E.H. Smith. (2009). Emerging Treatments for Retinopathy of Prematurity. *Semin Ophthalmol.* 24(2): 82–86.

Ikenoue T, Kanai F, Hikiba Y, Obata T, Tanaka Y, Imamura J, Ohta M, Jazag A, Guleng B, Tateishi K, Asaoka Y, Matsumura M, Kawabe T, Omata M. (2005). Functional analysis of PIK3CA gene mutations in human colorectal cancer. *Cancer Res.*1;65(11):4562-7.

Ingber DE, Folkman J. (1989). Mechanochemical switching between growth and differentiation during fibroblast growth factor-stimulated angiogenesis in vitro: role of extracellular matrix. *J Cell Biol*; 109(1):317-30.

Jain RK. (2003). Molecular regulation of vessel maturation. *Nat Med.*9(6):685-93.

Jakobsson L, Franco CA, Bentley K, Collins RT, Ponsioen B, Aspalter IM, Rosewell I, Busse M, Thurston G, Medvinsky A, Schulte-Merker S, Gerhardt H. (2010). Endothelial cells dynamically compete for the tip cell position during angiogenic sprouting. *Nat Cell Biol.* (10):943-53.

Jiang BH, Zheng JZ, Aoki M, Vogt PK. (2001). Phosphatidylinositol 3-kinase signaling mediates angiogenesis and expression of vascular endothelial growth factor in endothelial cells. *Proc Natl Acad Sci U S A.* 97(4):1749-53.

Junge HJ, Yang S, Burton JB, Paes K, Shu X, French DM, Costa M, Rice DS, Ye W. (2009). TSPAN12 regulates retinal vascular development by promoting Norrin- but not Wnt-induced FZD4/beta-catenin signaling. *Cell.* 139(2):299-311.

Kalluri R. (2003). Basement membranes: structure, assembly and role in tumour angiogenesis. *Nat Rev Cancer.* 3(6):422-33.

Kangas J, Nätynki M, Eklund L. (2018). Development of Molecular Therapies for Venous Malformations. *Basic Clin Pharmacol Toxicol.*123 Suppl 5:6-19.

Katso R, Okkenhaug K, Ahmadi K, White S, Timms J, Waterfield MD. (2001). Cellular function of phosphoinositide 3-kinases: implications for development, homeostasis, and cancer. *Annu Rev Cell Dev Biol.*17: 615–675.

Kennedy D. (2006). Breakthrough of the year. *Science.* 314(5807):1841.

Kerr, B.A., et al. (2016). Stability and function of adult vasculature is sustained by Akt/Jagged1 signalling axis in endothelium. *Nat Commun.* 7: p. 10960.

Kim I, Kim HG, So JN, et al. (2000). Angiopoietin-1 regulates endothelial cell survival through the phosphatidylinositol 30-kinase/Akt signal transduction pathway. *Circ Res.* 86:24–29.

Kinross,K.M.,Montgomery,K.G.,Kleinschmidt,M.,Waring,P.,Ivetac,I.,Tikoo,A.,Saad,M.,Hare,L.,Roh,V.,Mantamadiotis,T.,Sheppard,K.E.,Ryland,G.L.,Campbell,I.G.,Gorringe,K.L.,Christensen,J.G,Cullinane,C.,Hicks,R.J.,Pearson,R.B.,Johnstone,R.W.,McArthur,G.

A.,Phillips,W.A. (2012). An activating Pik3ca mutation coupled with Pten loss is sufficient to initiate ovarian tumorigenesis in mice.*J.Clin.Investig.* 122(2),553–557.

Kontos CD, Stauffer TP, Yang WP, York JD, Huang L, Blanar MA, Meyer T, Peters KG. (1998). Tyrosine 1101 of Tie2 is the major site of association of pp85 and is required for activation of phosphatidylinositol 3-kinase and Akt. *Mol Cell Biol* .18: 4131–4140.

Koren S, Reavie L, Couto JP, De Silva D, Stadler MB, Roloff T, Britschgi A, Eichlisberger T, Kohler H, Aina O, Cardiff RD, Bentires-Alj M. (2015). PIK3CA (H1047R) induces multipotency and multi-lineage mammary tumours. *Nature.* 525(7567):114-8.

Kostourou V.,Papalazarou V. (2014). Non-collagenous ECM proteins in blood vessel morphogenesis and cancer. *Biochim. Biophys. Acta Gen. Subj.,* 1840, 2403–2413.

Kurek KC, Luks VL, Ayturk UM, Alomari AI, Fishman SJ, Spencer SA, Mulliken JB, Bowen ME, Yamamoto GL, Kozakewich HP, Warman ML. (2012). Somatic mosaic activating mutations in PIK3CA cause CLOVES syndrome. *Am J Hum Genet.* 90(6):1108-15.

Lamalice L, Le Boeuf F, Huot J. (2007). Endothelial cell migration during angiogenesis. *Circ Res.* 100(6):782-94.

Lampugnani MG. (2012). Endothelial cell-to-cell junctions: adhesion and signaling in physiology and pathology. *Cold Spring Harb Perspect Med.* 2(10).

Laviña B, Castro M, Niaudet C, Cruys B, Álvarez-Aznar A, Carmeliet P, Bentley K, Brakebusch C, Betsholtz C, Gaengel K. (2018). Defective endothelial cell migration in the absence of Cdc42 leads to capillary-venous malformations. *Development.*145:1–20.

Lawrence MS, Stojanov P, Mermel CH, Robinson JT, Garraway LA, Golub TR, Meyerson M, Gabriel SB, Lander ES, Getz G. (2014). Discovery and saturation analysis of cancer genes across 21 tumour types. *Nature.* 505(7484):495-501.

Legiehn G.M.Heran M.K.S. (2008). Venous malformations: Classification, development, diagnosis, and interventional radiologic management. *Radiol Clin North Am.* 46: 545-597

Lee BB, Baumgartner I, Berlien P, et al. (2015). Diagnosis and Treatment of Venous Malformations. Consensus Document of the International Union of Phlebology (IUP): updated 2013. *Int Angiol.*34:97-149.

Lelievre E, Bourbon PM, Duan LJ, Nussbaum RL, Fong GH. (2005). Deficiency in the p110alpha subunit of PI3K results in diminished Tie2 expression and Tie2(-/-)-like vascular defects in mice. *Blood.* 105(10):3935-8.

Lenard A, Ellertsdottir E, Herwig L, Krudewig A, Sauteur L, Belting HG, Affolter M. (2013). In vivo analysis reveals a highly stereotypic morphogenetic pathway of vascular anastomosis. *Dev Cell.* 25(5):492-506.

Lee MY, Luciano AK, Ackah E, Rodriguez-Vita J, Bancroft TA, Eichmann A, Simons M, Kyriakides TR, Morales-Ruiz M, Sessa WC. (2014). Endothelial Akt1 mediates angiogenesis by phosphorylating multiple angiogenic substrates. *Proc Natl Acad Sci U S A.* 111(35):12865-70.

Li B, Dewey CN. (2011). RSEM: accurate transcript quantification from RNA-Seq data with or without a reference genome. *BMC Bioinformatics.* 12:323.

Liao YF, et al. (2002) The EIIIA segment of fibronectin is a ligand for integrins alpha 9beta 1 and alpha 4beta 1 providing a novel mechanism for regulating cell adhesion by alternative splicing. *J. Biol.Chem.*277:14467–14474.

Limaye N, Wouters V, Uebelhoer M, Tuominen M, Wirkkala R, Mulliken JB, Eklund L, Boon LM, Vikkula M (2009). Somatic mutations in angiopoietin receptor gene TEK cause solitary and multiple sporadic venous malformations. Nat Genet 41(1):118–124.

Limaye N, Kangas J, Mendola A, Godfraind C, Schlögel MJ, Helaers R, Eklund L, Boon LM, Vikkula M. (2015). Somatic Activating PIK3CA Mutations Cause Venous Malformation. *Am J Hum Genet.* 3:97(6):914-21.

Lindblom P, Gerhardt H, Liebner S, et al. (2003). Endothelial PDGF-B retention is required for proper investment of pericytes in the microvessel wall. *Genes Dev.* 17: 1835–1840.

Ling TL, Mitrofanis J, Stone J. (1989). Origin of retinal astrocytes in the rat: evidence of migration from the optic nerve. *J Comp Neurol.* 286(3):345-52.

Lindhurst MJ et al. (2012). Mosaic overgrowth with fibroadipose hyperplasia is caused by somatic activating mutations in PIK3CA. *Nat. Genet.* 44:928–933.

Lobov IB, Brooks PC, Lang RA. (2002). Angiopoietin-2 displays VEGF-dependent modulation of capillary structure and endothelial cell survival in vivo. *Proc Natl Acad Sci U S A.* 99(17):11205-10.

Lobov IB, Renard RA, Papadopoulos N, Gale NW, Thurston G, Yancopoulos GD, Wiegand SJ. (2007). Delta-like ligand 4 (Dll4) is induced by VEGF as a negative regulator of angiogenic sprouting. *Proc Natl Acad Sci U S A.* 104(9):3219-24.

Loibl S, Majewski I, Guarneri V, et al. (2016). PIK3CA mutations are associated with reduced pathological complete response rates in primary HER2-positive breast cancer: pooled analysis of 967 patients from five prospective trials investigating lapatinib and trastuzumab. *Ann Oncol.* 27: 1519–1525.

Love MI, Huber W, Anders S. (2014). Moderated estimation of fold change and dispersion for RNA-seq data with DESeq2. *Genome Biol.* 15(12):550.

Lowe LH, Marchant TC, Rivard DC, Scherbel AJ. (2012). Vascular malformations: classification and terminology the radiologist needs to know. *Semin Roentgenol.* 47(2):106-17.

Lu X, Le Noble F, Yuan L, Jiang Q, De Lafarge B, Sugiyama D, Bréant C, Claes F, De Smet F, Thomas JL, Autiero M, Carmeliet P, Tessier-Lavigne M, Eichmann A. (2004). The netrin receptor UNC5B mediates guidance events controlling morphogenesis of the vascular system. *Nature.*432(7014):179-86.

Madsen RR, Vanhaesebroeck B, Semple RK (2018) Cancer-associated PIK3CA mutations in overgrowth disorders. *Trends Mol Med* 24:856–870.

Madsen RR, Knox RG, Pearce W, Lopez S, Mahler-Araujo B, McGranahan N, Vanhaesebroeck B, Semple RK. (2019). *Proc Natl Acad Sci.* 23;116(17):8380-8389.

Magnuson B, Ekim B, Fingar DC (2012). Regulation and function of ribosomal protein S6 kinase (S6K) within mTOR signalling networks. *Biochem J.* 441(1):1-21.

Maisonpierre PC, Suri C, Jones PF, Bartunkova S, Wiegand SJ, Radziejewski C, Compton D, McClain J, Aldrich TH, Papadopoulos N, Daly TJ, Davis S, Sato TN, Yancopoulos GD. (1997). Angiopoietin-2, a natural antagonist for Tie2 that disrupts in vivo angiogenesis. *Science.* 277(5322):55-60.

Malka-Mahieu H, Newman M, Désaubry L, Robert C, Vagner S. (2017). Molecular Pathways: The eIF4F Translation Initiation Complex-New Opportunities for Cancer Treatment. *Clin Cancer Res.* 23(1):21-

Manning BD, Cantley LC. (2007). AKT/PKB signaling: navigating downstream. *Cell.* 129(7):1261-74.

Manning BD, Toker A. (2017). AKT/PKB Signaling: Navigating the Network. *Cell.* 169(3):381-405.

Marcinkiewicz C, et al. (2000). Inhibitory effects of MLDG-containing heterodimeric disintegrins reveal distinct structural requirements for interaction of the integrin alpha 9beta 1 with VCAM-1, tenascin-C, and osteopontin. *J. Biol. Chem*; 275: 31930–31937.

Mattassi RLD, Vaghi M. (2009). Hemangiomas and vascular malformations. An atlas of diagnosis and treatment. Milano: Springer; 2009.

Mattila KA, Kervinen K, Kalajoki-Helmio T, Lappalainen K, Vuola P, Lohi J et al. (2015). An interdisciplinary specialist team leads to improved diagnostics and treatment for paediatric patients with vascular anomalies. *Acta Paediatr.*104:1109–16.

Michell BJ, Griffiths JE, Mitchelhill KI, Rodriguez-Crespo I, Tiganis T, Bozinovski S et al. (1999). The Akt kinase signals directly to endothelial nitric oxide synthase. *Curr Biol.* 9:845–848.

Milde F, Lauw S, Koumoutsakos P, Iruela-Arispe ML. (2013). The mouse retina in 3D: quantification of vascular growth and remodeling. *Integrative Biology*. 5(12),1426.

Millán J, Cain RJ, Reglero-Real N, Bigarella C, Marcos-Ramiro B, Fernández-Martín L, Correas I, Ridley AJ. (2010). Adherens junctions connect stress fibres between adjacent endothelial cells. *BMC Biol.* 2;8:11.

Morello F, Perino A, Hirsch E. (2009). Phosphoinositide 3-kinase signalling in the vascular system. *Cardiovasc Res.*82(2):261-71.

Morris PN, Dunmore BJ, Tadros A, Marchuk DA, Darland DC, D'Amore PA et al. (2005). Functional analysis of a mutant form of the receptor tyrosine kinase Tie2 causing venous malformations. *J Mol Med.*;83:58–63.

Mulliken JB, Glowacki J. (1982). Hemangiomas and vascular malformations in infants and children: a classification based on endothelial characteristics. *Plast Reconstr Surg*. 69: 412–422.

Mulliken JB, Burrows PE, Fishman SJ. (2013). Mulliken and Young's Vascular Anomalies Hemangiomas and Malformations, 2nd edn.Oxford University Press, New York, USA.

Murohara T, Witzenbichler B, Spyridopoulos I, Asahara T, Ding B, Sullivan A, Losordo DW, Isner JM. (1999). Role of endothelial nitric oxide synthase in endothelial cell migration. *Arterioscler Thromb Vasc Biol*;19 (5):1156-61.

Nätynki M, Kangas J, Miinalainen I, Sormunen R, Pietila R, Soblet J et al. (2015). Common and specific effects of TIE2 mutations causing venous malformations. *Hum Mol Genet*; 24:6374–89.

Nicoli S, Knyphausen CP, Zhu LJ, Lakshmanan A, Lawson ND. (2012). miR-221 is required for endothelial tip cell behaviors during vascular development. *Dev Cell.* 22(2):418-29.

Oellerich MF, Potente M. (2012). FOXOs and sirtuins in vascular growth, maintenance, and aging. *Circ Res.* 110(9):1238-51.

Papapetropoulos A, Fulton D, Mahboubi K, Kalb RG, O'Connor DS, Li F, Altieri DC, Sessa WC. (2000). Angiopoietin-1 inhibits endothelial cell apoptosis via the Akt/survivin pathway. *J Biol Chem.*275(13):9102-5.

Phng LK and Gerhardt H. (2009). Angiogenesis: a team effort coordinated by notch. *Dev. Cell.*16, 196–208.

Phng LK, Gebala V, Bentley K, Philippides A, Wacker A, Mathivet T, Sauteur L, Stanchi F, Belting HG, Affolter M, Gerhardt H. (2015). Formin-mediated actin polymerization at endothelial junctions is required for vessel lumen formation and stabilization. *Dev Cell.* 32(1):123-32.

Phung TL, Ziv K, Dabydeen D, Eyiah-Mensah G, Riveros M, Perruzzi C, Sun J, Monahan-Earley RA, Shiojima I, Nagy JA, Lin MI, Walsh K, Dvorak AM, Briscoe DM, Neeman M, Sessa WC, Dvorak HF, Benjamin LE. (2006). Pathological angiogenesis is induced by sustained Akt signaling and inhibited by rapamycin. *Cancer Cell.*; 10(2):159-70.

Pitulescu ME, Schmidt I, Benedito R, Adams RH. (2010). Inducible gene targeting in the neonatal vasculature and analysis of retinal angiogenesis in mice. *Nat Protoc.* 5(9):1518-34.

Potente M, Urbich C, Sasaki K, Hofmann WK, Heeschen C, Aicher A, Kollipara R, DePinho RA, Zeiher AM, Dimmeler S. (2005). Involvement of Foxo transcription factors in angiogenesis and postnatal neovascularization. *J Clin Invest.* 115(9):2382-92.

Potente M, Gerhardt H, Carmeliet P. (2011). Basic and therapeutic aspects of angiogenesis. *Cell.*146(6):873-87.

Potente M, Carmeliet P. (2016). The Link Between Angiogenesis and Endothelial Metabolism. *Annu Rev Physiol.* 79:43-66.

Ren, B., et al. (2010). ERK1/2-Akt1 crosstalk regulates arteriogenesis in mice and zebrafish. *J Clin Invest.* 120(4): p. 1217-28.

Robinson G, et al. (2012). Novel mutations target distinct subgroups of medulloblastoma. *Nature.* 488(7409):43-8.

Roderick R. McInnes. (2003). Developmental Biology: Frontiers for Clinical Genetics. *Clin Genet.* 63: 340–351

Saharinen P, Eklund L, Miettinen J, Wirkkala R, Anisimov A, Winderlich M, Nottebaum A, Vestweber D, Deutsch U, Koh GY, Olsen BR, Alitalo K. (2008). Angiopoietins assemble distinct Tie2 signalling complexes in endothelial cell-cell and cell-matrix contacts. *Nat Cell Biol.* 10(5):527-37.

Saint-Geniez M, D'Amore P. (2004). Development and pathology of the hyaloid, choroidal and retinal vasculature. *Int. J. Dev. Biol.* 48: 1045 - 1058

Samuels Y, Wang Z, Bardelli A, Silliman N, Ptak J, Szabo S, Yan H, Gazdar A, Powell SM, Riggins GJ, et al. (2004). High frequency of mutations of the PIK3CA gene in human cancers. *Science.* 304:554.

Samuels Y, Diaz LA Jr, Schmidt-Kittler O, Cummins JM, Delong L, Cheong I, Rago C, Huso DL, Lengauer C, Kinzler KW, Vogelstein B, Velculescu VE. (2005). Mutant PIK3CA promotes cell growth and invasion of human cancer cells. *Cancer Cell.*7(6):561-73.

Samuels Y, Waldman T. (2010). Oncogenic mutations of PIK3CA in human cancers. *Curr Top Microbiol Immunol.* 2010;347:21-41.

Sarbassov D, Ali SM, Sengupta S, Sheen JH, et al. (2006). Prolonged rapamycin treatment inhibits mTORC2 assembly and Akt/PKB. *Mol Cell.* 22:159–168.

Sasan b., et al. (2016) Venous malformations: clinical diagnosis and treatment. *Cardiovasc Diagn Ther.* 6(6): 557–569.

Sauteur L, Krudewig A, Herwig L, Ehrenfeuchter N, Lenard A, Affolter M, Belting HG. (2014). Cdh5/VE-cadherin promotes endothelial cell interface elongation via cortical actin polymerization during angiogenic sprouting. *Cell Rep.* 9(2):504-13.

Schmidt M, Paes K, De Mazière A, Smyczek T, Yang S, Gray A, French D, Kasman I, Klumperman J, Rice DS, Ye W. (2007). EGFL7 regulates the collective migration of endothelial cells by restricting their spatial distribution. *Development.* 134(16):2913-23.

Schmidt S, Friedl P. (2010). Interstitial cell migration: integrin-dependent and alternative adhesion mechanisms. *Cell Tissue Res.*339(1):83-92.

Semenza GL. (2003). Targeting HIF-1 for cancer therapy. *Nat Rev Cancer.* 3(10):721-32.

Senger DR, Davis GE. (2011). Angiogenesis. *Cold Spring Harb Perspect Biol.* 3(8):a005090.

Serban D, Leng J, Cheresh D. (2008). H-ras regulates angiogenesis and vascular permeability by activation of distinct downstream effectors. *Circ Res.* 102(11):1350-8.

Seront E., Vikkula M., Boon L.M. (2018). Venous malformations of the head and neck. *Otolaryngol Clin North Am.* 51: 173-184.

Seront E, Van Damme A, Boon LM, Vikkula M. (2019). Rapamycin and treatment of venous malformations. *Curr Opin Hematol.* 26(3):185-192.

Serra, H. et al. (2015).PTEN mediates Notch-dependent stalk cell arrest in angiogenesis. *Nat Commun.* 6, 7935.

Shiojima I, Walsh K. (2002). Role of Akt signaling in vascular homeostasis and angiogenesis. *Circ Res.* 90(12):1243-50.

Soblet JLN, Uebelhoer M, Boon LM, Vikkula M (2013) Variable somatic TIE2 mutations in half of sporadic venous malformations. *Mol Syndromol* 4(4):179–183

Soblet J, Kangas J, Natynki M, Mendola A, Helaers R, Uebelhoer M et al. (2017). Blue rubber bleb nevus (BRBN) syndrome is caused by somatic TEK (TIE2) mutations. *J Invest Dermatol*;137:207–16.

Soler A, Angulo-Urarte A, Graupera M.(2015). PI3K at the crossroads of tumor angiogenesis signaling pathways. *Mol Cell Oncol.* 2(2):e975624.

Somanath PR, Malinin NL, Byzova TV. (2009). Cooperation between integrin alphavbeta3 and VEGFR2 in angiogenesis. *Angiogenesis.*12(2):177-85.

Song SM, Salmena L, Pandolfi PP (2012). The functions and regulation of the PTEN tumour suppressor. *Nat Rev Mol Cell Biol.* **13**(5): p. 283-96.

Stahl A, Connor KM, Sapieha P, Chen J, Dennison RJ, Krah NM, Seaward MR, Willett KL, Aderman CM, Guerin KI, Hua J, Löfqvist C, Hellström A, Smith LE. (2010). The mouse retina as an angiogenesis model. *Invest Ophthalmol Vis Sci.* 51(6):2813-26.

Stanczuk L, Martinez-Corral I, Ulvmar MH, Zhang Y, Laviña B, Fruttiger M, Adams RH, Saur D, Betsholtz C, Ortega S, Alitalo K, Graupera M, Mäkinen T. (2015). cKit Lineage Hemogenic Endothelium-Derived Cells Contribute to Mesenteric Lymphatic Vessel. *Cell Rep.* 10(10):1708-1721.

Staniszewska I, et al. (2007). Interaction of alpha9beta1 integrin with thrombospondin-1 promotes angiogenesis. *Circ. Res;*100:1308–1316.

Stenzel D, Lundkvist A, Sauvaget D, Busse M, Graupera M, van der Flier A, Wijelath ES, Murray J, Sobel M, Costell M, Takahashi S, Fässler R, Yamaguchi Y, Gutmann DH, Hynes RO, Gerhardt H. (2011). Integrin-dependent and -independent functions of astrocytic fibronectin in retinal angiogenesis. *Development.*138 (20):4451-63.

Stone J, Dreher Z. (1987). Relationship between astrocytes, ganglion cells and vasculature of the retina. *J Comp Neurol.* 255(1):35-49.

Stone J, Itin A, Alon T, Pe'er J, Gnessin H, Chan-Ling T, Keshet E. (1995). Development of retinal vasculature is mediated by hypoxia-induced vascular endothelial growth factor (VEGF) expression by neuroglia. *J Neurosci.* 15(7 Pt 1):4738-47.

Stratton MR, Campbell PJ, Futreal PA. (2009). The cancer genome. *Nature.* 458(7239):719-24.

Subramanian A., et al. (2005). Gene set enrichment analysis: A knowledge-based approach for interpreting genome-wide expression profiles. *Proc. Natl. Acad. Sci.* USA 102, 15545-15550.

Taddei A, Giampietro C, Conti A, Orsenigo F, Breviario F, Pirazzoli V, Potente M, Daly C, Dimmeler S, Dejana E. (2008). Endothelial adherens junctions control tight junctions by VE-cadherin-mediated upregulation of claudin-5. *Nat Cell Biol.*10(8):923-34.

Tammela, T. et al. (2011). VEGFR-3 controls tip to stalk conversion at vessel fusion sites by reinforcing Notch signalling. *Nat Cell Biol.* 13, 1202–1213

Timothy D Le Cras and Elisa Boscolo. (2019). Cellular and molecular mechanisms of PIK3CA-related vascular anomalies. *Vascular biology.* H33–H40.

Thorpe LM, Yuzugullu H, Zhao JJ. (2015). PI3K in cancer: divergent roles of isoforms, modes of activation and therapeutic targeting. *Nat Rev Cancer.* 15(1):7-24.

Uebelhoer M, Boon LM, Vikkula M. (2012). Vascular anomalies: from genetics toward models for therapeutic trials. *Cold Spring Harb Perspect Med.* 1;2(8).

Uebelhoer M, Nätynki M, Kangas J, Mendola A, Nguyen H-L, Soblet J, Godfraind C, Boon LM, Eklund L, Limaye N, Vikkula M. (2013). Venous malformation-causative TIE2 mutations mediate an AKT-dependent decrease in PDGFB. *Hum. Mol. Genet.* 22:3438–3448.

Uemura A, Ogawa M, Hirashima M, Fujiwara T, Koyama S, Takagi H, Honda Y, Wiegand SJ, Yancopoulos GD, Nishikawa S. (2002). Recombinant angiopoietin-1 restores higher-order architecture of growing blood vessels in mice in the absence of mural cells. *J Clin Invest.* 110(11):1619-28.

Uemura A, Kusuhara S, Wiegand SJ, Yu RT, Nishikawa S. (2006). Tlx acts as a proangiogenic switch by regulating extracellular assembly of fibronectin matrices in retinal astrocytes. J Clin Invest.116(2):369-77.

Van der Flier A, Sonnenberg A. (2001). Function and interactions of integrins. *Cell Tissue Res.* 305(3):285-98.

Van Keymeulen A, Lee MY, Ousset M, Brohée S, Rorive S, Giraddi RR, Wuidart A, Bouvencourt G, Dubois C, Salmon I, Sotiriou C, Phillips WA, Blanpain C. (2015). Reactivation of multipotency by oncogenic PIK3CA induces breast tumour heterogen eity. *Nature.*3; 525(7567):119-23.

Vanhaesebroeck B, Ali K, Bilancio A, Geering B & Foukas LC. (2005). Signalling by PI3K isoforms: insights from gene- targeted mice. *Trends Biochem. Sci.* 30, 194–204.

Vanhaesebroeck B, Guillermet-Guibert J, Graupera M, Bilanges B. (2010). The emerging mechanisms of isoform-specific PI3K signalling. *Nat Rev Mol Cell Biol.*11(5):329-41.

Vanhaesebroeck B, Stephens L, Hawkins P. (2012). PI3K signalling: the path to discovery and understanding. *Nat Rev Mol Cell Biol.* 13(3):195-203.

Venot Q, Blanc T, Rabia SH, et al. (2018). Targeted therapy in patients with PIK3CA related overgrowth syndrome. *Nature.* 558:540–546.

Vikkula M, Boon LM, Carraway KL III, Calvert JT, Diamonti AJ, Goumnerov B, Pasyk KA, Marchuk DA, Warman ML, Cantley LC, Mulliken JB, Olsen BR. (1996). Vascular dysmorphogenesis caused by an activating mutation in the receptor tyrosine kinase TIE2. *Cell.* 87:1181–1190.

Vlahakis NE, Young BA, Atakilit A, Hawkridge AE, Issaka RB, Boudreau N, et al. (2007). Integrin α9β1 directly binds to Vascular Endothelial Growth Factor (VEGF)-A and contributes to VEGF-A-induced angiogenesis. *J Biol Chem.* 282:15187-96.

Wang GL, Jiang BH, Rue EA, Semenza GL. (1995). Hypoxia-inducible factor 1 is a basic-helix-loop-helix-PAS heterodimer regulated by cellular O2 tension. *Proc Natl Acad Sci U S A.* 92(12):5510-4.

Wassef M, Blei F, Adams D, Alomari A, Baselga E, Berenstein A, Burrows P, Frieden IJ, Garzon MC, Lopez-Gutierrez JC, Lord DJ, Mitchel S, Powell J, Prendiville J, Vikkula M. (2015). Vascular Anomalies Classification: Recommendations From the International Society for the Study of Vascular Anomalies. *Pediatrics.* 136(1):e203-14.

Wilhelm K, Happel K, Eelen G, Schoors S, Oellerich MF, Lim R, Zimmermann B, Aspalter IM, Franco CA, Boettger T, Braun T, Fruttiger M, Rajewsky K, Keller C, Brüning JC, Gerhardt H, Carmeliet P, Potente M. (2016). FOXO1 couples metabolic activity and growth state in the vascular endothelium. *Nature.* 529: 216-20.

Williams MR, Arthur JS, Balendran A, van der Kaay J, Poli V, Cohen P, Alessi DR. (2000). The role of 3-phosphoinositide-dependent protein kinase 1 in activating AGC kinases defined in embryonic stem cells. *Curr Biol.*10:439–448.

Wu CY, Keivens VM, O'Toole TE, McDonald JA, and Ginsberg MH. (1995). Integrin activation and cytoskeletal interaction are essential for the assembly of a fibronectin matrix. *Cell.* 83:715–724.

Yamamoto H, Ehling M, Kato K, Kanai K, van Lessen M, Frye M, Zeuschner D, Nakayama M, Vestweber D, Adams RH. (2015). Integrin β1 controls VE-cadherin localization and blood vessel stability. *Nat Commun.* 6:6429.

Yoshioka K, Yoshida K, Cui H, et al. (2012). Endothelial PI3K-C2alpha, a class II PI3K, has an essential role in angiogenesis and vascular barrier function. *Nat Med.*18:1560–1569.

Yuan TL, Choi HS, Matsui A, Benes C, Lifshits E, Luo J, Frangioni JV, Cantley LC. (2008). Class 1A PI3K regulates vessel integrity during development and tumorigenesis. *Proc Natl Acad Sci U S A.*105(28):9739-44.

Zhao L, Vogt PK. (2008). Class I PI3K in oncogenic cellular transformation. *Oncogene.* 27:5486–5496.

Zhang Y, et al. (2017) A pan-cancer proteogenomic atlas of PI3K/AKT/mTOR pathway alterations. Cancer Cell 31:820–832.e3.

Zhou X, Rowe RG, Hiraoka N, George JP, Wirtz D, Mosher DF, Virtanen I, Chernousov MA, Weiss SJ (2008). Fibronectin fibrillogenesis regulates three dimensional neovessel formation. Genes Dev. 22, 1231–1243.

Zovein AC, Luque A, Turlo KA, Hofmann JJ, Yee KM, Becker MS, Fassler R, Mellman I, Lane TF, Iruela-Arispe ML. (2010). Beta1 integrin establishes endothelial cell polarity and arteriolar lumen formation via a Par3-dependent mechanism. Dev. Cell 18, 39–51.

Appendix

A first author manuscript based on my thesis work is under preparation to be submitted to an international journal relevant to the field.